NPS-MR-93-002

# NAVAL POSTGRADUATE SCHOOL
## Monterey, California


# ADVANCES IN DYNAMICAL PREDICTIONS AND MODELLING OF TROPICAL CYCLONE MOTION

Russell L. Elsberry

March 1993

Approved for Public Release; Distribution Unlimited
Prepared for: Office of Naval Research,
Code 1122MM, Arlington, VA 22217

Naval Postgraduate School
Monterey, California 93943-5000

Rear Admiral T. A. Mercer
Superintendent

H. Shull
Provost

This report was prepared for and partially funded by the Office of Naval Research, Code 1122MM, Arlington, VA, 22217-5000. The remainder of the funding was provided by the Naval Postgraduate School Direct Research Fund.



This report was prepared under the direction of:

UNCLASSIFIED
SECURITY CLASSIFICATION OF THIS PAGE

## REPORT DOCUMENTATION PAGE

Form Approved OMB No 0704 0188

| | |
|---|---|
| 1a REPORT SECURITY CLASSIFICATION: UNCLASSIFIED | 1b RESTRICTIVE MARKINGS: |
| 2a SECURITY CLASSIFICATION AUTHORITY: | 3 DISTRIBUTION/AVAILABILITY OF REPORT: Approved for public release; distribution unlimited |
| 2b DECLASSIFICATION/DOWNGRADING SCHEDULE: | |
| 4 PERFORMING ORGANIZATION REPORT NUMBER(S): NPS-MR-93-003 | 5 MONITORING ORGANIZATION REPORT NUMBER(S): |
| 6a NAME OF PERFORMING ORGANIZATION: Naval Postgraduate School; 6b OFFICE SYMBOL (If applicable): MR | 7a NAME OF MONITORING ORGANIZATION: Office of Naval Research (Code 1122MM) |
| 6c ADDRESS (City, State, and ZIP Code): Monterey, CA 93943-5000 | 7b ADDRESS (City, State, and ZIP Code): Arlington, VA 22217-5000 |
| 8a NAME OF FUNDING/SPONSORING ORGANIZATION: Office of Naval Research; 8b OFFICE SYMBOL (If applicable): Code 1122MM | 9 PROCUREMENT INSTRUMENT IDENTIFICATION NUMBER: N0001493 WR 24009 |
| 8c ADDRESS (City, State, and ZIP Code): Arlington, VA 22217-5000 | 10 SOURCE OF FUNDING NUMBERS: PROGRAM ELEMENT NO 0601153N; PROJECT NO RR033-03-01; TASK NO; WORK UNIT ACCESSION NO |

11 TITLE (Include Security Classification): ADVANCES IN DYNAMICAL PREDICTIONS AND MODELLING OF TROPICAL CYCLONE MOTION

12 PERSONAL AUTHOR(S): Russell L. Elsberry

| 13a TYPE OF REPORT | 13b TIME COVERED | 14 DATE OF REPORT (Year, Month, Day) | 15 PAGE COUNT |
|---|---|---|---|
| Interim | FROM 10/92 TO 3/93 | 93 March | 121 |

16 SUPPLEMENTARY NOTATION: The views expressed in this report are those of the author and do not reflect the official policy or position of the Department of Defense.

| 17 COSATI CODES | | | 18 SUBJECT TERMS (Continue on reverse if necessary and identify by block number) |
|---|---|---|---|
| FIELD | GROUP | SUB-GROUP | |
| | | | |
| | | | |

19 ABSTRACT (Continue on reverse if necessary and identify by block number)

Recent advances in the use of numerical models for dynamical track predictions and modelling of tropical cyclone motion are reviewed. New applications of barotropic models for operational track predictions are described first. Barotropic models continue to be used by researchers to illustrate the importance of the symmetric and asymmetric components of the initial vortex in the model. New numerical techniques such as adaptive grids are shown to be well suited to the tropical cyclone prediction problem. New data assimilation techniques are first being tested with barotropic models in an effort to improve the initial conditions for track predictions.

Selected baroclinic models on limited regions are described in terms of numerical characteristics, representations of physical processes and specifications of the initial conditions. Improvements in these operational limited-region models have yielded more accurate track predictions, and the future goals are to predict the tropical cyclone-related precipitation and the

| 20 DISTRIBUTION/AVAILABILITY OF ABSTRACT | 21 ABSTRACT SECURITY CLASSIFICATION | |
|---|---|---|
| ☒ UNCLASSIFIED/UNLIMITED ☐ SAME AS RPT ☐ DTIC USERS | UNCLASSIFIED | |
| 22a NAME OF RESPONSIBLE INDIVIDUAL: Russell L. Elsberry | 22b TELEPHONE (Include Area Code): (408) 656-2373 | 22c OFFICE SYMBOL: MR |

DD Form 1473, JUN 86 — Previous editions are obsolete. — S/N 0102-LF-014-6603

19. Abstract continuation:

trends in the intensity as well. Recent results from research versions of limited-region baroclinic models appear to promise future improvements in all three aspects, and especially in the specifications of the initial conditions.

Global forecast models now have horizontal resolution that allows representation of the tropical cyclone circulation, and these circulations may move from the tropics into the midlatitudes during the 5-10 day predictions. Thus, many of these global models now include special techniques for improving the specifications of tropical cyclones. Although only limited verifications have been performed of the tropical cyclone track predictions, it appears that the error growth rates in these global models have been reduced. Even though the global model track predictions are received later by the tropical cyclone forecast centers, the smaller error growth rates and absence of domain boundaries that limit the forecast length suggest that the global models may contribute to more accurate track guidance and for longer intervals (perhaps to 120 h).

The physical mechanisms contributing to tropical cyclone motion in the baroclinic models are much more complex than the relatively simple dynamics of the barotropic models. A review of some recent idealized baroclinic models to assist in understanding tropical cyclone motion is given in the appendix. Even though the tropical cyclone has a baroclinic structure, the first-order motion is due to advection by the lower- to mid-tropospheric environmental flow (steering) plus advection of the environmental potential vorticity gradient by the cyclone circulation. Diabatic and frictional contributions to the motion appear to be smaller due to counter-balancing adjustments in the circulation. Little observational evidence is found to support hypotheses of significant track deflections due to vertical wind shear effects that were based on highly simplified models. The more sophisticated baroclinic models suggest that the negative potential vorticity anomalies associated with tropical cyclone outflow have relatively small effects on the motion.

Contents

Contents continued:

LIST OF TABLES

LIST OF FIGURES

## ACKNOWLEDGEMENTS

Preparation of this review was greatly facilitated by numerous authors supplying advance copies of manuscripts. Funding was provided by the Office of Naval Research Marine Meteorology Program. Dr. L. E. Carr, III, provided helpful comments on the manuscript, which was ably prepared in several versions by Mrs. Penny Jones.

## 1. Introduction

### a. Midlatitude and tropical prediction with dynamical models

Great advances have been made in the prediction of midlatitude circulation systems with numerical models. Accurate short-term (6-12 h) predictions and improved initialization procedures have led to the implementation of four-dimensional data assimilation systems that utilize the analysis-forecast-analysis cycle to improve the representation of the initial state of the atmosphere. The accuracy of the 72-h numerical predictions of midlatitude circulations is now equivalent to that of the 36-h forecasts of a decade ago. Improvements in accuracy have been achieved beyond 72 h as well, so that useful medium-range forecasts are now possible.

By contrast, advances in accuracy of the prediction of tropical circulation systems have been considerably slower. This is in part due to the inadequacy of the observing systems in the tropics. In addition to the sparsity of observation sites, especially over the tropical oceans, the horizontal gradients of meteorological properties such as temperature and geopotential heights in the tropics are of the same order as the measurement inaccuracies. Another important factor is the limited understanding of the basic dynamical and physical mechanisms of tropical circulations. Whereas the strong guidance of quasi-geostrophic theory has been exploited in improving midlatitude predictions, a similar dynamical basis does not exist for the tropics. Indeed, the importance of latent heat release in convective clouds makes the thermodynamics and dynamics of tropical circulations much more complex. It also follows that moisture measurements are more important in the tropics than in the midlatitudes, and yet the rawinsonde moisture observation may be representative of only a small area around the station. Convective scale processes have typically been parameterized in terms of large-scale circulations. However, it is unclear whether the basic assumption of parameterizability is applicable for the smaller scale tropical circulations.

Better tropical predictions are required to improve weather forecasts in tropics, and in the midlatitudes on time scales beyond 72 h. The most important weather phenomenon in the tropics is the tropical cyclone. Many of the 80 named tropical cyclones each year cause tremendous damage (estimates exceed US $20 billion for Hurricane Andrew during 1992) and loss of life. More accurate forecasts of the tracks of these cyclones can allow more timely preparations and avoid some of the property damage and loss of life. On time scales of 5-10 days, a tropical cyclone may form, move into the midlatitudes and transition into a dangerous weather system. In addition, the energy inputs in tropical circulations such as the Intertropical Convergence Zone or monsoon systems have an impact on the medium-range forecasts in midlatitudes. It is for these reasons that considerable interest has been focused on improving tropical predictions, and especially the tropical cyclone.

b. Dynamical track predictions -- shortcomings and potential

Previous assessments of dynamical predictions of tropical cyclones (e.g., Elsberry 1979, Elsberry 1987) had focused on limited area or regional models. As indicated above, global models intended for predictions beyond 72 h must include the tropics. Present global models have the horizontal resolution of regional models of a decade ago. Consequently, these models now include representations of tropical cyclone circulations, and it is essential that these representations be as accurate as possible.

The above assessments (and many other evaluations) have described the shortcomings of dynamical models for tropical cyclone track prediction. Both the initial direction and translation speed of the dynamical track predictions have typically been poor. In addition to the model storm starting from the wrong location, an initial adjustment period typically occurred in which the storm milled around before proceeding along a steady path. This early track behavior led to a "slow bias". Furthermore, many of the dynamical models (e.g., Ueno 1991; Mathur 1991; Mathur and Shapiro 1992) exhibit a northward track bias for west-moving tropical cyclones in low latitudes. Some of these shortcomings are likely related to inadequate horizontal resolution in the dynamical

models. Model resolutions of 50-100 km can only represent the outer circulation. The details of the tropical cyclone structure will not be resolved until grid spacings of 5-10 km are achieved. A false spinup in the storm circulation may also occur, and an unrepresentative storm structure typically results in coarse-grid models.

Even given these shortcomings, the dynamical models have been the source of much of the optimism for improving tropical cyclone predictions. Although the dynamical models typically start poorly, the predicted tracks at 48 h to 72 h are among the most skillful of the objective guidance techniques (Elsberry 1987). Indeed, as the specifications of the initial conditions in the dynamical models have been improved, the forecast tracks have become skillful relative to a standard technique such as CLIPER (climatology and persistence) at earlier times. The dynamical models are also expected to be most useful during the difficult forecast periods when adjacent synoptic systems are affecting the tropical cyclone motion. For example, the interaction with the subtropical ridge cell and a midlatitude trough during potential recurvature situations is one of the most difficult track forecast problems. Because this interaction is an inherently nonlinear process, an accurate dynamical model is expected to offer the best guidance as to the likely path.

c. Recent advances in understanding tropical cyclone motion

As described by Elsberry and Abbey (1991), programs of the Office of Naval Research and other agencies (especially the NOAA Hurricane Research Division (HRD), Geophysical Fluid Dynamics Laboratory and National Hurricane Center) have contributed to new understandings of tropical cyclone motion. Coordination among four international field experiments (Elsberry 1990) has led to the best data set every available to study western North Pacific tropical cyclones (Elsberry *et al.* 1990; Harr *et al.* 1991). The NOAA HRD also has gathered important new data sets in Atlantic hurricanes as part of their annual data collection efforts (e.g., Lord and Franklin 1987; Franklin 1990).

Some of these advances in understanding tropical cyclone motion have already been incorporated in the dynamical track prediction models. Other aspects can form a basis for

future improvements. Especially in the case of the global models, the desire to improve tropical cyclone track prediction may only be an auxiliary goal. Improvements in horizontal resolution or physical processes representations may be motivated by other considerations, but these can also lead to improved tropical cyclone track predictions. One of the objectives of this report is to relate recent advances in understanding tropical cyclone motion to improvements in operational dynamical track predictions and our capability to model tropical cyclones. Consequently, some of these advancements in understanding are summarized here (more details are available in Elsberry and Abbey 1991).

(*i*) Lower and middle tropospheric steering is the primary factor in tropical cyclone motion. Although the first-order importance of the steering concept has been known for some time, recent observational studies (see Elsberry and Abbey 1991; 1992) have put this concept on a more solid basis. In particular, the most consistent representation of the steering vector is a vertical average over the 850-300 mb layer. However, recent studies by Velden and Leslie (1992) suggest that the vertical average should be over a shallower layer for less intense storms. The most important implication for dynamical track prediction is that the model forecast will only be as good as the analysis and prediction of this lower tropospheric steering. Where observations are lacking, such as over the tropical oceans, poor initial specifications of the steering will need to be corrected.

(*ii*) Propagation of the tropical cyclone can account for systematic departures relative to steering. Regardless of the definition of the steering that may have been used, the tropical cyclone has a propagation vector relative to the steering. The implication for dynamical track prediction is that the inability of observe the small (1-3 m/s) propagation vector will require an independent specification in the initial conditions.

(*iii*) Propagation in a purely barotropic framework is a function of beta and the environmental wind field (linear shear and relative vorticity gradients), and of the outer storm structure. This dependency on the environmental wind field puts additional

emphasis on the initial condition specification for dynamical models. Not only must the steering vector in the region of the tropical cyclone be specified, the first and second derivatives of the environmental flow must also be specified. An equally important implication is that the outer wind structure in the tropical cyclone must be correctly specified and predicted if the propagation vector is to be accurate. Thus, the synthetic observations (bogus vortex) used to define the tropical cyclone location should also represent the actual wind structure.

(*iv*) Propagation effects arise in a baroclinic model in association with asymmetric heating and wind distributions and vertical shear effects. [Because several baroclinic model studies have appeared since the publication of Elsberry and Abbey (1991), a review of some idealized studies to reveal tropical cyclone motion mechanisms is given in Appendix A.] Since the latent heat release is being represented on a square grid in the dynamical model, an asymmetric component may be real or fictitious, and may be highly time-dependent compared to the asymmetric circulations associated with the barotropic processes in (*iii*) above. Model horizontal resolution is obviously an important factor for correctly representing these asymmetries. In addition, the solutions may be quite sensitive to the latent heat release parameterizations in the dynamical model.

(*v*) Mesoscale convective systems embedded within the tropical cyclone circulation may cause track meanders of 100 km on time scales of a day. One potential mechanism for these meanders is that the mesoscale convective system (MCS) represents an asymmetric latent heat release as in (*iv*) above. However, the effect may be due to a vortex-vortex interaction analogous to the Fujiwhara effect. This implies the horizontal wind distributions in the tropical cyclone and the MCS must be accurately specified in the initial conditions and predicted in the model as the cyclone and MCS interact.

d. Plan for the paper

Recent activities in tropical cyclone track prediction and research studies with dynamical models will be reviewed. The next section begins with the simpler barotropic

models, which will be shown to have utility as operational models. In addition, these models are natural test beds for research approaches that will later find application in operational barotropic models, or in the baroclinic models. The following section will describe the baroclinic models that have been (and continue to be) the primary focus of research. Both global and regional models will be compared. The final section will summarize the outlook for the future of tropical cyclone track prediction with dynamical models.

## 2. Barotropic models

### a. Characteristics and utility of operational models

Two recently developed barotropic models are selected for discussion. In terms of the considerations discussed above, the justification for using a barotropic model for tropical cyclone prediction would be to allow high horizontal resolution to better resolve the storm structure and the interaction between the vortex and its environment. However, that environment also evolves due to baroclinic processes, especially during recurvature in association with a midlatitude trough. Thus, such a barotropic model is expected to be useful for situations where the lower tropospheric flow in the tropics is more barotropic, and for limited periods of time (before baroclinic processes significantly change the environmental circulations affecting the tropical cyclone). The first (HRD) model discussed below does indeed have better numerics and resolution, and the second (Bureau of Meteorology Research Centre--BMRC) model is highly flexible and is intended for interactive use.

(1) Operational track prediction. The HRD model (called VICBAR) utilizes a nested grid (Table 1) with a higher resolution near the center and coarser grids at greater distances (DeMaria *et al.* 1992). In the operational version, the inner grid resolution is 50 km. As this barotropic model has previously been used by Shapiro and Ooyama (1990) with up to seven nested grids and an inner grid spacing of 10 km, the veracity of the cubic B spline representation of the fields and of the nesting technique have been established.

Table 1 Characteristics of selected barotropic models used for tropical cyclone track prediction.

PREDICTION MODEL

| | Type | Layer Depth | Grid Sizes | X Domain | Y Domain | Time Step | Horiz. BC |
|---|---|---|---|---|---|---|---|
| VICBAR 1990 | SWE | 750 m | 50 km<br>100<br>200<br>400 | 600 km<br>1800<br>4800<br>14,400 | 600 km<br>1800<br>4800<br>11,200 | 110s<br>200<br>400<br>800 | Global Spectral model |
| BMRC | NDB | --- | 70 (Var) | 9990 | 5550 | --- | Regional model analysis |

ANALYZED FIELDS

| | Layer Average | Background Field | Fitting Routine | Vortex Specification | | |
|---|---|---|---|---|---|---|
| | | | | Symmetric | Steering | Asymmetric |
| VICBAR 1990 | 850-200 | 12-h global forecast | Cubic B spline | Profile fit to $V_m$, $r_m$ size | Specified initial motion | No |
| BMRC | 850-300 single level | Regional analysis | Barnes analysis 2 passes | Profile | Specified initial motion | No |

Abbreviations:

VICBAR - Hurricane Research Division Model (De Maria *et al.* 1992)
BMRC - Bureau of Meteorology Research Centre (Holland *et al.* 1991)
SWE - Shallow water equations
NDB - Nondivergent, barotropic
BC - Boundary conditions
$V_m$ - Maximum velocity
$r_m$ - Radius of maximum winds
NA - Not applicable

Various specifications of the lateral boundary conditions have been tested (DeMaria *et al.* 1992), and time-dependent values are now specified from the current (or prior 12 h) global model integration.

Operational track forecasting also requires an analysis scheme to specify initial conditions. HRD has also used the cubic B spline approach for analyses on nested grids (Lord and Franklin 1987; Franklin 1990). In this operational case, the analysis is of layer-average (850-200 mb) winds and heights using the prior 12-h global forecast fields as the background (Table 1). As indicated above, a crucial part of the analysis is the specification of the fields near the storm where inadequate observations exist to specify the steering and the storm structure. A symmetric vortex profile is fit to the maximum wind, eye size and storm size values estimated by the National Hurricane Center (NHC) forecasters. In particular, the wind profile decreases to 5 m/s at a radius that is 250 km beyond an "influence radius" determined from surface analyses and satellite loops that is believed to represent the radius of the area influenced by the storm circulation. DeMaria *et al.* (1992) state that the track of the vortex is sensitive to the outer structure (~ 400-800 km), but not to the inner structure, as demonstrated previously by research models. An example of the layer-mean analyses for a small hurricane (wind decreased to 5 m/s at 600 km) is shown in Fig. 1.

These synthetic observations to represent the symmetric vortex are superposed on a constant wind vector field equal to the initial storm motion provided by the NHC. This pre-processing technique of replacing the steering estimates within 600 km of the storm center assures that the initial direction and speed in the model forecast will be equal to persistence. However, the asymmetry created by adding the symmetric vortex to a uniform flow is not the asymmetric circulation that research models have demonstrated to cause the propagation of the tropical cyclone relative to the steering current (Elsberry and Abby 1991).

The VICBAR model is normally initiated whenever a named kt) exists in the

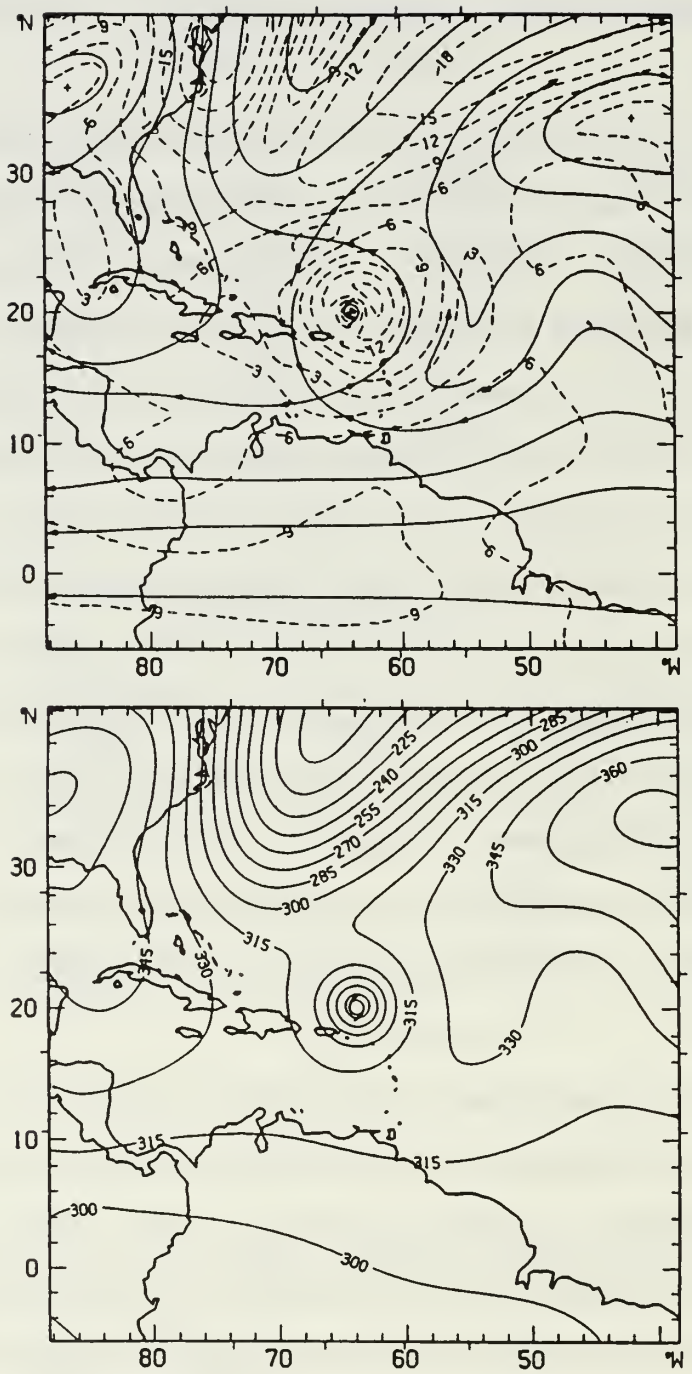


Fig. 1 (top) Initial streamline (solid) and isotachs (dashed) and (bottom) height deviations analyses on meshes 1-3 of the VICBAR prediction model (DeMaria *et al.* 1992) for Hurricane Dean at 00 UTC 4 August 1989. Isotach and height contour intervals are 3 m $s^{-1}$ and 15 m respectively.

Atlantic basin. Forecasts also are only verified for cases of tropical-storm tropical cyclone (35 kt) exists in the Atlantic basin. Forecasts also are only verified for cases of tropical-storm strength or greater. A general result is that the forecast errors are smaller when the storm is of hurricane intensity. During 1989 (Fig. 2), the VICBAR track errors had skill relative to CLIPER, and were generally equivalent in skill to the statistical-dynamical aid called NHC83, which has generally been the best objective aid. In addition, the VICBAR had smaller errors in 1989 than the baroclinic model called QLM (to be discussed below). A particular advantage of the VICBAR is that it has skill relative to CLIPER already at 12 h, when the QLM (during 1989) had large errors, which has been a characteristic of dynamical models (see Section 1). The VICBAR skill at 12 h is due to the pre-processing technique of using the initial storm motion as a steering vector. Notice also that the VICBAR skill relative to CLIPER begins to decrease after 36 h, which is an indication that baroclinic processes are beginning to become more important after 36 h.

During 1990 (Fig. 3), the VICBAR skill relative to CLIPER was slightly smaller than during 1989. However, the skill was essentially the same as the statistical-dynamical technique (now called NHC90). The performance of the QLM was substantially improved during 1990 by the inclusion of a pre-processing technique (Mathur 1991, Mathur and Shapiro 1992, to be discussed below). Consequently, the QLM had skill relative to CLIPER by 24 h and continued to improve in skill until 72 h (Fig. 3b). In particular, the QLM was more skillful than VICBAR at 48 h and 72 h.

These statistical comparisons during 1989 and 1990 indicate the year-to-year variability in the performance of dynamical models. This is in part due to the real differences in the character (e.g., more hurricanes during 1989 than 1990) and locations (more low-latitude, westward-moving storms in 1989). However, both the VICBAR and QLM were substantially modified prior to the 1990 season. Such facts make it difficult for the forecasters to utilize dynamical model tracks as guidance.

(2) Interactive analysis-forecast system. Holland *et al.* (1991) have installed a

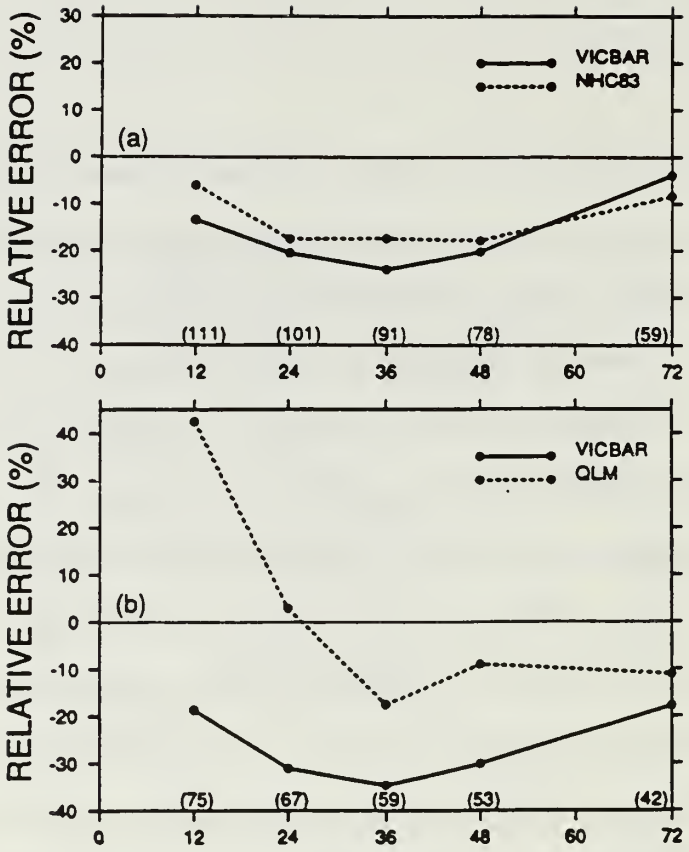


Fig. 2 Average relative track errors from VICBAR and (a) NHC83 and (b) QLM during 1989 tests. The relative track error is with respect to CLIPER and homogeneous samples are compared with the number of cases at each forecast time indicated along the bottom (DeMaria *et al.* 1992).

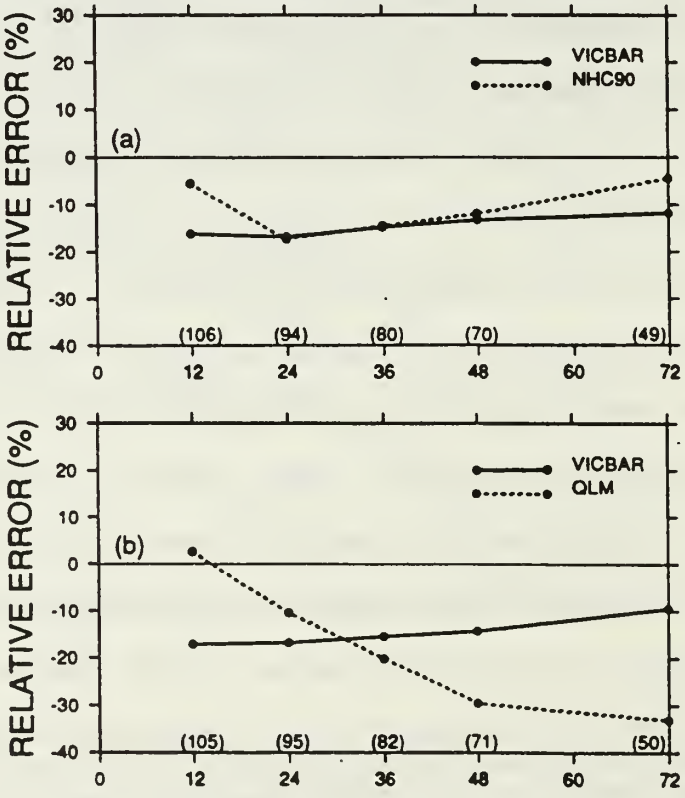


Fig. 3 As in Fig. 2 except during the 1990 tests, and NHC90 replaced NHC83 as the statistical dynamical model.

barotropic model for track forecasting on a workstation at BMRC. The primary purpose for choosing a barotropic model in this case is that the model can be integrated so quickly that it is feasible to do multiple integrations (Fig. 4). Thus, the forecaster can use the model interactively to test various scenarios that might apply in a particular situation, e.g., what if the storm was displaced or was represented with a different structure (Fig. 5). The basic assumption is that it is advantageous to be able to integrate a degraded (barotropic) model several times compared to a single integration of a more complex baroclinic model. A justification for this assumption (at least to 36 h) is implied by the accuracy of the VICBAR model in Figs. 2 and 3.

The characteristics of the BMRC barotropic forecast model and analysis approach are summarized in Table 1. Only a single grid (typically 70 km) is used. If a finer resolution is specified, the domain size would be correspondingly reduced. With a smaller domain than VICBAR, it is expected that errors associated with boundary conditions will degrade the solution more quickly, and the BMRC model is normally only run to 48 h. The initial conditions for the BMRC model (Table 1) may be provided from a Barnes analysis, which requires no global or regional analysis as a background, or a statistical interpolation technique. Various forms of a bogus vortex are available for the forecaster to test. As in the VICBAR, these symmetric vortices are superposed on an steering vector equal to the initial storm motion vector in order to get the model storm moving in the correct direction and speed. Holland *et al.* (1991) do not provide track statistics as in Figs. 2 and 3. Rather, they illustrate the flexibility of such an interactive version of a barotropic model for track prediction (Fig. 5). These cases indicate the sensitivity of the forecasts to the specifications of the environmental flow and the storm structure, as would be expected from recent research described above in Section 1. It remains to be demonstrated that a forecaster with the BMRC barotropic model as a tool will be able to produce consistently better forecasts.

b. Research applications of barotropic models

As indicated above, barotropic models are useful to test in a research mode

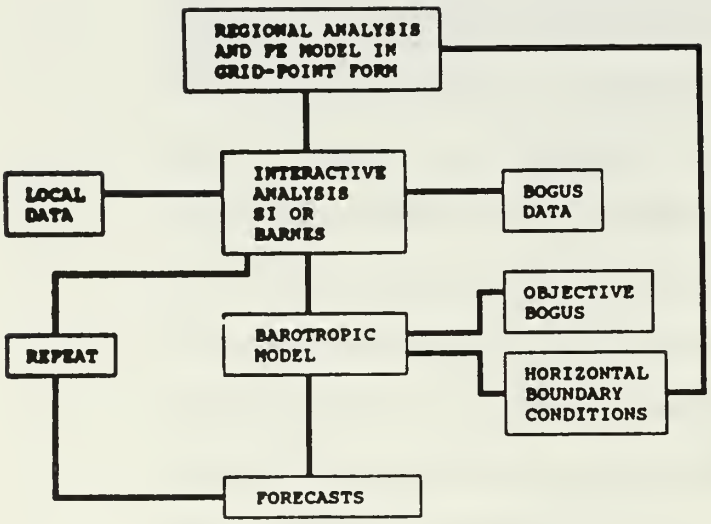


Fig. 4 Schematic structure of the interactive analysis and forecast system for tropical cyclones at the BMRC (Holland *et al.* 1991).

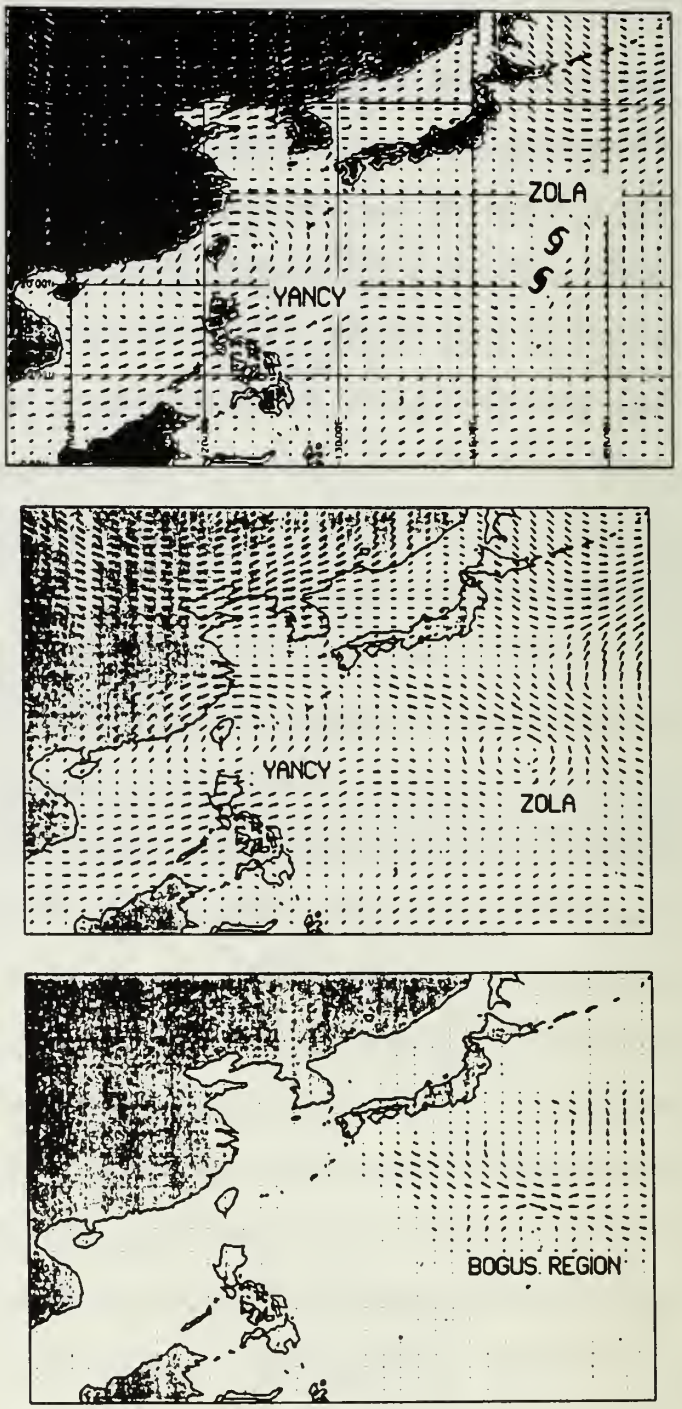


Fig. 5 (a) Original 500 mb NOGAPS wind analysis for Typhoon Zola indicating analyzed (open symbol) and actual (closed symbol) positions; (b) revised analysis following insertion of bogus vortex; and (c) analysis differences subtracting (b) from (a). Maximum vector length is 25 m $s^{-1}$ (Holland *et al.* (1991).

some concepts or approaches that will later be applied in an operational barotropic model or in more complex baroclinic models. Several examples related to tropical cyclone motion and track prediction will be given here. For purposes of background, recall that Fiorino and Elsberry (1989) demonstrated (with a nondivergent barotropic model and no background flow) that larger propagation vectors for vortices with stronger outer winds were due to more intense asymmetric circulations. Wavenumber one gyres with an anticyclonic (cyclonic) gyre to the right (left) of the storm have a flow between them that is nearly equal in direction and speed to the propagation vector. Various analytical theories have been developed to describe the steady-state (e.g., Carr 1989) or time evolution (e.g., see review by Smith 1992) of the wavenumber one gyres. Observational documentation for the existence of these gyres is somewhat indirect (Elsberry and Abbey 1991, 1992).

(1) Effect of symmetric vortex profile. The impact of the choice of the symmetric wind profile for the bogus vortex has been demonstrated by Holland and Leslie (1993) with a barotropic model. Four profiles (Fig. 6) used by the Fleet Numerical Oceanography Center (Goerss *et al.* 1991), Japan Meteorological Agency (Ueno and Ohnogi 1992), U. S. National Meteorological Center (Mathur 1991), the Australian Bureau of Meteorology (Davidson and Puri 1992a) and DeMaria (1987) were tested in a 303 x 211 gridpoint model with 30 km resolution. All wind profiles were calculated to 1000 km from the center and then linearly reduced to zero at 1500 km. Although the four profiles are qualitatively similar in the core region, marked differences are found in the outer regions. Based on Fiorino and Elsberry (1989), such differences in outer wind structure would be expected to produce quite different asymmetric circulations (Fig. 7) and propagation vectors. The Rankine vortex (Fig. 7a) developed a gyre structure that covered much of the integration domain within 48 h, and it is twice the intensity of the gyre developed by the weakest vortex (Holland) in Fig. 7d.

Ohnishi (1992a) has also illustrated the sensitivity of the beta drift to the imposed vortex structure. He specifies the symmetric vortex in terms of empirical constants that

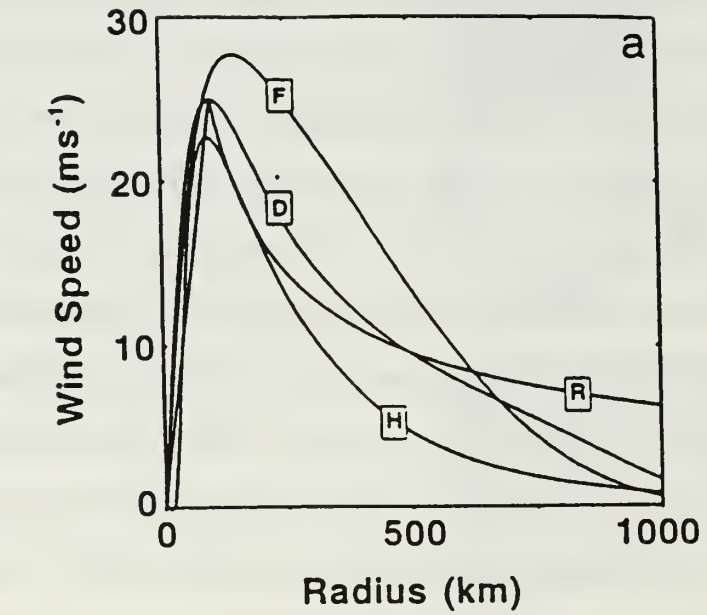


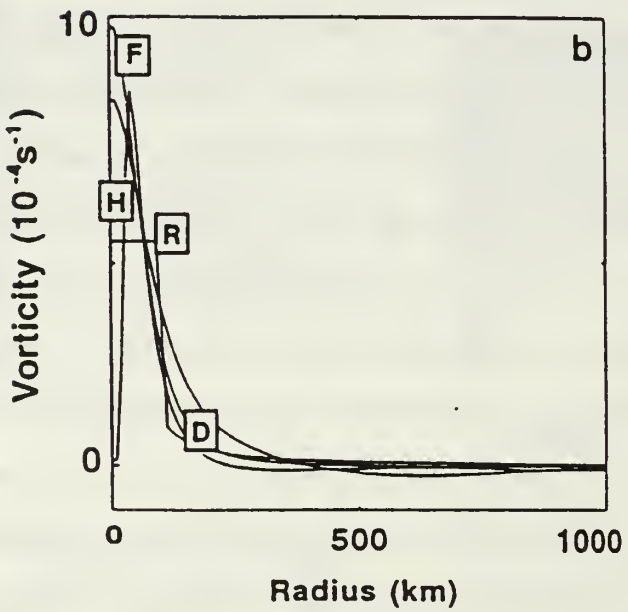


Fig. 6 Axisymmetric profiles of (a) tangential wind component and (b) relative vorticity of four vortices tested by Holland and Leslie (1993). R, D, H and F refer to profiles proposed by Rankine, DeMaria, Holland and Fujita respectively.

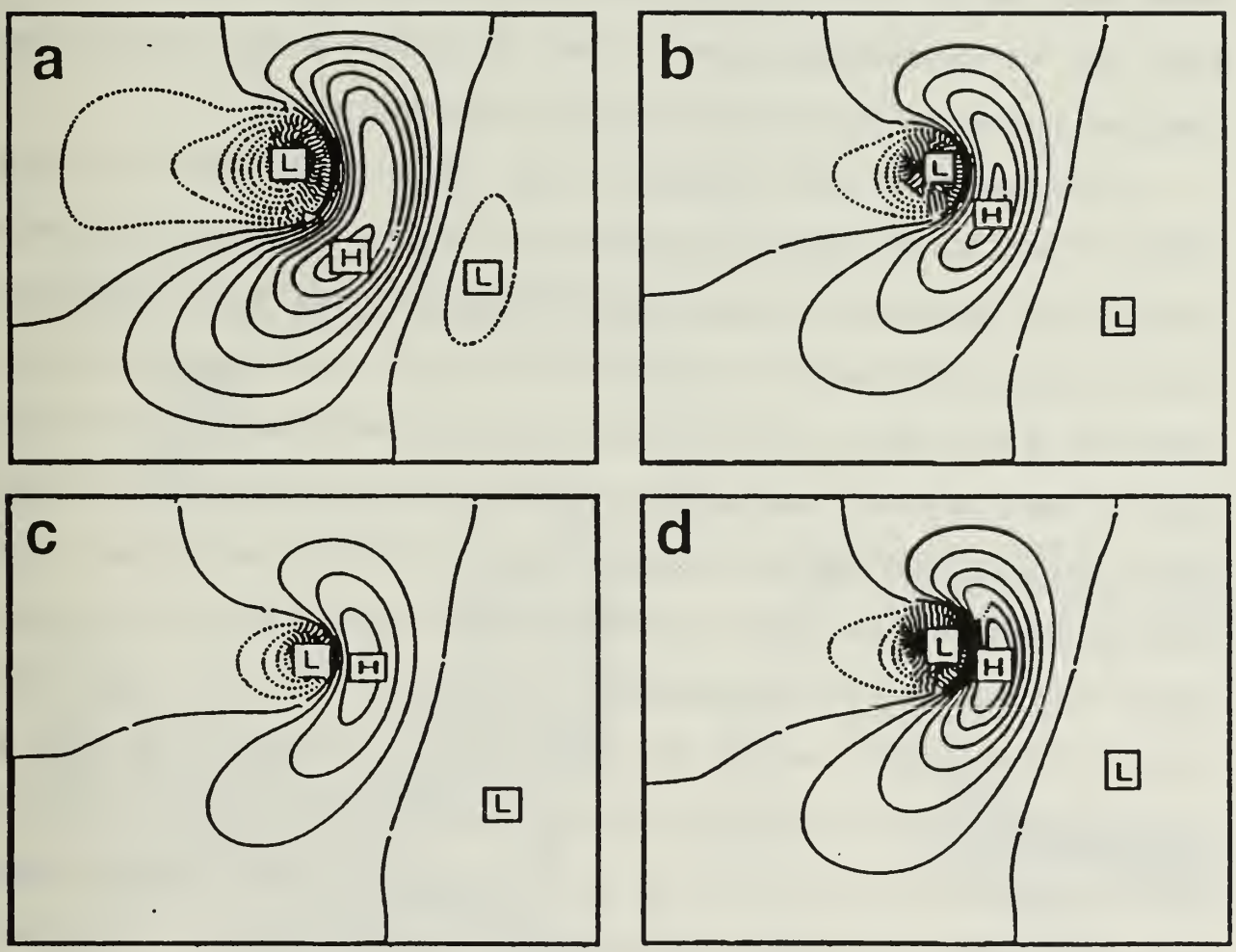


Fig. 7 Streamfunction field after 48 h integrations of a barotropic model with the four initial vortex wind profiles from Fig. 6: (a) Rankine, (b) DeMaria, (c) Holland and (d) Fujita. Negative (dashed) values indicate the cyclones (Holland and Leslie 1993).

determine the strength, size and concentration of high winds near the center. Because the phase speeds for the vorticity and the streamfunction centers differ, a stream flow through the vorticity center will be created, which establishes a nonlinear advective effect on the vortex center. Analytical expressions for this advective effect for different wind profiles were checked against numerical integrations of a barotropic model. Whereas a "tight vortex" drifts to the north (as in many previous studies), Ohnishi (1992a) illustrates that a "broad vortex" may first drift to the south because the vorticity center is displaced westward faster than the streamfunction center. Later, the centers become coincident and meridional displacement ceases, and eventually the vortex drifts poleward.

These barotropic model integrations by Holland and Leslie (1993) and Ohnishi (1992a) illustrate the sensitivity of the asymmetric circulation to the outer wind profile specified in the bogus vortex for dynamical track prediction models. Such a profile should thus reflect actual storm conditions, especially at outer radii. It also emphasizes again the importance of the satellite cloud-drift wind estimates at low levels around the tropical cyclone. That is, the outer wind profiles in Fig. 6 can not be simply inserted as a bogus vortex in a environment with no real observations to "control" the specified values. The Japan Meteorological Agency extracts detailed low-level cloud-drift winds (Fig. 8) from 15 minute visual imagery of their Geostationary Meteorological Satellite once a day (Ohnishi 1992b). Although these low-level wind estimates are only possible in quadrants not obscured by thick cirrus overcast, the azimuthally-averaged wind profile with radius may reflect the actual storm structure (Fig. 8). Notice that the profile slope appears to change at a radius of about 600 km, which may indicate that the tropical cyclone vortex should be confined to about 600 km in this case. A long-standing problem has been to develop a consistent and accurate procedure for separating the vortex from the environment in nature (Elsberry and Bohner 1992).

(2) Inclusion of asymmetric circulation. As indicated in Section 1b, a common problem in dynamical predictions of tropical cyclone tracks is the slow bias and incorrect

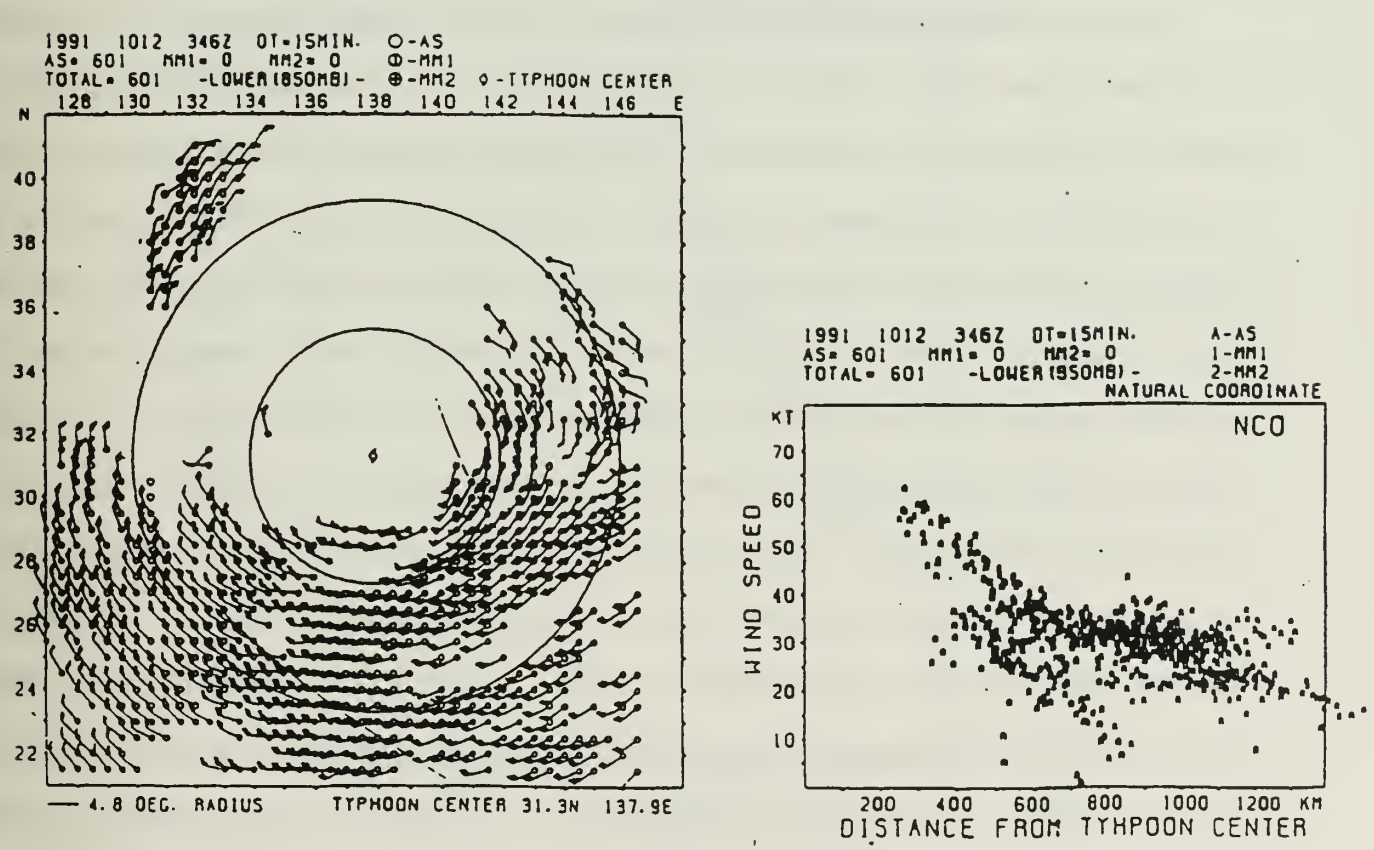


Fig. 8 (Left) Detailed low-level cloud-drift winds estimated from 15 minute GMS imagery of Typhoon Orchid (9121) at 0346 UTC 12 October 1991. (Right) Tangential wind speeds (kt) as a function of distance from the typhoon center extracted from the imagery on the left (Ohnishi 1992b).

direction during the early period. Carr and Elsberry (1992) use a barotropic model to demonstrate that a proper specification of the initial conditions that includes an asymmetric circulation may greatly reduce this problem. Carr and Elsberry point out that omission of the asymmetric circulation omits also the propagation effect that contributes to the motion, at least until the model develops the appropriate gyres. As shown in Fig. 9, the model with only a symmetric vortex is displaced northwestward about 150 km less during 0-48 h than occurs during the nearly steady-state translation period from 36 - 48 h. However, inclusion of the appropriate wavenumber one gyres for the initial symmetric vortex immediately produces an essentially steady propagation, which reduces the along-track error to less than 60 km.

Mathur (1991) and Mathur and Shapiro (1992) have designed an *ad hoc* asymmetric circulation in part inspired by the barotropic model of Fiorino and Elsberry (1989) to address the problem of northward bias in the tracks of westward-moving tropical cyclones in low latitudes. The frequent occurrence of such cyclones during 1989 contributed to the large QLM errors in the early forecasts in Fig. 2b. Mathur and Shapiro (1992) created a dipole circulation with westward flow between the centers that would be superposed on the symmetric vortex and thus direct the model storm on a more westward path (Fig. 10). Whereas the initial analysis of Hurricane Gilbert had a nearly symmetric flow (Fig. 10b), superposition of the dipole resulted in stronger (weaker) winds to the north (south). With the dipole, the initial motion was more westward and agreed more closely with the observed track than did the case without the dipole. Mathur (1991) generalized the dipole pattern to orient the direction of flow between the gyres in any desired direction. Because they then specify this direction and speed to be the observed storm vector, they are combining the problems of specifying the initial environmental flow (steering) and the inclusion of propagation into a single step. Nevertheless, implementation of the dipole circulation during 1990 contributed to an improved performance of the QLM (Fig. 3b).

Another example of barotropic model research results applying to baroclinic models

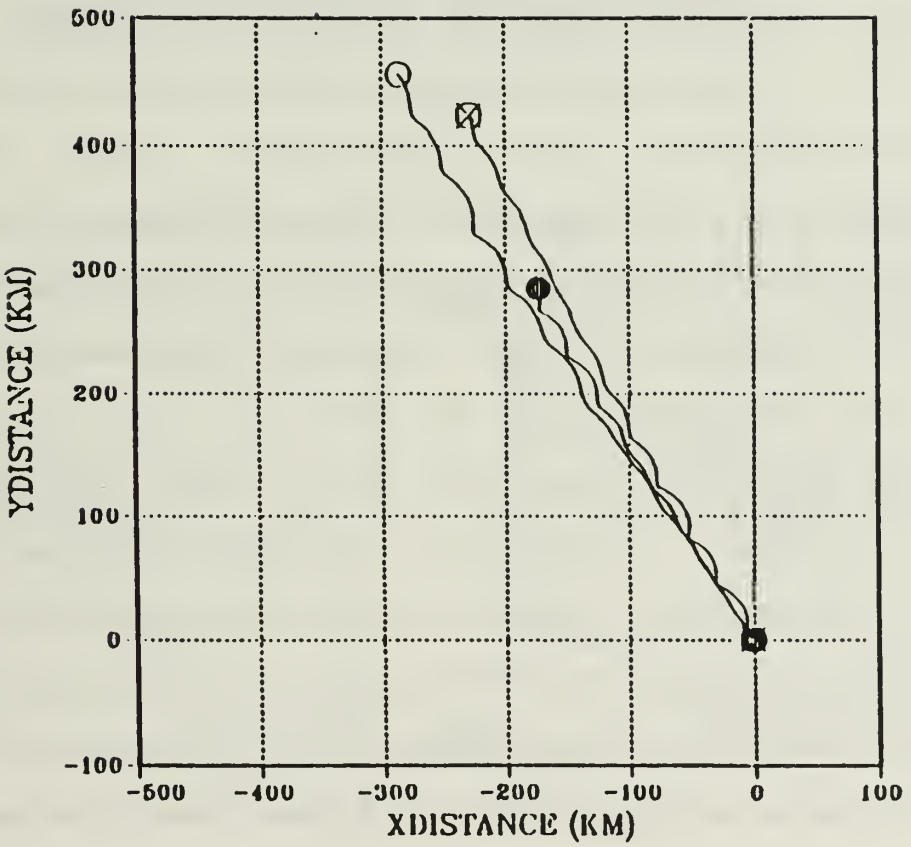


Fig. 9 Tracks predicted by a nondivergent, barotropic numerical model for: symmetric initial vortex, 0-48 h (solid circle); symmetric initial vortex, 36-84 h repositioned to same starting point (crossed circle); and asymmetric initial vortex including wavenumber one gyre, 0-48 h (open circle) (Carr and Elsberry 1992).

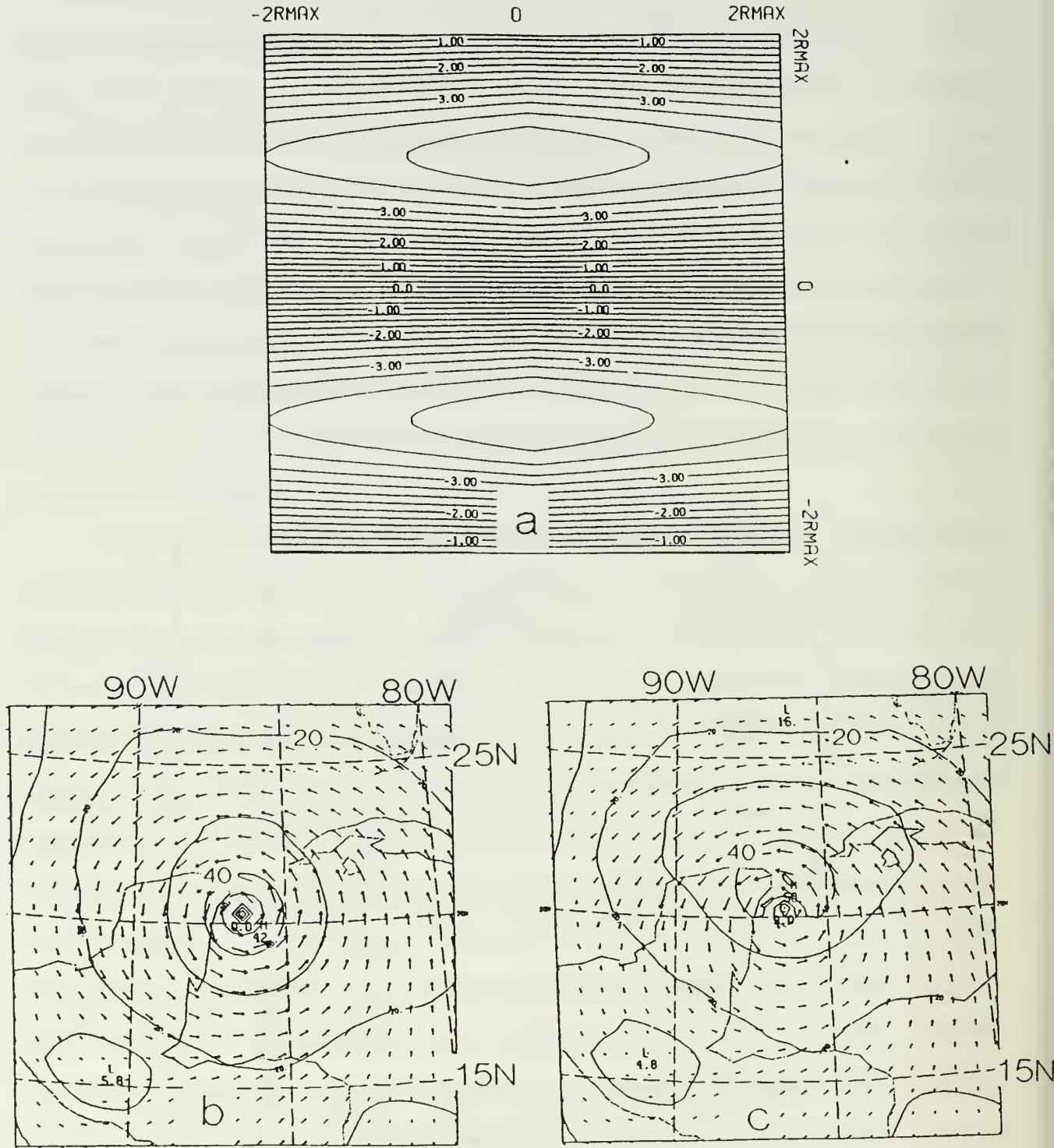


Fig. 10(Top) Dipole streamfunction structure of Mathur and Shapiro (1992) for case of Hurricane Gilbert at 12 UTC 14 September 1988. Winds at 850 mb without (lower left) and with (lower right) the dipole streamfunction added.

has been provided by Ross and Kurihara (1992). They describe a simplified scheme to specify the asymmetric circulation due to the beta effect, which is a key component in their initialization procedure for high resolution baroclinic model predictions of tropical cyclone tracks and intensity (Kurihara *et al.* 1992). Ross and Kurihara express the vorticity and wind fields in terms of azimuthal wavenumbers and then test truncations of wavenumbers 1, 2 and 3 in comparison to the complete numerical solution. Recall that it is wavenumber one that is associated with the propagation effect. Wavenumbers 0 (symmetric vortex), 2 and 3 do not have a direct effect (because they have no net flow component across the vortex center), but they may have an indirect effect via the beta effect in changing wavenumber 1. Ross and Kurihara show that the influence of wavenumber 3 is negligibly small. Thus, they conclude that a model truncated at wavenumber 2 is adequate for generating the asymmetric circulation associated with the beta effect.

Another important theoretical result of Ross and Kurihara was that time dependence of the symmetric vortex must be allowed to achieve the proper propagation. The reason is that the same processes that generate the gyres also modify the vortex profile by decreasing the cyclonic flow at larger radii. As Fiorino and Elsberry (1989) show, even small changes in the outer wind structure can affect the propagation vector. Previous theoretical solutions by Smith and Ulrich (1990), Smith (1991) and Peng and Williams (1990) have assumed that the symmetric vortex is constant.

Ross and Kurihara also show that their simplified model is accurate for a variety of vortex sizes, whereas the Smith and Ulrich (1990) theory does not yield a good estimate of the track of a small vortex (Fig. 11). The simplified model including wavenumber two and the time-dependent symmetric vortex (labelled K012) is closer to the control position (labelled SU numerical) than is the simplified model including only wavenumber one (labelled K1) or the Smith and Ulrich analytical model (labelled SU analytic). It will be shown below that inclusion of this simplified (barotropic) solution for the asymmetric circulation at all levels in the Kurihara *et al.* (1992) baroclinic model improves the initial

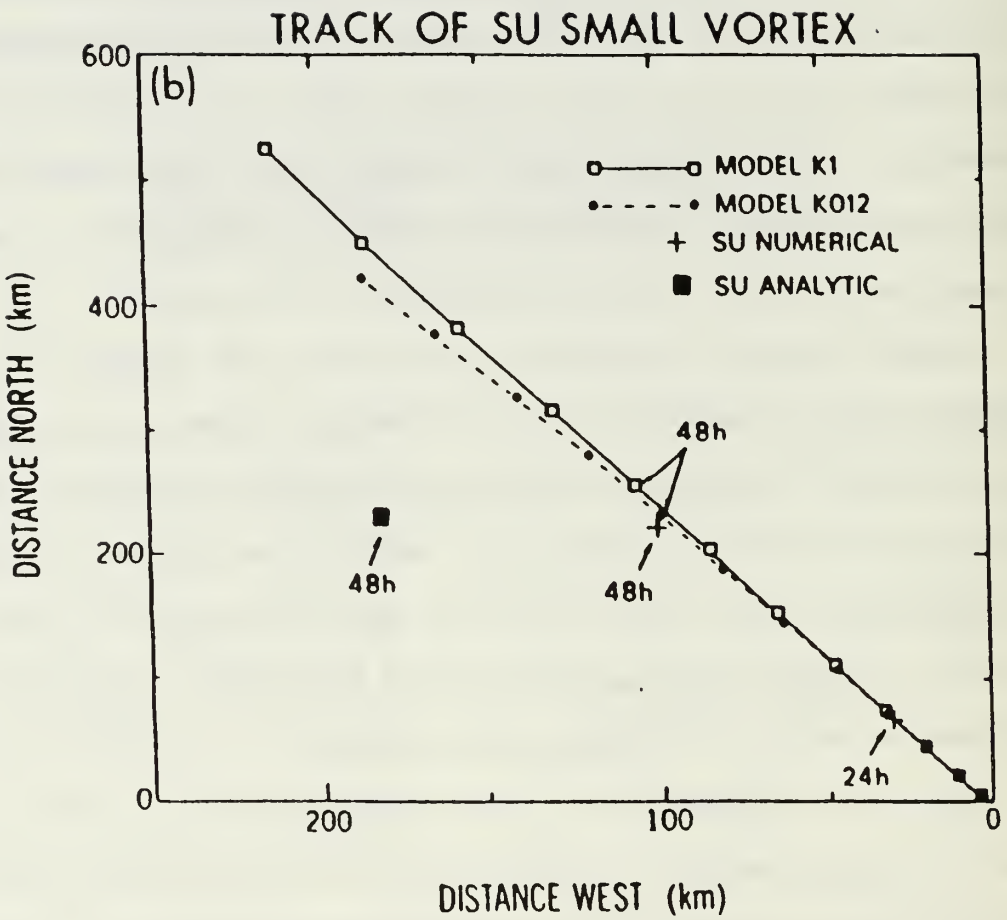


Fig. 11 Vortex positions each 6 h from the Ross and Kurihara (1992) models with only wavenumber one (K1) and with wavenumbers one and two plus a time-dependent symmetric vortex (K012) for a small vortex case. Corresponding 24 h and 48 h positions are shown for the Smith *et al.* (1990) numerical model and the 48 h position of the Smith *et al.* analytical solution.

track of the tropical cyclone.

(3) Adaptive grids for tropical cyclone modelling. Nested grid models have been used for 20 years to improve the resolution near the central region of the tropical cyclone. Recent applications include the HRD model (Shapiro and Ooyama 1990; Shapiro 1992; DeMaria *et al.* 1992) and the Geophysical Fluid Dynamics Laboratory (GFDL) model (Kurihara *et al.* 1992; Bender *et al.* 1992). However, such nested models have not been used with multiple storms, which would require separate nests for each storm. The merger of two storms would probably involve a pretty complex interaction between the two nests.

Holland and Dietachmayer (1992) have used an adaptive grid barotropic model to simulate the interaction of two and three tropical vortices. The grid adaptation is to improve the accuracy of the numerical solutions of the shallow water equations by the technique of grid-stretching. An appropriate spatial distribution of gridpoints is determined automatically and is time dependent. Although the grid is non-uniform and non-orthogonal in physical space, the gridpoints are regular and stationary in computational space. Holland and Dietachmayer define a weighting function that is a linear combination of the geopotential perturbation magnitude and the wind speed squared, which ensures enhanced grid resolution in the vortex core and in surrounding regions of strong winds. A splitting technique is used to separate the slow (advective) and fast (inertia-gravity) modes in the solutions. Other details can be found in Dietachmayer (1992) and Dietachmayer and Droegemeir (1992).

An example of the adaptive grid simulation of the merger of two large, intense vortices placed 550 km apart is shown in Fig. 12. The combination of the two vortices drifted westward and poleward in response to the beta effect as the vortices approached and merged. After only 12 h (Fig. 12a), a rotation through about 120$^{o}$ has occurred, and spiral bands of higher vorticity trail behind each vortex. The rotation accelerated by 18 h (Fig. 12b) and the cores were approaching. Most of the merger process occurred in the 3-h period from 21-24 h (Fig. 12c) and involved substantial distortion of the original vortices.

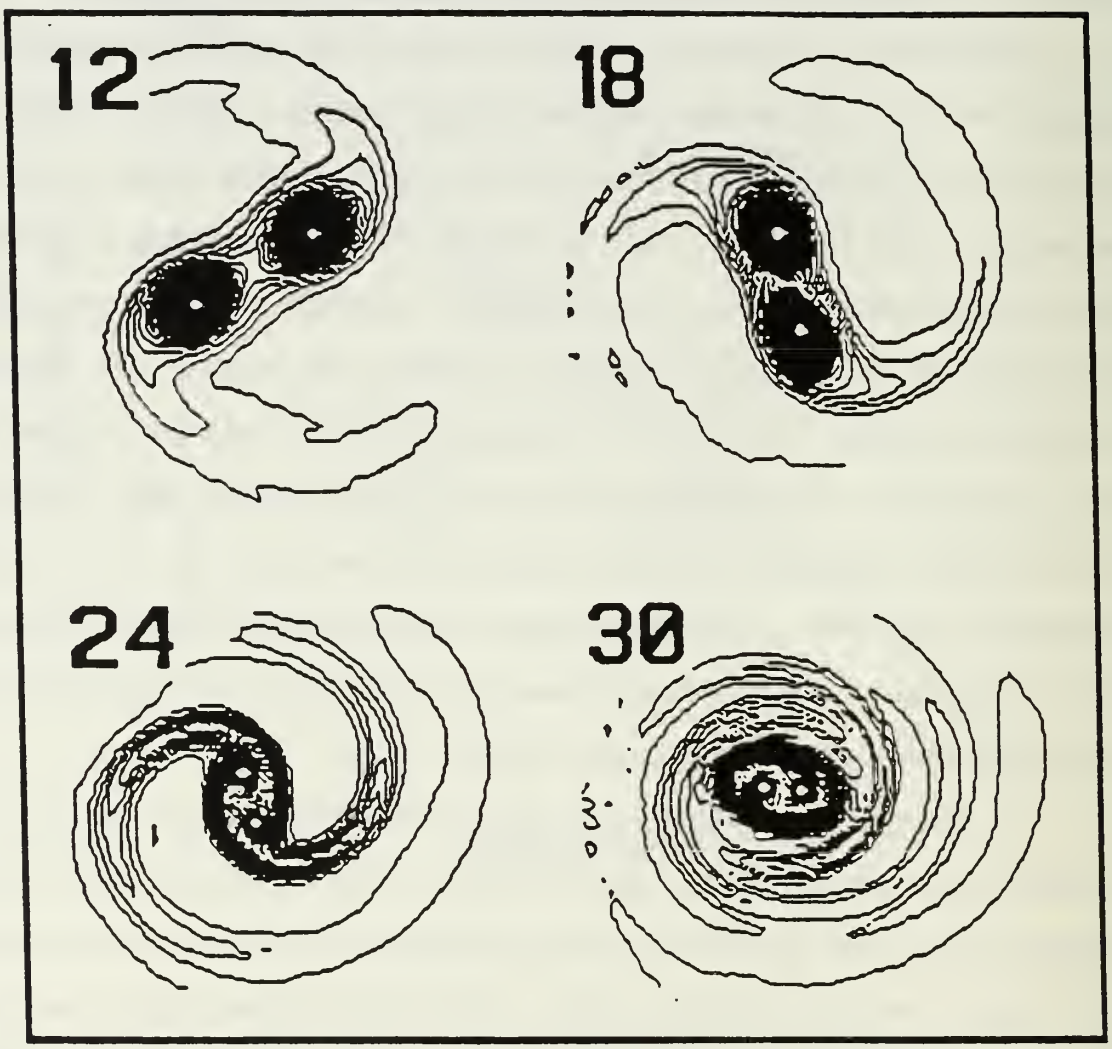


Fig. 12 Evolution each 6 h from 12 h through 30 h of the relative vorticity fields of the Holland and Dietachmayer (1992) adaptive grid model with two Southern Hemisphere cyclonic vortices separated by 5° longitude at the initial time. The white dots indicate the cores of the original vortices.

The importance of the adaptive grid in resolving this stage is evident. Substantial amounts of fluid with cyclonic vorticity were lost to filamentation in the spiralling wake. The remnants of the two original vortex cores were retained and continued to orbit the core of the new composite vortex at 30 h (Fig. 12d).

Liu and Zeng (1992) have applied an adaptive mesh model to some tropical cyclone track predictions. They use a variational that includes factors to force smoothness in the grid-stretching, near-orthogonality in the mapping, and a weighted volume of the grids. The weighting function varies exponentially with the radial distances from the center in the physical space so that the density of grid points is concentrated and resolution is improved. Their transformation of wind and geopotential variables in the shallow water equations is designed to conserve total energy and mass for periodic or fixed boundary conditions. No control predictions are given for comparison with their tropical cyclone track predictions. Thus, it is difficult to evaluate the additional benefits that the adaptive grid approach may have provided in terms of accuracy or efficiency.

(4) New data assimilation techniques. Leslie and Holland (1992) have reviewed trends in data assimilation that are relevant for tropical cyclone prediction. They define data assimilation as the process by which an initial state ($t=0$) for the forecast model is produced by incorporating data over the time period $-T < t < 0$, where T may be 6, 12 or 24 h (Fig. 13). The present data assimilation schemes are either intermittent or continuous. An example of the intermittent scheme is the typical 6-h cycling procedure that begins with an analysis, a 6-h model forecast is then used to define the background (first-guess) conditions for the next analysis, etc. Notice that observations at times other than the 6-h analysis time must be translated in time to the analysis time. In the continuous data assimilation techniques, the model solution beginning at $t=-T$ is compared to the observations (or target analyses at discrete intervals), and additional forcing terms are added to the governing equations to "nudge" the model solution toward these observations or target analyses. For example, this nudging technique is incorporated in the tropical

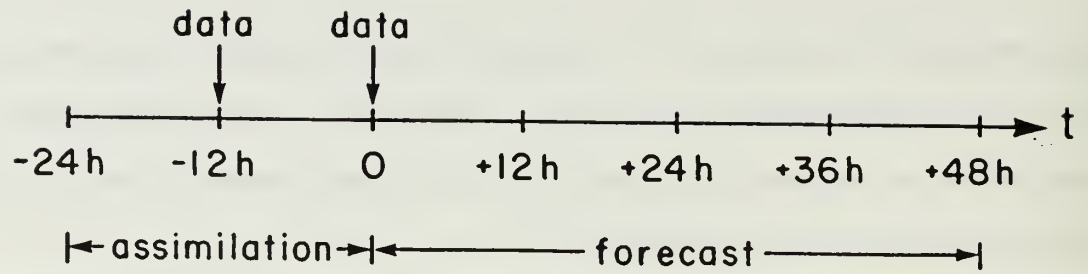


Fig. 13 Time diagram illustrating the data assimilation procedures with initial conditions at t = - 24 h, additional analyses at t = - 12 h and t = 0 h. Observed boundary conditions are available from t = - 24 h to t = 0 h and forecast boundary conditions from a global model are supplied from t = 0 h to t = 48 h (Bennett *et al.* 1992).

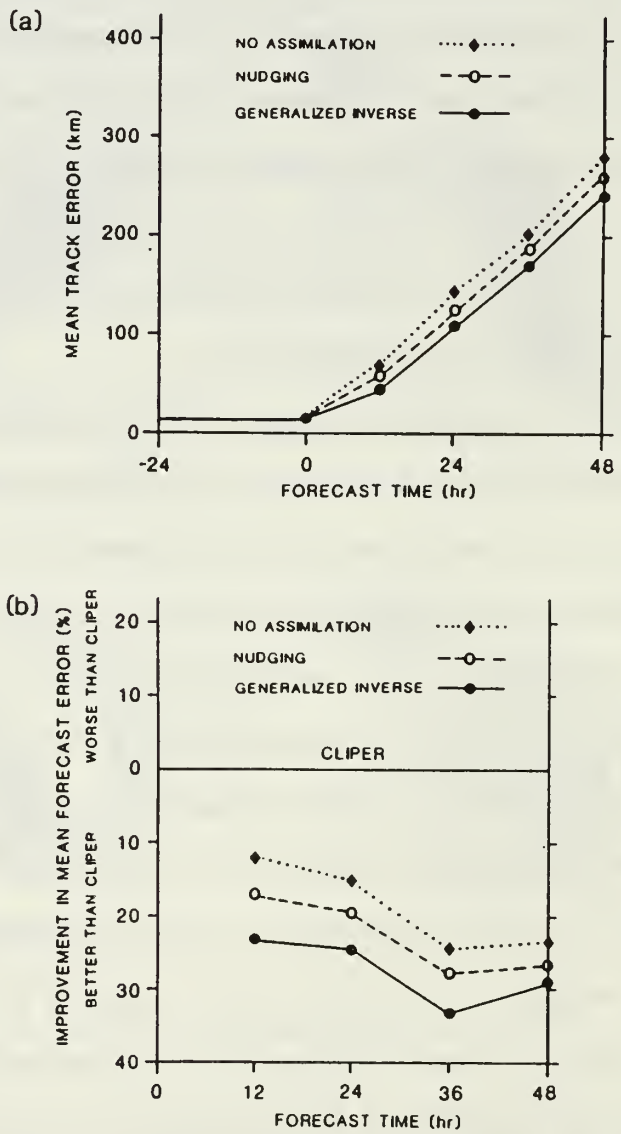


Fig. 14 (a) Mean track forecast errors for the 10 cases in the assimilation tests of Bennett *et al.* (1992). (b) Improvement relative to CLIPER for the 10 cases in (a).

model at the Australian Bureau of Meteorology (Puri *et al.* 1992; Davidson and Puri 1992b). The assimilation cycle is 12 h and uses target analyses at -12 h, - 6 h and 0 h. The objective is to combine the recent past analyses into the initial conditions at t = 0 and yet have these conditions be consistent with the model physics. Thus, no initialization step is involved that removes divergence, or reduces the vertical motion and delays the onset of convection and latent heat release in the model (so-called precipitation spin-up problem). However, the model fields are likely to be noisy and not completely adjusted to new observations at t = 0 because the nudging process takes time to reduce the differences between the observations and the model values.

Recent research in data assimilation techniques has utilized a variational approach that minimizes errors by the method of least squares (Leslie and Holland 1992). In addition to minimizing errors in the observations or analyzed fields, the potential model errors or boundary errors can be included (Bennett *et al.* 1992). One of the first applications of the variational method for tropical cyclone track forecasts was by Jones and DeMaria (1991, 1993) and DeMaria and Jones (1993). Because the previous analyses at -6 h and -12 h also included properly positioned hurricanes, the assimilation method may be considered to be an optimal method for including the persistence of past motion into the dynamical model initial fields at time t = 0. Each of their analyses of Hurricane Hugo utilized the HRD procedure of superposing a bogus vortex within 600 (or 800) km of the storm on a constant vector that represents the initial motion of the storm. Another similarity with DeMaria *et al.* (1992) above is that the same four nested grids with an inner grid of 50 km resolution was used in the balanced equivalent barotropic model.

Jones and DeMaria (1991) first applied a strong dynamical constraint (assuming that the model is a perfect representation of the atmospheric dynamics) and minimized a "cost function"

$$CF = \sum_{n=0}^{N} \sum_{i=0}^{I} \sum_{j=0}^{J} W_{ij}^{n} \left( P_{ij}^{n} - \bar{P}_{ij}^{n} \right)^2 , \qquad (1)$$

where $\tilde{P}_{ij}^{n}$ is the observed (from the analyses) potential vorticity and $W^n$ are arbitrary weights. The summations are over the i,j gridpoints and the n observation times. The least squares problem is solved by the method of Lagrange multipliers in which the constraint equations multiplied by a Lagrange multiplier are added to the cost function (1). A cycle of one integration of the model forward and one backward integration over the data assimilation is required. The backward integration in this "adjoint procedure" is required to determine the values of the Lagrange multipliers. That is, knowing the misfit of the $P^n$ at the initial time, the backward integration of the model to the earliest analysis time allows a comparison of the model solution with the conditions at that time. The weighting factors in the cost function (1) then can be calculated to put more or less weight on the analyzed values at each point as necessary to bring the forward integration closer to the analyzed values at time t = 0. This adjoint cycle must be repeated until the cost function (1) is sufficiently converged, i.e., additional cycles would not change significantly the solution. However, if many of these cycles of forward-backward integrations over the assimilation period are used, much more computer time will be required to obtain the initial conditions than to integrate the model from time t = 0 to 72 h for the track forecast. For example, Jones and DeMaria compared solutions after 8 cycles and after 32 cycles.

The measure of goodness for the data assimilation is the improvement over simply starting the model from the initial conditions at t = 0. For a sample of 17 forecasts of Hurricane Hugo, Jones and DeMaria (1991) found the assimilation (non assimilation) errors at 0, 12, 24, 36, 48, 60 and 72 h were 8 (9), 22 (38), 46 (61), 65 (84), 94 (110), 132 (138) and 175 (163). Thus, the percentage improvements were largest at 12 h and diminished at later times. The improvement at early times is reasonable as the data assimilation procedure is blending previous storm positions into the model initial conditions at t = 0, and thus introduces a persistence of past motion into the dynamical model solution.

Bennett *et al.* (1992) use a nested, non-divergent barotropic model to test a more

generalized inverse procedure that also allows for potential model inaccuracies in predicting the atmosphere, and potential inaccuracies in the specifications of the boundary values. Including potential model errors is called a weak dynamical constraint in contrast to the strong dynamical constraint of Jones and DeMaria (1991). Adding these additional effects increases the complexity of the solution of the inverse problem. Bennett *et al.* provide the details of the solution method for the Euler-Lagrange equations for a least-squares penalty functional. They tested the inverse method for only 10 cases during the TCM-90 program. Predictions of the tracks to 48 h were compared with the operational Bureau of Meteorology operational barotropic model that has no assimilation procedure and with a simple nudging assimilation approach over the prior 24 h. The Bennett *et al.* inverse method reduced the 24-h track errors about 14% and 10% relative to the operational and nudging approaches respectively, and the 48-h errors by 10% and 7% respectively (Fig. 14a). Comparison of these errors with CLIPER (Fig. 14b) indicates the inverse method had skill with improvements of 26% and 29% at 24 h and 48 h respectively. In their post-analysis of the inverse technique, they found that improvements due to inclusion of potential model errors or boundary condition errors were negligible. That is, it would have been sufficient for this small sample of cases to impose these conditions as a strong constraint. This may not be a general conclusion because the environmental flow conditions around the tropical cyclones in this sample did not vary strongly, and these changes were well resolved by the limited observations. In more variable environmental conditions, or with less complete and accurate data sets than were available during TCM-90, it might be advantageous to apply the model as a weak constraint.

Jones and DeMaria (1993) tested the strong constraint, weak constraint and an alternating between strong and weak constraints during the assimilation cycle. The best track forecasts were achieved with the alternating strong-weak cycle. It was also beneficial to use 06 UTC or 18 UTC fields that are simply interpolations of the 00 UTC and 12 UTC synoptic fields except with insertion of the new storm location, structure and initial motion

vector. Although these tests need to be repeated with larger samples, this data assimilation research with barotropic models indicates the potential for better use of the available observations to define the initial conditions for dynamical track predictions. In addition, these methods incorporate persistence of past motion information into the dynamical models, and thus start the model storm in about the correct direction and speed at the initial time. Thus, these methods have promise for reducing one of the dynamical model shortcomings described in Section 1b.

3. Limited region baroclinic models

Elsberry (1987) discussed four limited region baroclinic models being used for operational tropical cyclone track prediction during the early 1980s. Except for the One-way influence Tropical Cyclone Model (OTCM) of the U. S. Navy, each of the other three models has been replaced by more recent models (Table 2). The models selected for discussion here are operational models for which some track error statistics are available, and two sophisticated research baroclinic models that have been tested with real data.

Development and testing of baroclinic models are underway in several other countries, but only limited samples of predictions are available. Some comprehensive reviews for the former USSR are given by Sitnikov (1991) and for the People's Republic of China by Y.-T. Zhu (1992). Experience in Japan, U.S., Australia, etc. suggests that these baroclinic models are so complex that a considerable period of development and testing will be required before stable results may be expected. Thus, the discussion will be limited to the relatively mature models in Table 2, which are indicative of the status of regional baroclinic models during the late 1980s and early 1990s. Since these models (and those in other countries) are being modified frequently, the reader is advised to continually monitor these modifications.

a. Characteristics of operational models

One of the interesting changes since the mid-1980s has been the expanded objectives for these limited-region baroclinic models. The single objective of each of the

Table 2a Characteristics of selected operational and semi-operational limited-region baroclinic models for tropical cyclone track prediction. Part 1. Numerical characteristics.

| | Vertical Layers | Horiz. Grid | Domain X | Domain Y | Time Integration | Horizontal BC |
|---|---|---|---|---|---|---|
| | | | OPERATIONAL | | | |
| Typhoon Tatsumi (1986) | 8 | 50 km | 5400 km | 5400 km | Semi implicit | One-way hemispheric 12 h fcst |
| QLM Mathur (1991) | 8 | 40 km | 4400 km | 4400 km | Quasi-Lagrangian | One-way global 0 h fcst |
| BMRC Davidson & Puri (1992a, b) | 8 | 100 km | 45° long. | 45° lat. | Semi-implicit | One-way global 0 h fcst |
| Taiwan Peng *et al.* (1993a, b) | 9 | 70 km | 8500 km | 6000 km | Split explicit | One-way global 12 h fcst |
| | | | SEMI-OPERATIONAL | | | |
| MRI Yamasaki (1992) | 10 | 5/12°<br>1.25<br>3.75° | 30° long.<br>90°E-180<br>global | 25° lat.<br>15°S-60°N<br>30°S-NP | Centered space-time | ? |
| GFDL Kurihara *et al.* (1993a) | 17 | 1/6°<br>1/3°<br>1° | 5°<br>11°<br>75° | 5°<br>11°<br>75° | ? | One-way global ? |

four models in Elsberry (1987), except for the Movable Fine-mesh Model (MFM) of the U. S. NMC, was to predict the tropical cyclone positions. The MFM was a more sophisticated model that was also capable of precipitation forecasts. The new models now generally include tropical cyclone-related precipitation prediction as a secondary objective. In addition, the model developers are somewhat optimistic that trends in the intensity of tropical cyclone may also be predicted with these higher resolution baroclinic models, even though the resolution is still not adequate to represent the details of the inner core wind distribution.

Various characteristics of these models are summarized in the three-part Table 2. Numerical characteristics are first discussed (Table 2a), and then the physical processes included in the baroclinic models will be summarized briefly (Table 2b). Both of these aspects must be understood to assess the capability of these baroclinic models to better predict the tropical cyclone and its environment. Given the limited computer resources of operational numerical weather prediction centers, multi-level and full physics baroclinic models may be expected to have larger grid sizes and smaller domains than the operational barotropic models discussed in Section 2a(1). Two important advantages to be expected (Section 1b) from the baroclinic models relative to the barotropic model are: (*i*) better predictions of the steering flow, especially after 36 h when baroclinic effects become more evident; and (*ii*) vertical shear effects in the tropical cyclone structure and in the environment will now be represented. However, the real key to the success of these recent baroclinic models is the specification of the initial conditions to represent the location, structure and initial motion of the tropical cyclones, which are summarized in Table 2c. As indicated in the list of shortcomings in Section 1b, improvements in the baroclinic model predictions required a better specification of the initial conditions.

(1) Numerical characteristics. Comparison of the operational models in Table 2a indicates considerable similarities. In contrast to the OTCM (summarized in Elsberry 1987), which has only three layers with no boundary layer, each of the four operational

models has at least eight layers. In general, one or more of these layers will be used to represent the boundary layer through which the tropical cyclone receives energy from the ocean. In addition, a layer in the lower stratosphere is generally also now included as an upper boundary condition.

A tradeoff must be made by the dynamical model designer between the horizontal grid resolution and the horizontal domain to be covered. Each reduction in the grid size by a factor of two in a finite difference model requires an increase of a factor of eight in computer speed, because the time step must also be reduced by a factor of two. The alternative of reducing the domain size below 4000 km square is not viable because the tropical cyclone may move great distances during the 72 h forecast, especially following recurvature. Peng *et al.* (1993a) give an example in which the difference between a poor track forecast and a good forecast was the distance between the tropical cyclone and the western edge of the domain. This again illustrates one of the well-known disadvantages of limited-area models, which is the presence of the artificial boundaries that degrade the solutions due to inaccurate boundary conditions. It is clearly an advantage if these domain boundaries can be far removed from the center of the domain where the tropical cyclone is found. An additional consideration for the western North Pacific region is that multiple tropical cyclones are a frequent occurrence (Iwasaki *et al.* 1987). Thus, the domain must be quite large if all cases are to be predicted simultaneously, which is particularly necessary if the cyclones are close enough to interact. However, the number of gridpoints increases rapidly as the domain size is increased. Thus, it may be necessary to accept a coarser horizontal resolution than is really desirable for tropical cyclone prediction.

The time integration method must be both accurate and efficient. In the split explicit approach, a shorter time step is used for the terms in the primitive equations that allow rapidly moving gravity waves, and a longer time step is used for advective terms. Iwasaki *et al.* (1987) found they could not fully exploit this efficiency for tropical cyclone conditions because the interaction between the moist processes and gravity waves is not

well represented if the theoretical limit of the advective time step is attempted. The quasi-Lagrangian approach in the QLM has the advantage of more accuracy than the traditional centered spatial finite differences. The BMRC model utilizes a semi-implicit time integration.

As indicated above, the disadvantage of the limited area model is the requirement to provide accurate values at the horizontal boundaries. Numerous limited-area model tests have demonstrated that the accuracy of the longer-term solutions is directly related to the accuracy of the boundary values. In research applications, these boundary values are often provided from the actual analyses at the appropriate times (perfect-prog approach). This approach is not possible with an operational model. In each case in Table 2a, these boundary values are provided from a larger scale model.

The dilemma here for the numerical model designer is between accuracy and timeliness. The most accurate values are provided if the larger scale model is integrated first, and the required values on the limited-area domain boundaries are stored. However, the global models typically do not run until six or more hours past synoptic time. Thus, the limited-region model could not be run until perhaps 8 h after synoptic time, and the dynamical track prediction could not be used by the tropical cyclone forecaster until 12 h after valid time. The alternative is to use boundary values derived from the previous 12 h forecast of the global model, which will already be available as soon as the new synoptic time observations are received for use in the limited-area model. Although the tropical cyclone track forecast is available 6 h earlier, many tests have demonstrated that the accuracy is reduced by use of the 12-h old boundary values. Normally, this improvement in timeliness is a more important consideration than the reduction of accuracy.

(2) Representation of physical processes. The most important physical process in the tropical cyclone is the release of latent heat in convective and large-scale clouds. Each of the operational models in Table 2b uses some modification of the Kuo (1975)

Table 2b. As in Table 2a. Part 2. Representation of physical processes.

| | Cumulus Convection | Surface fluxes Ocean | Surface fluxes Land | Radiation | Friction Surface | Friction Internal |
|---|---|---|---|---|---|---|
| **OPERATIONAL** | | | | | | |
| Typhoon Iwasaki *et al.* (1987) | Kuo-modified in subcloud layer | Bulk $C_0(V)$ | None | None | Bulk $C_D(V)$ | 4th order horizontal diffusion |
| QLM Mathur (1991) | Kuo | $C_0(V)$ | None | None | Bulk $C_D(V)$ | 2nd order horizontal divergence damping |
| BMRC Davidson and Puri (1992a, b) | Kuo | Bulk | Bulk | Diurnally varying | Bulk | ? |
| Taiwan Peng *et al.* (1993a, b) | Kuo plus artificial heating | Bulk | Bulk | Longwave Shortwave | Stability dependent | ? |
| **SEMI-OPERATIONAL** | | | | | | |
| MRI Yamasaki (1992) | Predicted cloud water, rainwater | ? | ? | ? | ? | ? |
| GFDL Kurihara *et al.* (1993a) | Convective adjustment | Roughness dependent | Roughness Vegetation dependent | Diurnally varying | Roughness Stability dependent | Turbulence closure |

representation of cumulus convection. This technique relates the total latent heat release to the moisture convergence in the column, and partitions the moisture supply between moistening and heating of the environmental air during a moist adiabat ascent from the boundary layer. Because the original Kuo technique is known to have deficiencies, various modifications have been applied. For example, Iwasaki *et al.* (1987) found it necessary to offset excessive cooling in the subcloud layer to maintain a tropical cyclone. Peng *et al.* (1993a, b) artificially add heat to maintain the tropical cyclone against dispersion and diffusion.

The energy source for the tropical cyclone is the latent and sensible heat gained from the warm tropical oceans. Thus, the modern operational models directly predict these surface fluxes over the ocean and over the land (except in the case of the QLM). In most cases, the exchange coefficients for moisture, heat and momentum are dependent on wind speed. Although radiative processes are generally not considered to be of importance on time scales of 36 h, the prediction of the tropical cloudiness cycles in the environment of the cyclone on longer time scales probably require the inclusion of radiative processes.

In addition to the frictional boundary layer processes, most of the models include some scale-selective diffusion or damping processes. The objective is to eliminate computationally or physically-produced short wavelength features before they contaminate the larger scale features being predicted.

(3) Specification of initial conditions. As indicated in Section 1, inadequate observations are available to analyze the three-dimensional structure of the tropical cyclone. As Elsberry (1987) pointed out, a common error in the early dynamical models was the "misplaced vortex" problem. That is, the analysis scheme would produce a vortex in the wrong location due to insufficient and/or unequally distributed observations around the tropical cyclone. Recent studies, especially with barotropic models, have indicated that an accurate representation of the symmetric vortex (Section 2b.1) and the asymmetric circulation (Section 2b.2) are necessary. Since the asymmetric circulation is related to the

propagation vector (defined as the difference between the actual storm motion and the steering vector), the proper representation of the initial storm motion in the dynamical models has been a continuing source of problems.

The capability to attack this initial condition problem systematically by all numerical weather prediction centers was advanced by an initiative from the second International Workshop on Tropical Cyclones (WMO 1990). Based on discussions at the workshop, a common format was developed for reporting the location and characteristics of each tropical cyclone by the analysis centers. This digital report is transmitted via the Global Telecommunication System (GTS) and provides uniform information for inserting "synthetic observations" (previously called a bogus vortex) to represent the tropical cyclone. The first advantage is that the cyclone position is generally improved, although some initial position error still remains due to interpolation between horizontal grid points separated 40-100 km (Table 2a).

Different approaches are used to represent the horizontal and vertical structure of the symmetric vortex (Table 2c). The twin objectives here are to represent well the actual storm structure and to have a vortex that is compatible with the numerical prediction model. The Iwaskai *et al.* (1987) approach was to specify the surface pressure profile following Fujita (1952) based on the central pressure and an environmental surface pressure. However, the sharp pressure gradients near the center of an intense typhoon can not be resolved on a 50 km grid. Thus, a less steep pressure slope is specified that is more consistent with the model resolution. Iwasaki *et al.* also specify the anticyclonic geopotential height deviations at cloud top level in the tropical cyclone. Temperature patterns are calculated that are hydrostatically consistent with the surface pressure and the anticyclone aloft, and with the Kuo convective parameterization scheme. Then the gradient wind equation is used to calculate the wind field from the geopotential heights at each level. They also calculate the radial inflow that is in steady state with the tangential winds at the top of the boundary layer. A relative humidity of 90% is inserted near the

Table 2c. As in Table 2a, Part 3. Specification of initial conditions.

| | Specification of TC | Size Dependence | Derived Quantity | Secondary Circulation | Relative Humidity | Initial Motion | Merging TC | Merging Blend Zone |
|---|---|---|---|---|---|---|---|---|
| | | | | OPERATIONAL | | | | |
| Typhoon Iwasaki et al. (1987) | Empirical surface p and cloud top D value | Radius of 15 $m\ s^{-1}$ | Gradient wind balance | Diagnostic boundary layer | 90% in lower troposphere | Via asymmetric circulation | 100% within $R_i$ ($R_i$, $R_e$ depend on $R_{15}$) | Cosine $R_i<r<R_e$ |
| QLM Mathur (1991) | Empirical surface p $\geq$ 970 mb vertical function | Outer closed isobar $\geq$ 170 km | Gradient wind | No | ~100% at center for strong storm | Global model modified with dipole | Cosine 0<r<size | |
| BMRC Davidson and Puri (1992a,b) | Synthetic winds inserted | Size | Mass | Beta-plane asymmetry | Satellite cloud temp | Inside TC | Blending with real observations by dynamic nudging | |
| Taiwan Peng et al. (1993a,b) | Spinup vortex (Three options) | Two large or one small | None | Wavenumber one asymmetry | Spinup Vortex | Observed | < 630km | < 840km |
| | | | | SEMI-OPERATIONAL | | | | |
| MRI Yamasaki (1992) | Empirical wind field | Size | Mass | No | Global field | No | ? | Size dependent |
| GFDL Kurihara et al. (1993) | Spinup vortex | Controlled by obs | None | Asymmetry from barotropic model | Spinup vortex | Global model plus asymmetry | Size dependent | Size dependent |

tropical cyclone to insure moisture convergence to trigger the convective latent heat release via the Kuo technique.

Mathur (1991) also uses the observed central surface pressure observation in the QLM, except that values less than 970 mb are set to equal to 970 mb. The reported size (radius of the outer closed surface isobar) is used to scale the symmetric vortex, except that the size must be at least 170 km. Mathur uses an empirical vertical structure function to represent the cyclonic portion of the vortex. The anticyclonic portion aloft is assumed to be represented in the global model background fields, or will be developed during the integration. A gradient wind is calculated, but no secondary circulation or initial vertical motion is imposed as an initial condition. A relative humidity of almost 100% is specified near the center to trigger convective latent heat release quickly.

In the BMRC model, both the symmetric and asymmetric circulation are represented by synthetic observations. However, these observations are then combined with surrounding observations in the objective analysis step, presumably with high weighting values to ensure that the analysis tends to closely fit these synthetic observations. However, the horizontal grid size of 100 km (Table 2a) will not allow much detail of the vortex structure to be captured. In this case, the mass field is derived from the wind field using the balance equation. The main focus of Davidson and Puri (1992b) is the nudging assimilation technique (see discussion in Section 2b.4 above) to make the observations consistent with the model equations. During the assimilation, the heating from the Kuo scheme is replaced with a heating function determined from satellite-observed cloud-top temperatures each 6 h. This nudging process defines a vertical motion field that is consistent with the satellite cloud imagery and enhances rainfall rates during the early hours of the forecast, which improves retention of the cyclone circulation during the 48-h integration.

Peng *et al.* (1993a, b) use the "spin-up vortex" approach to ensure that the symmetric vortex is consistent with the numerical model resolution and physics. In this approach, a

two-dimensional version of the model on an *f*-plane is integrated to near-steady state for a representative sea-surface temperature and an environmental thermodynamic profile. Peng *et al.* define three categories of vortices (strong, weak and large, or weak and small) that are pre-integrated, and the duty forecaster selects the catalogued vortex that most closely matches the present storm. Peng *et al.* (1993b) indicate more than three vortices will need to made available in the future to better match actual storms.

The third important step is to specify the initial conditions in such a manner as to get the tropical cyclone moving in the correct direction and speed. Considerable success has been achieved in this regard with operational barotropic models (Section 2a.1) and with research barotropic models (Section 2b.2), and especially with developing procedures for including the asymmetric circulation. Iwasaki *et al.* (1987) include the pre-processing option used in barotropic models (Table 1) of replacing the background flow pattern with the desired initial motion vector and superposing the symmetric vortex. This vortex is blended with background field in the outer region. The generalized dipole that Mathur and Shapiro (1992) insert in the QLM has been described in Section 2b.2 (see example in Fig. 10). The combination of the symmetric vortex and the dipole asymmetric circulation is blended with the background field from the global model over an annular ring that is dependent on the size of the storm. In 1989 and 1990, the spinup vortex in the Taiwan model was superposed on the background field from the global model. Peng (1993a) showed that the poorer forecasts during this early period were frequently due to a poor initial storm direction. Peng (1993b) reported improved predictions when the past typhoon movement vector was inserted in the region of the storm. In addition, a prototype wavenumber one asymmetry based on the previous motion (analogous to the Mathur approach) was also tested and found to improve the predictions. The combination of the past typhoon movement vector and the wavenumber one asymmetry was implemented in the Taiwan system prior to the 1991 typhoon season.

b. Utility of operational models

Some track error statistics that have been provided for the operational models in Table 2 are presented here as an illustration of their present capabilities. Ueno (1991) summarized the performance of the typhoon (TYM) model and the Asian Spectral Model (ASM) and Global Spectral Model (GSM) of the Japan Meteorological Agency during 1990 (Fig. 15). A total of 373 TYM forecasts that were produced for typhoons and tropical depressions were compared with a persistence (PER) forecast (linear extrapolation of past motion) whenever the verifying storm intensity was tropical storm or greater. The relative error is defined as

$$\text{Relative Error (\%)} = 100 \times \frac{\text{PER error - TYM error}}{\text{PER error + TYM error}}$$

A positive value indicates an improvement of the track forecast by the dynamical model over persistence. As shown in Fig. 15, the TYM does not have skill relative to persistence until after 24 h except for storms after recurvature. Then TYM has skill through 60 h, especially for storms after recurvature, where the improvement is about 40%. Although the TYM has the smallest forecast errors at 24 h, the ASM is slightly (12 km) better at 48 h, when both of these models are considerably better than the GSM. The performance of TYM and the other dynamical models has contributed (H. Ohnishi, personal communication) to the improvement in the official forecasts by the Regional Specialized Meteorological Center (RSMC) Tokyo Typhoon Center in recent years (Fig. 16).

The performance of the QLM during 1989 and 1990 is shown in Figs. 2 and 3 in relation to VICBAR. A homogeneous summary of track errors during the 1990 Atlantic hurricane season is shown in Table 3. A large number of the hurricanes during this season were in the central Atlantic. All of the techniques had 12-h errors only slightly larger than the official errors. The statistical-dynamical model (NHC 90) was better than official errors at 24 h, but had larger errors at 48 h and 72 h. The QLM had the smallest error growth with time and had only 233 n mi errors at 72 h. In addition to skill relative to

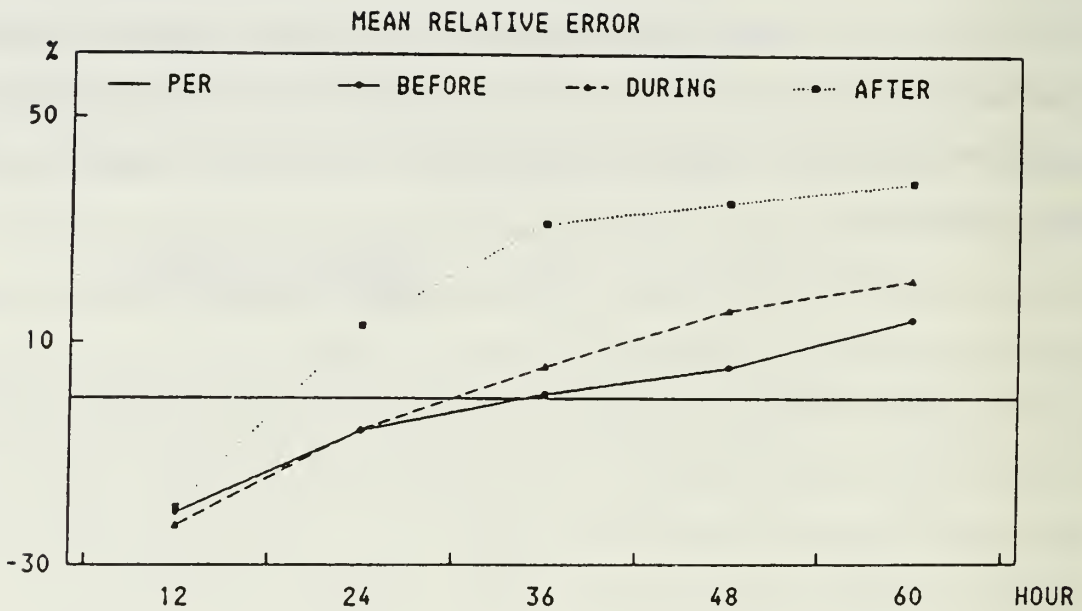


Comparison of track forecast errors of the TYM, ASM and GSM in km

| MODEL | T = 12 | T = 24 | T = 36 | T = 48 |
|---|---|---|---|---|
| TYM | 92 (186) | 165 (186) | 235 (186) | 315 (186) |
| ASM | 126 (186) | 185 (186) | 236 (186) | 303 (186) |
| GSM | 141 (186) | 217 (186) | 292 (186) | 372 (186) |
| PER | 58 (186) | 168 (186) | 314 (186) | 497 (186) |

Fig. 15 (Top) Mean relative track error for Typhoon Model (TYM) before, during and after recurvature for 1990 season. Homogeneous sample (N = 186) of track errors (km) for TYM, Asian Spectral Model (ASM) and Global Spectral Model (GSM) forecasts during 1990 (Ueno 1991).

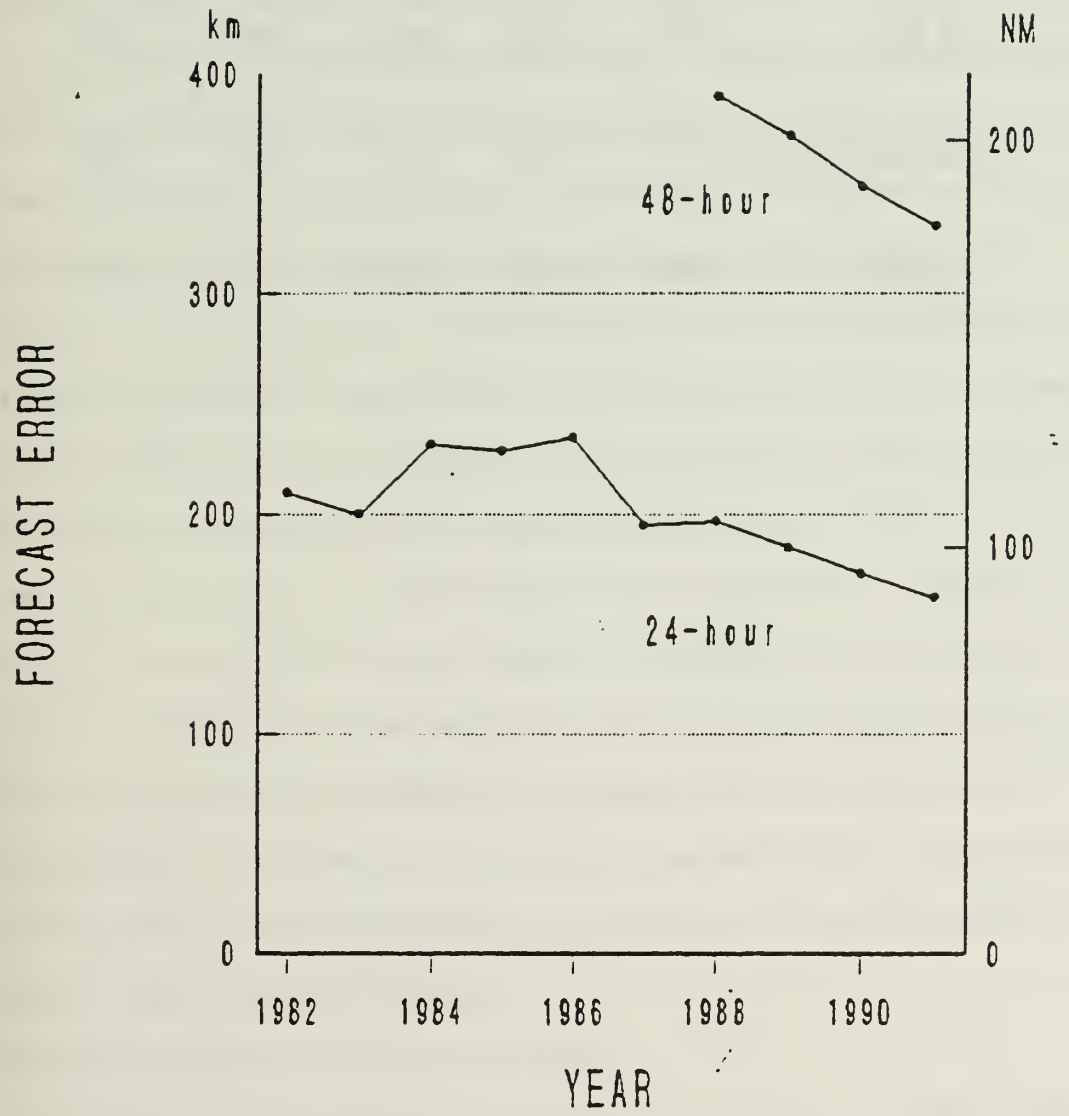


Fig. 16 Annual mean official track forecast errors at 24 h and 48 h since 1988 for the Regional Specialized Meteorological Center Tokyo Typhoon Center (H. Ohnishi, personal communication).

Table 3 Homogeneous comparison of the QLM track errors (n mi) with the other objective track aids and the official NHC forecasts during the 1990 Atlantic hurricane season (provided by Dr. M. Mathur).

| MODEL | 12H | 24H | 36H | 48 | 72H |
|---|---|---|---|---|---|
| CLIPER | 62 | 121 | 193 | 256 | 411 |
| NHC90 | 58 | 98 | 157 | 214 | 358 |
| QLM | 63 | 105 | 143 | 169 | 233 |
| OFFICIAL | 57 | 107 | 156 | 201 | 321 |
| CASES | (111) | (101) | (88) | (77) | (56) |

CLIPER, these 72-h errors were considerably smaller than the official forecast errors for the same cases.

Davidson and Puri (1993b) describe individual cases in which the BMRC nudging initialization procedure improved the initial representation of tropical cyclones. One of the cases illustrated a correct forecast of a storm that slowed down as it approached the northeast coast of Australia, and then recurved parallel to the coast. Evidently, the diabatic nudging procedure contributed to the correct forecast of recurvature and direction change events. As indicated previously, another objective for the BMRC model is to improve precipitation forecasts in the tropical region. The use of nudging to adjust the model vertical motion fields to the satellite cloud imagery enhances and more accurately depicts the rainfall during the early hours of the forecast, and improves the mass-wind balance so that the cyclone circulations are retained better during the integration.

Peng *et al.* (1993a) compared the performance of the Taiwan Typhoon Forecast System (TFS) with CLIPER during the development test period and the first operational system during 1990 (Table 4a). In both cases, the TFS did not have skill relative to CLIPER at 48 h, primarily due to the large directional errors. When the past motion vector was incorporated and a wavenumber one asymmetry was included, the TFS performance for selected cases from 1990 was markedly improved (Table 4b). By redirecting the model forecast along the initial motion vector, the TFS accuracy during the first 12-24 h was improved about 30%, and the positive effect continued through 48 h with a 26% improvement. As has been found with other dynamical models, incorporation of the initial motion reduces a major shortcoming and makes the Taiwan dynamical model fully competitive with other forecast techniques.

c. Research applications of baroclinic models

The objective in this section is to present two examples of highly sophisticated baroclinic models applied to the prediction of tropical cyclones. In the case of the Meteorological Research Institute (MRI) model, a triply-nested grid of high

Table 4 (a) Homogeneous comparison of the 48-h forecast errors (km) of the Typhoon Forecast System (TFS) of Taiwan versus CLIPER during the pre-1990 test period and the operational 1990 seasons (Peng *et al.* 1993a).

| | Sample size | CLIPER error | TFS error | Relative error % |
|---|---|---|---|---|
| Pre-1990 | 54 | 350 | 412 | - 7% |
| 1990 | 60 | 315 | 395 | -10% |

(b) Tests of the effect of including past motion vector and wavenumber one asymmetry in the bogus vortex for selected 1990 TFS track forecasts (Peng *et al.* 1993b).

| | 12 h | 24 h | 36 h | 48 h |
|---|---|---|---|---|
| Control | 143 | 241 | 346 | 474 |
| Test | 102 | 160 | 243 | 351 |
| Improvement | 29% | 34% | 30% | 29% |

resolution, and an explicit prediction of cloud water and rain water, are the highlights. In the limited test by Yamasaki (1992), selected cases from the TCM-90 period were simulated, but only using the operationally-analyzed fields rather than the full TCM-90 data set. The Geophysical Fluid Dynamics Laboratory (GFDL) model has been extensively expanded and tested for near real-time application (Kurihara *et al.* 1992; Bender *et al.* 1993; Kurihara *et al.* 1993a). The initialization scheme for specifying the vortex is described by Kurihara *et al.* (1993b), and the asymmetric component of that vortex specification is given in Ross and Kurihara (1982). These two advanced research models are likely forerunners of the operational baroclinic models of the future as they include high resolution necessary for tropical cyclones, advanced physical process representations, and specialized treatments of the initial conditions.

(1) Meteorological Research Institute model. Yamasaki (1986, 1987) has previously used the triply-nested MRI model to study the effect of the explicit predictions of cloud water and rain water on tropical cyclone formation. Numerical characteristics of the model are summarized at the bottom of Table 2a for ease of comparison with the operational models. A key feature is the 5/12 deg. lat. and long. horizontal resolution on a 25° lat. by 30° long. inner nest. The intermediate grid with 1.25 deg. resolution is also large, and the outer grid is from 30°S to the North Pole. With such a large horizontal domain, the boundaries are far removed from the center of the grid where the tropical cyclone is located.

The primary focus in the MRI model is the treatment of physical processes, which is quite different from the Kuo scheme of the operational models (Table 2b). Yamasaki (1986, 1987) has shown that the evaporation of rain water is a key factor in representing the latent heat release distribution in developing tropical cyclones. Yamasaki (1992) indicates future research will address the impact of physical processes on tropical cyclone motion.

Yamasaki (1992) used a simple tropical cyclone bogus to represent the tropical cyclone in the model (Table 2c). Because Yamasaki was using the operational analyses of

the Japan Meteorological Agency that already contain a tropical cyclone bogus (Ueno 1991), he found that inclusion of a bogus vortex did not impact the forecasts. He did not include the pre-processing procedure of inserting the past motion, which is an option in the Iwasaki *et al.* (1987) model.

Thus, the purpose of this first test with the MRI model was to evaluate its performance with operationally analyzed fields as a benchmark. Yamasaki (1992) describes 20 individual cases for eight typhoons during August-September 1990. Only one example (Fig. 17) is given here to illustrate a common problem and some notable successes found in this test. Typhoon Winona (T9011) had an unusual track toward the southeast and then a sharp turn to the north. The analysis at 00 UTC 7 August (Fig. 17) indicated that Tropical Depression Winona was to the southwest of Typhoon Vernon at the initial time. During the next 48 h, Vernon moved eastward and became a trough in the midlatitude westerlies. Notice the intensification of the subtropical high cell to the east of Winona at 00 UTC 9 August, which was a primary reason for the poleward deflection of Winona. The model integration from 00 UTC 7 August did not forecast the behavior of the subtropical high well (not shown). Although the model track turned northward, the turn occurred too far eastward and was delayed one day. However, the track prediction from 00 UTC 8 August was quite good during the first 36 h. The analysis on the fine grid and the 24 h forecast indicate the amplification and northwestward extension of the subtropical high to the east of Winona were predicted quite well. After 24 h, the model track was too slow. Although the landfall point was slightly to the east of the actual path, the predicted timing of the landfall was 14 h too late.

Yamasaki (1992) shows other examples of excellent forecasts and some marked failures. He concludes that these forecast errors are primarily due to the prediction of the subtropical high and to errors in the initial wind and conditional instability fields. Future tests with the complete TCM-90 data set may illustrate the impact of the data. The sensitivity to the initial conditional instability fields probably reflects the need for special

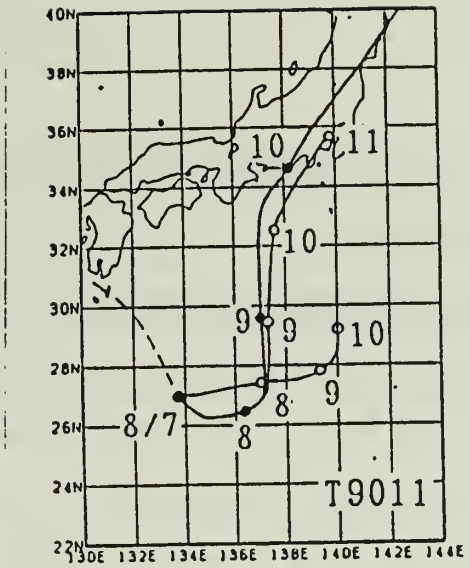


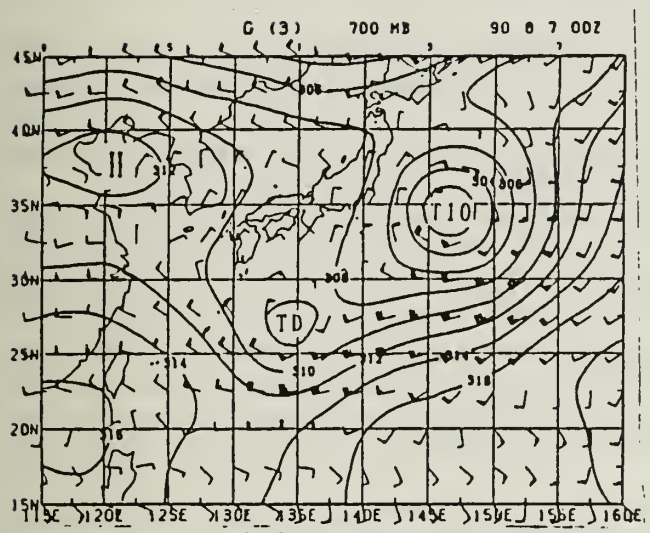


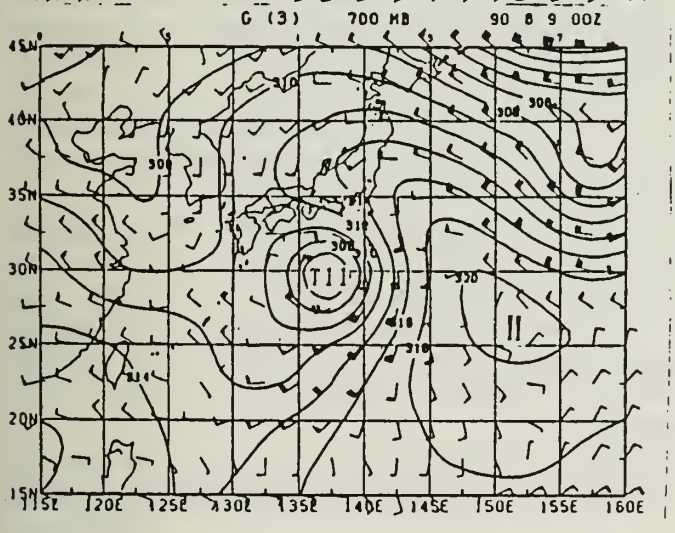


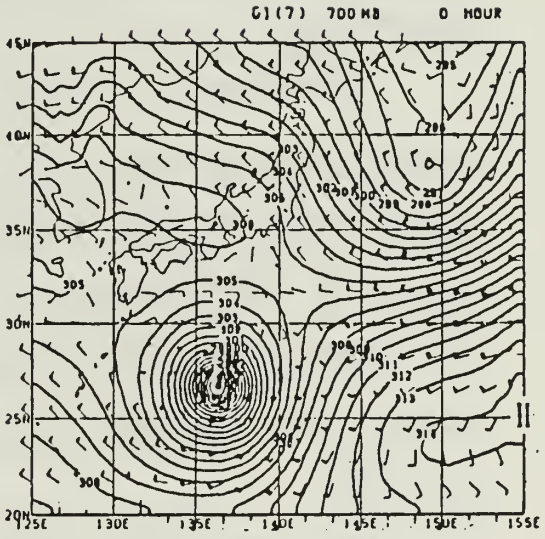


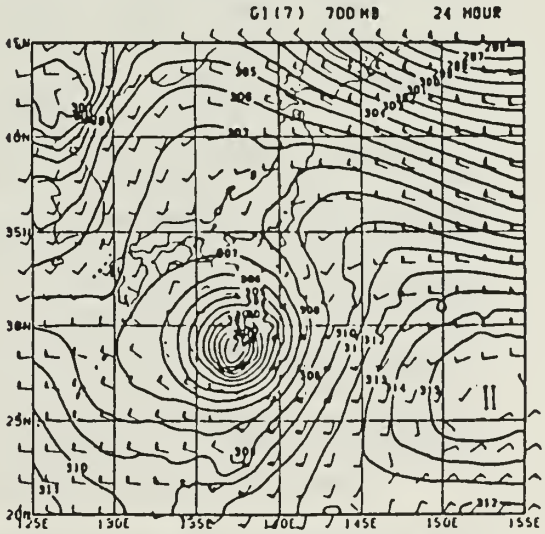


Fig. 17 (Top) Best track (dashed and thick solid) from 7 August to 10 August 1990 for Typhoon Winona and 72-h forecasts by MRI model (Yamasaki 1992) from 00 UTC 7 August and 00 UTC 8 August (thin solid lines). (Left) Analyzed wind and height fields at 700 mb for 00 UTC 7 August (top) and 00 UTC 9 August (bottom). (Right) Initial analysis (top) and 24-h forecast (bottom) from 00 UTC 8 August.

tuning to be compatible with the sophisticated moisture treatment in this model. Future testing should also improve this aspect.

(2) Geophysical Fluid Dynamics Laboratory model. Kurihara *et al.* (1990) had tested the GFDL multiply-nested model with real data for Hurricane Gloria. In addition to producing some excellent track forecasts, the model appeared to correctly predict some aspects of the hurricane intensification and wind structure on the high-resolution grid. This led to an effort to produce an automated hurricane prediction system at GFDL (Kurihara *et al.* 1993a).

As indicated at the bottom of Table 2a, the triply-nested model has much better resolution than the operational models. Both the inner grid of 1/6 deg. resolution and the intermediate grid of 1/3 deg. resolution move with the storm center to maintain high resolution. The coarse grid of 1 deg. resolution extends over 75° lat. and long., with horizontal boundary values updated from the global model. With the domain boundaries removed so far from the hurricane, the impact on the solution due to these boundary values is reduced.

The GFDL model also has the most sophisticated representation of physical processes (Table 2b). Perhaps the only weakness in the model is the use of convective adjustment to parameterize the convection in a tropical cyclone on a horizontal resolution of about 18 km. However, the other physical processes representations are very advanced, including land processes that take into account the vegetation cover. In summary, this model has physical processes representations comparable to the most advanced general circulation or operational global prediction models.

The GFDL group has devoted special efforts to specifying the initial conditions for the hurricane in the model (Kurihara *et al.* 1993a; Ross and Kurihara 1992). In their method, a crudely resolved tropical cyclone in the NMC global analysis is replaced with a vortex that is properly specified for use in the GFDL prediction model (Table 2c). Appropriate filters are first used to remove the vortex from the global analysis so that a

smooth environmental field that represents the steering remains. The GFDL bogus vortex consists of both symmetric and asymmetric components. The symmetric component is generated by a time integration of a two-dimensional version of the complete model so that the initial vortex will be dynamically and thermodynamically compatible with the resolution and physics of the model. During this integration, the tangential wind component is gradually forced toward a target wind profile specified from available observations of the individual hurricane. This procedure ensures more realism than selecting the best match from a catalogue of previously-integrated spinup vortices as in the Taiwan approach (Table 2c).

Another key step in the GFDL procedure (Ross and Kurihara 1992) is to generate an asymmetric wind field by time integration of a simplified barotropic vorticity equation including the beta effect (see Section 2b.2). This procedure does not include the effects of relative vorticity gradients and linear shear of the environment that have been found to be important in barotropic models (see review by Elsberry and Abbey 1991). However, it does produce an asymmetric circulation on a beta plane that is specifically tailored to the symmetric vortex structure, so that differences between large storms and small storms are included. The asymmetric component is assumed to be uniform in elevation.

The combination of the symmetric and asymmetric components of the vortex are added to the filtered environmental flow from the global analysis and merged into the larger scale fields from the global analysis. Imbalances between the mass and wind fields are removed by solving for the mass field from a divergence equation. Thus, no period of initial adjustment or false spinup of the model vortex occurs as in previous dynamical models.

Bender *et al.* (1993) tested the new initialization scheme with three cases from Hurricane Gloria and one case from Hurricane Gilbert. The differences between the analyzed vortex in the NMC global analysis for Gilbert and the specified vortex are shown in Fig. 18. Rather than having a 30 m $s^{-1}$ maximum wind hundreds of kilometers to the

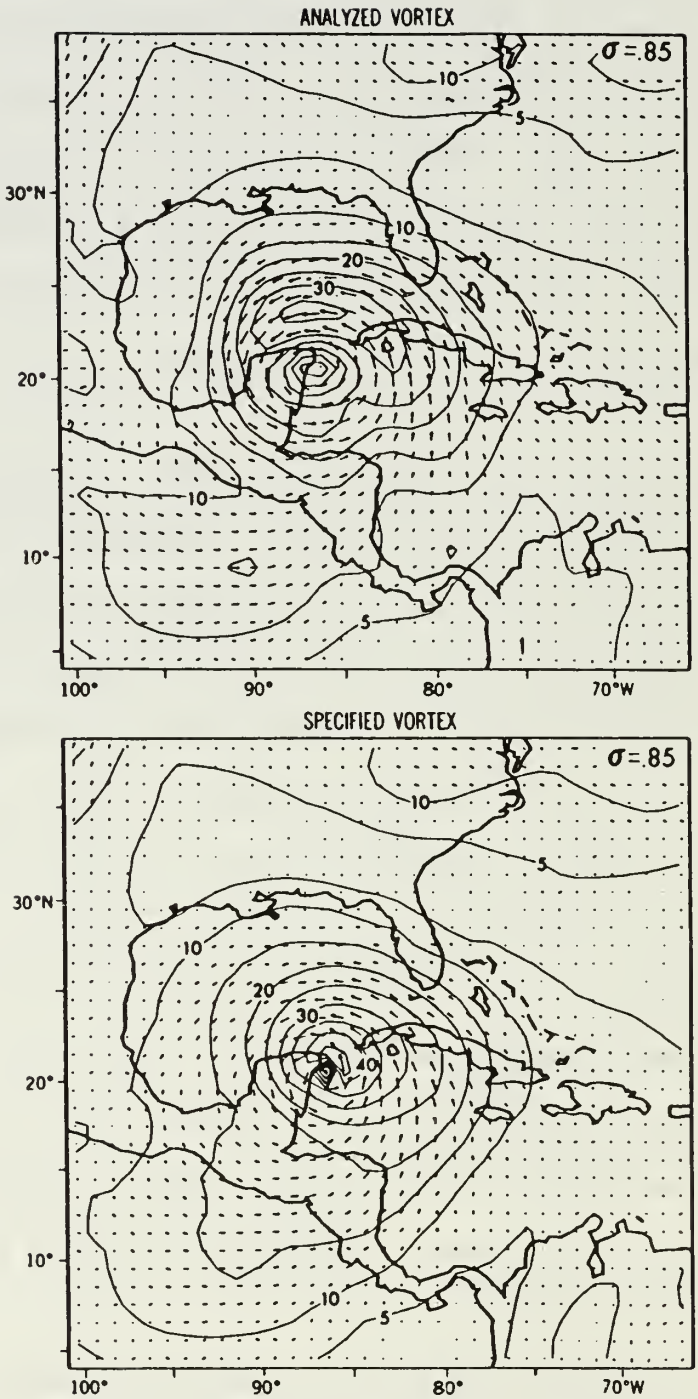


Fig. 18 Analyzed wind and isotachs (m $s^{-1}$) from NMC global analyses (top) and specified vortex after application of GFDL initialization scheme for Hurricane Gilbert (Bender *et al.* 1993).

north of the storm, winds exceeding 50 m $s^{-1}$ are analyzed adjacent to the correct center position. With these more realistic initial conditions, storm intensity and structure predictions can be considered. Bender *et al.* illustrate that the intensity trends in these four cases were predicted by the model. Where the track of Gloria was well forecast along the east coast of the U.S., the distribution of maximum low-level winds observed at gridpoints during the passage was predicted rather well (Fig. 19). Although the asymmetry in the wind distribution was reproduced to a first order in the forecast starting with the global analysis, the agreement with observations was much better with the specified vortex due to the more realistic radius of maximum wind and storm intensity.

Bender *et al.* (1993) demonstrated that the new initial condition specification eliminated the erratic initial storm motion found in prior integrations of the GFDL model. Dramatic improvements in track forecasts were found in the first 48 h. Track predictions to 72 h for one of the Gloria cases are shown in Fig. 20. Whereas the track from the NMC global analyses (G22N) starts from an incorrect position and has an erratic initial track, the new initial condition specification starts the storm at the correct position and has a smooth track with almost the correct direction. The other three test cases had similar improvements. Using the new scheme, the average 24-h and 48-h forecast errors for the four test cases were 58 and 94 km, whereas the non-initialized forecasts starting from the global analyses were 143 km and 191 km. Since the corresponding National Hurricane Center official forecast errors were 118 km and 212 km for these four cases, the GFDL model with the new initial condition specification appeared to have promise for accurate track prediction.

Kurihara *et al.* (1993b) describe some near-real time predictions after automation of the GFDL procedures. Note that the initial condition specification and the integration of the triply-nested model requires about 6 h of computer time, which results in the delayed provision of the forecasts. Track errors for seven test cases are shown in Fig. 21,

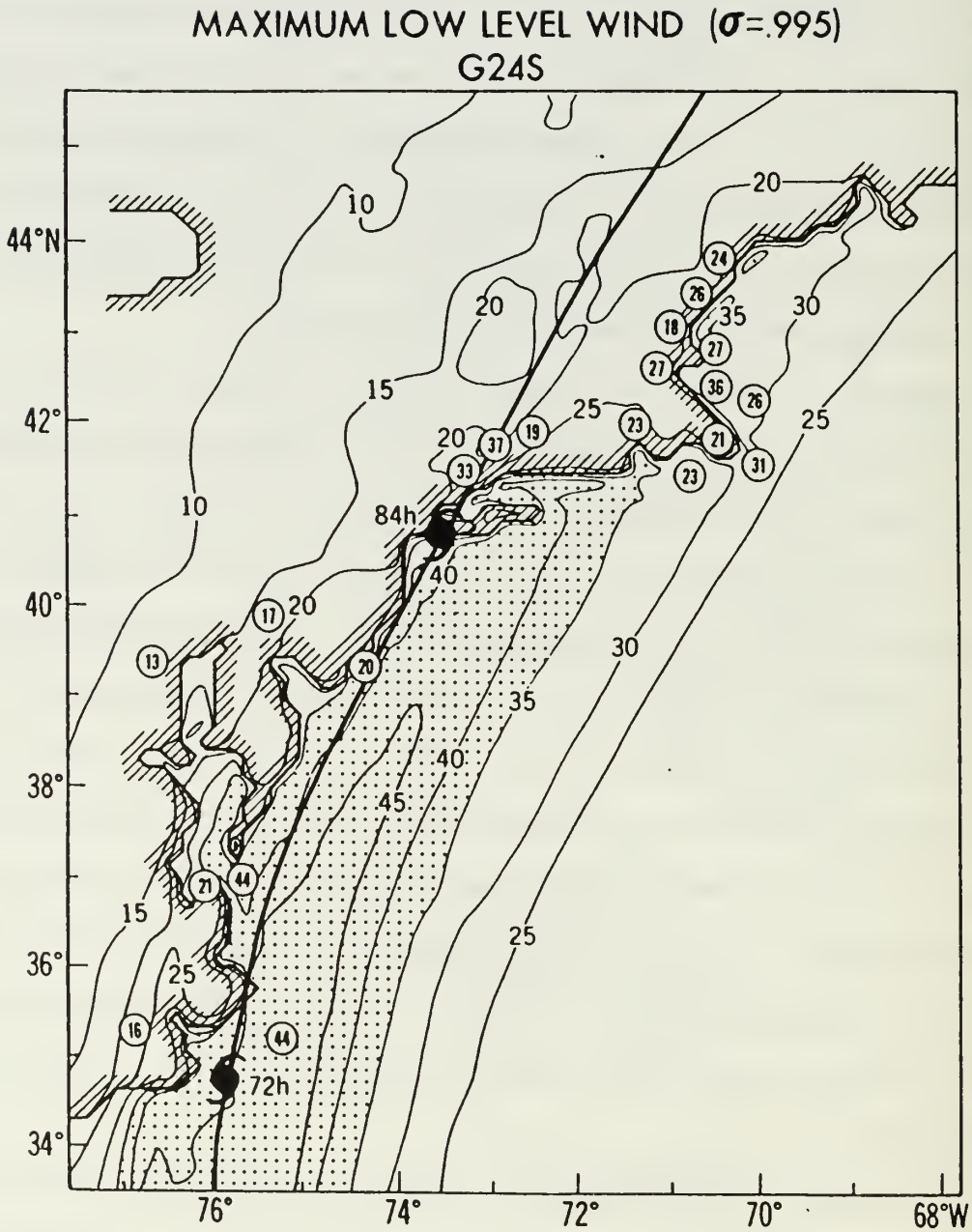


Fig. 19 Maximum wind speed (m $s^{-1}$) at $\sigma$ = 0.995 predicted by the GFDL model (Bender *et al.* 1993) for a test with Hurricane Gloria and station observations (circled). The predicted track is shown by the heavy solid line with hurricane symbols at the predicted 72 h and 84 h positions.

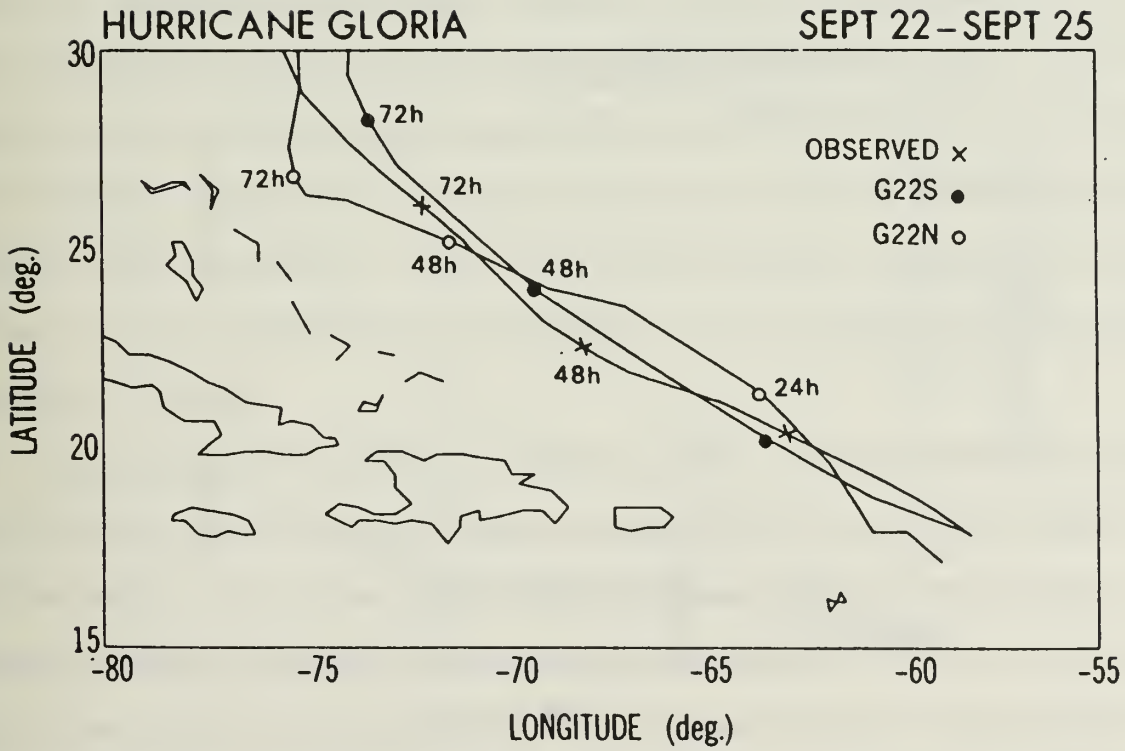


Fig. 20 Observed positions (X) at 00 UTC 22 September 1985 and 24-, 48-, and 72-h forecasts of the GFDL model (Bender *et al.* 1993) from the NMC global analyses (open circles) and from the GFDL initial condition specification (solid circles).

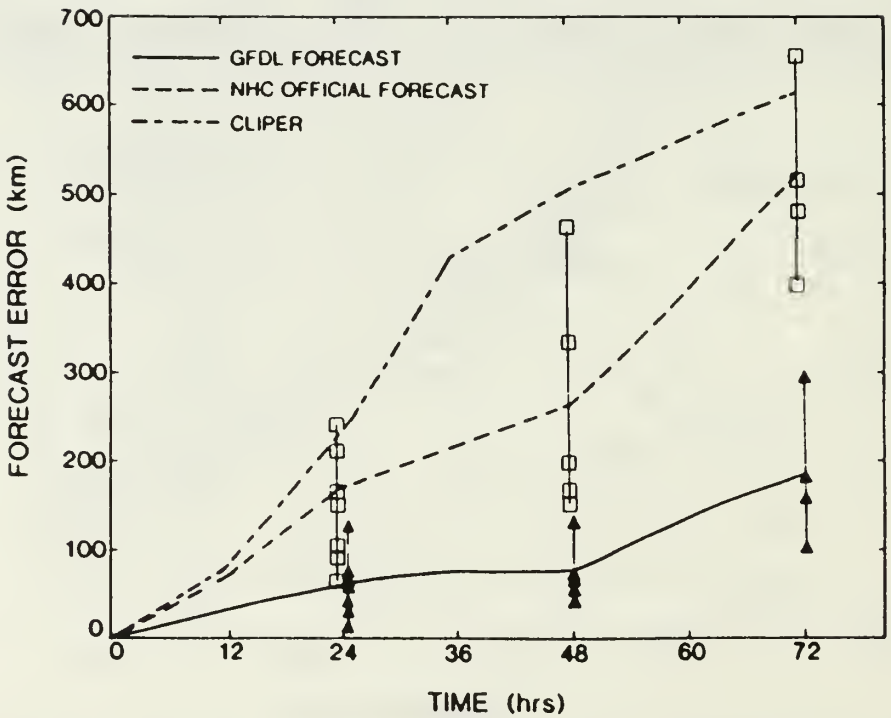


Fig. 21 Track errors (km) from the GFDL model (triangles and solid line), National Hurricane Center official forecasts (boxes and dashed line), and the CLIPER prediction (dash-dotted line) for seven test cases (Bender *et al.* 1993).

which includes the spread of the GFDL model and NHC forecasts about their mean values. The GFDL model has skill relative to CLIPER throughout the 24-72 h period. Although only four of these seven cases could be verified at 72 h, the rate of error growth in the GFDL model is very small. Reduction of errors in the later period are attributed to accurate prediction of the large-scale flow.

In summary, the advanced versions of the limited-region baroclinic models appear to promise future improvements in track prediction and trends in intensity. Additional cases of real-time predictions are required to demonstrate this potential.

## 4. Global baroclinic models

At the time of the Elsberry (1987) review, the possibilities of tropical cyclone forecasts within the global models was only beginning to be explored. Bengtsson *et al.* (1982) had found that the European Centre for Medium-range Weather Forecasts (ECMWF) operational model was able to simulate tropical cyclones with a frequency and distribution resembling observations. However, individual tropical cyclones were not forecast well by the ECMWF model with a horizontal resolution of 1.875° lat. by 1.875° long. After the higher resolution, triangular (T) 106 waves model was introduced, Heckley *et al.* (1987) and Chan and Lam (1989) examined specific cases in which the skill of the ECMWF model seemed to be improved. A tropical cyclone forecast error may later become an important contribution to midlatitude errors in the global models on medium time scales (5-10 days).

The objective of this section is to present a similar description of the characteristics and utility of the global baroclinic models as was given in Section 3 for the limited-region baroclinic models. Since these global models have such complex representations of the physical processes, a complete discussion is beyond the scope of this review. Suffice it to say that these global models include all of the physical processes of the limited-region baroclinic models in Table 2b. Miller (1992) indicates that increasingly complex representations of the physical processes (and other improvements) have substantially

reduced the systematic errors in the ECMWF model. For example, the time periods for which 850 mb winds forecasts are "useful" has increased from about 2.5 days in 1989 to about 4.5 days in 1991 (Fig. 22). Notice that this measure of the wind forecast accuracy indicates the longest useful forecasts are during the NH summer, with a secondary maximum during SH summer. Since the mean flow errors are smaller, the environmental flow that advects the tropical cyclone is better represented. This improvement, plus the absence of horizontal domain boundaries as in the limited-region models, are expected to be the two primary advantages of the global model for tropical cyclone forecasting. The key differences among the global models are in the specification of the initial conditions. Although the ECMWF inserts no synthetic observations, all of the other global model centers include some specification of the tropical cyclone position and structure. Some limited statistics will be presented to illustrate the performance of the global models for tropical cyclone track forecasting.

a. Characteristics of the global models

(1) Numerical characteristics. Global forecast models have been greatly improved since the early 1980's, e.g., horizontal and vertical resolution have been improved (Table 5a). During September 1991, a ECMWF model was implemented with T213 waves horizontal resolution and 31 (previously 19) vertical levels. Although the horizontal resolution of the physics grid of the T213 model is about 65 km, the effective grid length is probably about 100 km (Miller 1992).

The Japan Meteorological Agency (JMA) Global Spectral Model has a triangular T106 horizontal resolution and 21 levels in the vertical. Thus, the grid on which the physical processes are calculated is about 130 km (twice that of the ECMWF).

Only the United Kingdom Meteorological Office (UKMO) is using a grid point (rather than a spectral) representation in the horizontal. Since June 1991, the horizontal grid is $5/6^{o}$ lat. and $125^{o}$ long., which is roughly comparable to the JMA model. The 20 levels in the vertical are also similar to JMA, but much less than the ECMWF.

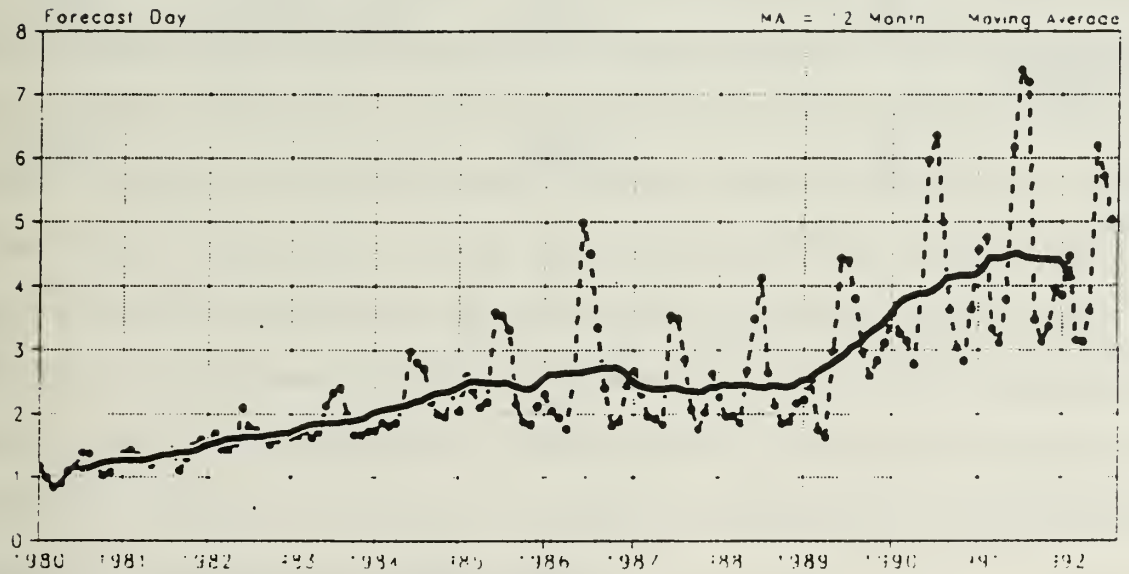


Fig. 22 Usefulness of ECMWF 850 mb vector wind forecasts between 20°S and 20°N in terms of the length of forecast interval for which the absolute correlation with the analyzed winds exceeds a threshold value of 70. The solid line is a 12-month running average of the monthly mean values indicated by the dashed line (Miller 1992).

Table 5a Characteristics of selected operational and research global baroclinic models for tropical cyclone track prediction. Part 1. Numerical characteristics.

| | Vertical Layers | Horiz Grid | Time Integration | Physics Grid |
|---|---|---|---|---|
| | | OPERATIONAL | | |
| ECMWF Miller (1992) | 31 | T213 | Semi-Lagrangian | 65 km |
| JMA | 21 | T106 | ? | 130 km |
| UKMO | 20 | 5/6° lat. 5/4° long. | ? | 5/6° lat. 5/4° long. |
| FNOC Goerss & Jeffries (1993) | 18 | T79 | Semi-implicit | 1.5° lat. |
| U.S. NMC | 18 | T126 | ? | 105 km |
| | | RESEARCH | | |
| FSU Krishnamurti *et al.* (1993) | 12 | T170 | Semi-implicit | 80 km |
| JMA Iwasaki (1991) | 21 | T213 | ? | 65 km |

The most coarse resolution model is the T79 spectral model of the U. S. Navy Fleet Numerical Oceanography Center (expected to increase to T126 or T160 during 1993). Thus, the physics are calculated on a 1.5° lat. by 1.5° long. grid, and at 18 levels in the vertical.

The final operational model in Table 5a is the National Meteorological Center, which has used a T126 and 18-level global model since March 1991.

In summary, most of the global models had (or will have in the case of FNOC) a significant increase in horizontal resolution since 1991. Thus, each model has become more capable of resolving the outer circulation of tropical cyclones. As indicated in the introduction to this section, the advanced physics packages in these global models will not be intercompared. However, the procedures to insert a representative tropical cyclone circulation will be discussed.

(2) Specification of initial conditions. Although the ECMWF researchers Andersson and Hollingsworth (1988) were one of the first groups to study methods of inserting synthetic observations to represent tropical cyclones, the ECMWF does not allow such observations (Table 5b). As a consequence, the only representation of the tropical cyclone circulation in the EMCWF initial conditions comes from the first-guess (prior 6-h forecast) and any observations. It is then crucial that the ECMWF forecast model develop tropical cyclone-like circulations at the correct time and location. In the western Pacific where there are more storms and more observations (especially low-level cloud-drift winds from the geostationary satellite), the ECMWF system does generate a tropical cyclone circulation at roughly the correct time, although not necessarily at the correct location. Typical initial position errors are about 200 km.

The JMA was one of the first to insert synthetic observations into their global model. Ueno and Ohnogi (1992) describe the changes in the operational bogussing method implemented during September 1991 and its impact on the JMA Global Spectral Model (GSM). The basic approach of specifying representative observations based on the

Table 5b. As in Table 5a, except Part 2. Specification of initial conditions.

| | Specification of TC | Size Dependence | Derived Quantity | Secondary Circulation | Insertion Stage | Initial Motion | Merging TC | Merging Blend Zone |
|---|---|---|---|---|---|---|---|---|
| | | | | OPERATIONAL | | | | |
| ECMWF | None | N/A | N/A | N/A | N/A | N/A | N/A | N/A |
| JMA<br>Ueno & Ohnogi | Empirical surface p | Radius of 15 m $s^{-1}$ | Gradient wind balance | ? | Analysis synthetic obs | No | Syn obs | Size dependent |
| UKMO<br>Hall (1987) | Center position | No | Mass | No | Analysis synthetic obs | No | Four syn obs | No |
| FNOC<br>Goerss & Jeffries (1993) | Empirical Rankine vortex (truncated) | 30 kt 50 kt wind radii | Mass | No | Analysis synthetic obs | No T20 background flow | 13 syn obs | 660 km (440 km if smaller storm) |
| U.S. NMC<br>Lord (1991) | Empirical surface p | Radii of 15 m $s^{-1}$ | Wind | No | Two-step analysis | Selected spectral background flow | Syn obs | Size dependent |
| | | | | RESEARCH | | | | |
| FSU<br>Krishnamurti (1993) | None | N/A | N/A | Yes | Physical initialization | No | N/A | |
| JMA<br>Iwasaki (1991) | (As in the operational JMA model above) | | | | | | | |

surface pressure profile of Fujita (1952) is similar to that used for their limited-region baroclinic model (Table 2c). The size of the storm (radius of gale-force winds) is taken into account in the surface pressure profile and in determining the number of synthetic observations to be inserted. More observations are inserted as necessary to keep the observation density uniform in space. Since Ueno and Ohnogi do not mention the use of the initial motion of the storm, their procedure for the global model appears to add synthetic observations that represent only the symmetric vortex. That is, these synthetic observations do not include either the asymmetries due to the background flow or the asymmetric circulation (Table 2c). Notice that the synthetic observations become part of the data set provided to the four-dimensional assimilation procedure. Although they are blended with real observations that represent the large-scale environmental flow, the number and distribution of these observations may or may not be sufficient to get the model storm moving in the correct direction and speed.

A recent report on the tropical cyclone bogussing procedures at UKMO is not available since Hall (1987). At that time, a very limited bogus was used primarily to re-position the tropical cyclone via insertion of winds near the center (Table 5b). This procedure was applied at the discretion of the quality control specialist.

The Fleet Numerical Oceanography Center (FNOC) began inserting synthetic observations in their global model during 1990 (Fiorino *et al.* 1993; Goerss and Jeffries 1993). The symmetric vortex is a Rankine vortex in which the exponent is specified to fit the observed maximum wind speed and the radii of 30 kt and 50 kt winds (if available). Synthetic height and wind soundings up to 400 mb are generated at 13 points: one at the storm center; four points located at 220 km north, south, east and west; four points 440 km to the northeast, northwest, southwest and southeast; and four points at 660 km to the north, south, east and west. The Rankine wind profile is truncated by reducing the 440 km values by 20% and the 660 km values by 40%. An asymmetry due to the background flow is added by interpolating a spectrally truncated (T20) wind field to the locations of the

13 synthetic observations. However, no wavenumber one gyres are inserted to represent the asymmetric circulation as in the barotropic models (Section 2b.2; Table 2c). The synthetic observations bypass the quality control checks and are assimilated into the initial fields for the global model by the multi-variate optimum interpolation analysis, with the assumption that they have the same error properties (weighting factors) as rawinsondes.

Lord (1991) described the bogussing system for the U.S. NMC (Table 5b), which uses the position and structure information transmitted from the tropical cyclone warning centers. The symmetric vortex is patterned after the Mathur (1991) and Mathur and Shapiro (1992) approach (Table 2c). This symmetric vortex is superposed on the spectrally truncated layer-mean wind field that is closest to the observed storm motion. This steering flow and vortex are combined and offered to the global model analysis in the form of rawinsonde observations of wind at mandatory levels up to 300 mb. In the second analysis pass, the horizontal correlation length scale is reduced from 500 km to 200 km so that the fit to the winds is more confined locally and more curvature is allowed.

In summary, all of the global model centers except ECMWF insert synthetic observations to at least define the position of the tropical cyclone. In most cases, the observations are adapted to the present storm intensity and size, at least to the extent that the horizontal resolution of the model permits. The FNOC and NMC superpose the synthetic vortex on a spectrally truncated background flow interpolated to the location of the synthetic observations. The NMC approach is the only one that uses the observed storm motion (through the selection of the closest background flow). All the centers add the synthetic observations to the analysis scheme, which blends these observations with actual observations in and around the tropical cyclones to provide the initial conditions for the global model.

b. Utility of global models. As indicated above, the global models have recently been improved considerably. Thus, long-term statistics on tropical cyclone track forecasts with a stable form of the model(s) are not available. A number of individual studies will be

reviewed here to indicate the relative accuracy of global model track forecasts.

(1) Tracking the center. One of the difficulties in intercomparing the global models is the lack of a standard, automated method for tracking the tropical cyclone in the global models. Studies such as Chan and Lam (1989) and an intercomparison by Muroi and Sato (1992) reconstructed the storm centers from 2.5° lat. and long. archived fields. Goerss and Jeffries (1993) had to revert to a manual analysis of center locations for the 1991 forecasts of the FNOC global model because their automated tracking system would occasionally begin to follow another feature. Muroi and Sato (1992) only had 12-h (24 h for UKMO) maps to trace the centers. Thus, they had to select the minimum sea-level pressure center within a 500 km radius circle from the typhoon pressure center, even though this center may not have time continuity with other positions. They suggest that each global model center develop an automated tracking routine that best represents the tropical cyclone circulation in time, and transmit these positions in an electronically readable format.

Lord (1991) describes an automated tracking algorithm for multi-level models. His algorithm traces six features: minimum wind speed, maximum relative vorticity and minimum geopotential height at 850 and 1000 mb. A simple linear programming algorithm is used to determine locations of extrema in the neighborhood of a guess position. The guess position is defined by the observed position at the initial time, by the extrapolated position using the observed initial motion vector at the first forecast time, and by linear extrapolation from preceding forecast positions at the second and succeeding forecast times. The final position is the weighted average of the six measures that have net threshold criteria. The weighting function ensures that forecast positions clustered near each other will contribute most to the final position, and that outlying positions receive little weight.

(2) JMA global and regional model comparisons. A comparison of the Global Spectral Model (GSM), Asian Spectral Model (ASM) and limited-region typhoon model

(TYM) was given in Fig. 15 for the 1990 season (Ueno 1991). At that time, the GSM clearly had larger errors than the ASM and TYM for all forecast intervals. Ueno and Ohnogi (1992) describe the improvements in the GSM and the ASM resulting from the bogussing procedures adopted in 1991 (Table 6). For these test samples, the GSM and ASM forecasts were improved at all times (notice the ASM is only integrated to 48 h) by the introduction of the new bogussing scheme. Since these small GSM and ASM samples are not homogeneous, it is not possible to intercompare these errors. However, it does appear that the error growth rate is smaller in the ASM.

(3) ECMWF global model. Chan (1992) compared the ECMWF model forecasts for four tropical cyclones during the TCM-90 field experiment with forecasts by TYM, OTCM and CLIPER. During this period, the ECMWF had a T106 horizontal resolution, and was run only once a day at 12 UTC. Thus, only 50 ECMWF forecasts were available, while 81 TYM and 241 OTCM and CLIPER forecasts were included. As shown in Table 7, only 17 of the ECMWF forecasts were verified. The surprising aspect in this sample is the small errors at 24 h, which may indicate that the additional observations during TCM-90 allowed a better initial position and field definition without the need for any synthetic observations. Although this is a small sample (and is not homogeneous), the small ECMWF errors relative to CLIPER and the other objective aids is certainly favorable.

Shun (1992) prepared a more extensive evaluation of the ECMWF track errors during 1990 and 1991. The verifying storm positions were provided by the Royal Observatory, Hong Kong and the RSMC Tokyo Typhoon Center. Only cyclones with maximum sustained winds in excess of 34 kt at the initial and the verifying times were included. Manual evaluations of the storm positions were based on the minima in sea-level pressures and 10 m vectors. The standard of comparison was a persistence forecast computed from best-track positions at the initial time and t-12 h.

Shun (1992) evaluated the ECMWF forecasts during the SPECTRUM field

Table 6 Track forecast errors (km) for the JMA Global Spectral Model (GSM) and Asian Spectral Model (ASM) for selected 1990-1991 typhoons using old and new bogussing procedures (Ueno and Ohnogi 1992).

| | Forecast interval (h) | | | | | |
|---|---|---|---|---|---|---|
| | 12 | 24 | 36 | 48 | 60 | 72 |
| | | | GSM | | | |
| OLD | 136 | 221 | 318 | 415 | 527 | 651 |
| NEW | 112 | 182 | 264 | 353 | 449 | 553 |
| Cases | 75 | 72 | 70 | 65 | 60 | 53 |
| | | | ASM | | | |
| OLD | 175 | 259 | 322 | 394 | -- | -- |
| NEW | 138 | 209 | 255 | 325 | -- | -- |
| Cases | 31 | 30 | 29 | 27 | | |

Table 7 Average track forecast errors (km) for selected models during the TCM-90 period (adapted from Chan 1992). Sample sizes are shown in parentheses.

| | Forecast interval (h) | | |
|---|---|---|---|
| | 24 | 48 | 72 |
| ECMWF | 164 (17) | 311 (17) | 461 (17) |
| CLIPER | 218 (105) | 422 (98) | 618 (85) |
| OTCM | 198 (101) | 337 (86) | 442 (68) |
| TYM | 221 (46) | 303 (37) | -- |

experiment that overlapped the TCM-90 experiment (Table 8). The forecast errors are slightly smaller than Chan (1992) found (Table 7). Shun also evaluated the T106 version of the ECMWF model forecast errors during 1991. Although the 24-h errors were larger than during SPECTRUM, the 72-h errors were smaller (Table 8). A combined sample of 1990 and 1991 cases with the T106 version had even larger 24-h errors (Table 8). The 48-h errors were larger than the SPECTRUM cases, but the 72-h errors were slightly smaller. This 1990-91 sample of T106 model errors had percentage errors relative to persistence of -4, +14 and +16 at 24 h, 48 h and 72 h respectively. These relative errors are comparable to the values for TYM during 1990 shown in Fig. 15. Finally, Shun summarized the errors after the higher resolution T213 was implemented in September 1991. Although the 24-h errors are not as small as during the SPECTRUM field experiment, the 48-h and 72-h errors with the T213 model are the smallest of the various samples. Compared to persistence, the relative errors are +1, +20 and +25% at 24 h, 48 h and 72 h respectively. This suggests that the error growth rate in the higher resolution T213 model is smaller. Although the ECMWF model does not start with a good initial position, such a small error growth rate will produce accurate forecasts at intervals beyond about 24 h.

(4) UKMO global model. Muroi and Sato (1992) have done a prototype intercomparison among the UKMO, ECMWF and JMA global models during 1991. As indicated above, the method of fixing the storm positions was not optimum, and the Muroi and Sato statistics for the ECMWF model differ slightly from the Shun (1992) evaluation in Table 8. Recall also that the JMA method of bogussing the vortex changed in September 1991 (Table 6). Although the Muroi and Sato study must be regarded as preliminary, it will be presented here because it is the only recent evaluation of the UKMO global model (Fig. 23). Since the UKMO and JMA models include synthetic observations to define the tropical cyclone and ECMWF does not (Table 5b), it is not surprising that the initial error is larger for ECMWF. However, the smaller error growth rate in the ECMWF model allows this model to provide more accurate forecasts than the UKMO or JMA models.

Table 8 Average track forecast errors (km) by the ECMWF model for selected samples (Shun 1992). Sample sizes are shown in parentheses.

| | Forecast interval (h) | | |
|---|---|---|---|
| SAMPLE | 24 | 48 | 72 |
| SPECTRUM | 151 (38) | 266 (31) | 452 (24) |
| T106 1991 | 185 (56) | 266 (41) | 394 (29) |
| T106 90-91 | 203 (138) | 301 (107) | 433 (82) |
| T213 1991 | 171 (71) | 248 (58) | 355 (45) |

Table 9 Average initial position and track forecast errors (km) for FNOC global model with and without insertions of synthetic observations to represent western North Pacific tropical cyclones during 1991. Sample sizes are shown in parentheses.

| | Forecast interval (h) | | | |
|---|---|---|---|---|
| | 00 | 24 | 48 | 72 |
| With synthetic observations | 76 (340) | 188 (289) | 299 (221) | 434 (167) |
| Without synthetic observations | -- | 333 | 453 | 605 |

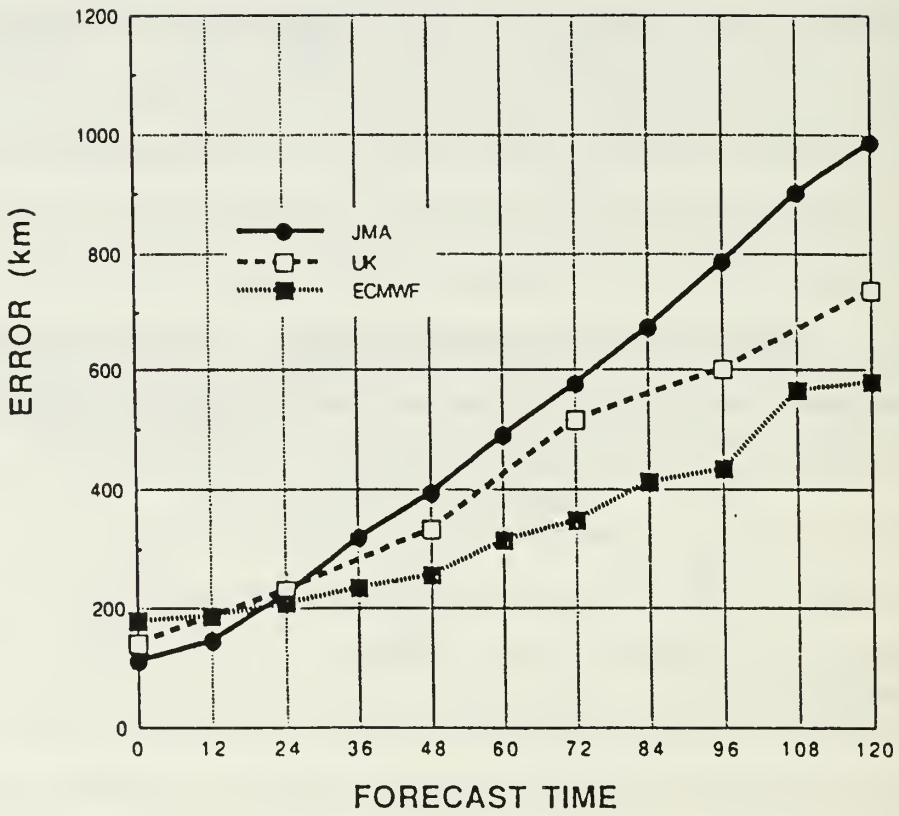


Fig. 23 Initial position and track forecast errors (km) for the ECMWF (dotted), UKMO (dashed) and JMA (solid) global models for western North Pacific tropical cyclones during 1991 (Muroi and Sato 1992).

Muroi and Sato note that the ASM 24- and 48-h forecast errors (not shown) were smaller than for the ECMWF model. The ASM includes a bogus vortex and has comparable resolution as the ECMWF model. However, the ASM is only integrated to 48 h.

Notice that this evaluation extended to 120 h, even though only about 25% of the forecasts can be verified at such long intervals. The advantage of the ECMWF model relative to the UKMO model extends to 120 h. At least for this small sample, the 120 h ECMWF forecast errors are of the same magnitude as the JMA global model at 72 h.

(5) FNOC global model. Fiorino *et al.* (1993) analyzed the ability of the T79 global model at FNOC to generate and/or maintain low-level (925 mb) cyclonic circulations (LLCC) during 72-h integrations. All LLCCs in each 12-h analysis and verifying 72-h forecast (valid at the time of the analysis) were manually extracted during 25 July through 24 December 1990, when 23 named tropical cyclones (09W-31W) existed in the western North Pacific. The relative vorticity at 925 mb calculated on a 2.5° lat. by 2.5° long. archive grid was used to define the LLCC centers. All gridpoints with relative vorticity exceeding a threshold value of $2 \times 10^{-5}$ $s^{-1}$ were identified and then a local maxima was interpolated between the gridpoints. The position within 2° lat. and long. of the JTWC warning position was identified as the inital center in the global model. The search zone, which is always centered on the prior position, expands in time to follow recurving and/or accelerating cyclones. If no center meeting the threshold relative vorticity is found, the LLCC is assumed to have dissipated.

Although the global model LLCCs were usually influenced by the synthetic observation procedure at FNOC (Table 5b) after a named tropical cyclone existed, periods of 12 h to 72 h existed early in the life cycle when the LLCC was based only on actual observations and the circulations generated by the model physics. After subjectively locating and numbering all closed cyclonic circulations and cyclonic troughs equatorward of 25°N in the 925 mb analyses, the verifying 72-h forecast was overlaid. Systems within 5° lat. and long. were assumed to be the same feature.

An example during the TCM-90 period is shown in Fig. 24. The JTWC forecasters trace many potential systems before issuing a tropical cyclone formation alert, which is a message indicating a suspect cloud cluster is expected to form into a tropical depression analysis/forecasts within 24 h. A LLCC in the global model analysis/forecasts at this early time could only have been produced from existing observations and/or generated by the model physics as no synthetic observations are inserted until the tropical storm stage. Of the 61 identified LLCCs during this 6-month study, eight were forecast at 72 h that did not appear in the verifying analysis, which is a false alarm rate of 13%. Another four appeared in the analysis, but not in the 72-h forecast. Excluding the false alarm cases, 23 of the 53 analyzed LLCCs became named tropical cyclones. A LLCC was already present in the global analysis at the time the JTWC forecaster first began to follow the system for 96% of these 23 cases. Furthermore, the verifying 72-h forecast at that time had a LLCC within 5° lat./long. in 20 of the 23 cases. According to Fiorino *et al.* (1993), the ability of the relatively coarse T79 model to generate and maintain LLCCs may be attributed to the Arakawa-Schubert convective parameterization. It would be useful to do a similar census of LLCCs in other global models to know the percentage of successful representations and the false alarm rates.

Goerss and Jeffries (1993) have summarized separately the FNOC global model forecast errors (Table 9) for analyses that included the synthetic observations (Table 5b) and those that did not include synthetic observations. Notice that this is not an impact test of two separate analysis systems running in parallel as in the JMA test in Table 6. Rather, the cases without synthetic observations were in the early stages of the life cycle, and the cases with synthetic observations are for named storms that are likely to be defined better. Initial position (t = 00 h) errors for the cases with synthetic observation insertions were only 76 km. A comparable initial error for the cases without synthetic observations was not determined since a reliable verifying position was not considered to be available. As expected, the track forecast errors for the cases without synthetic observations are much

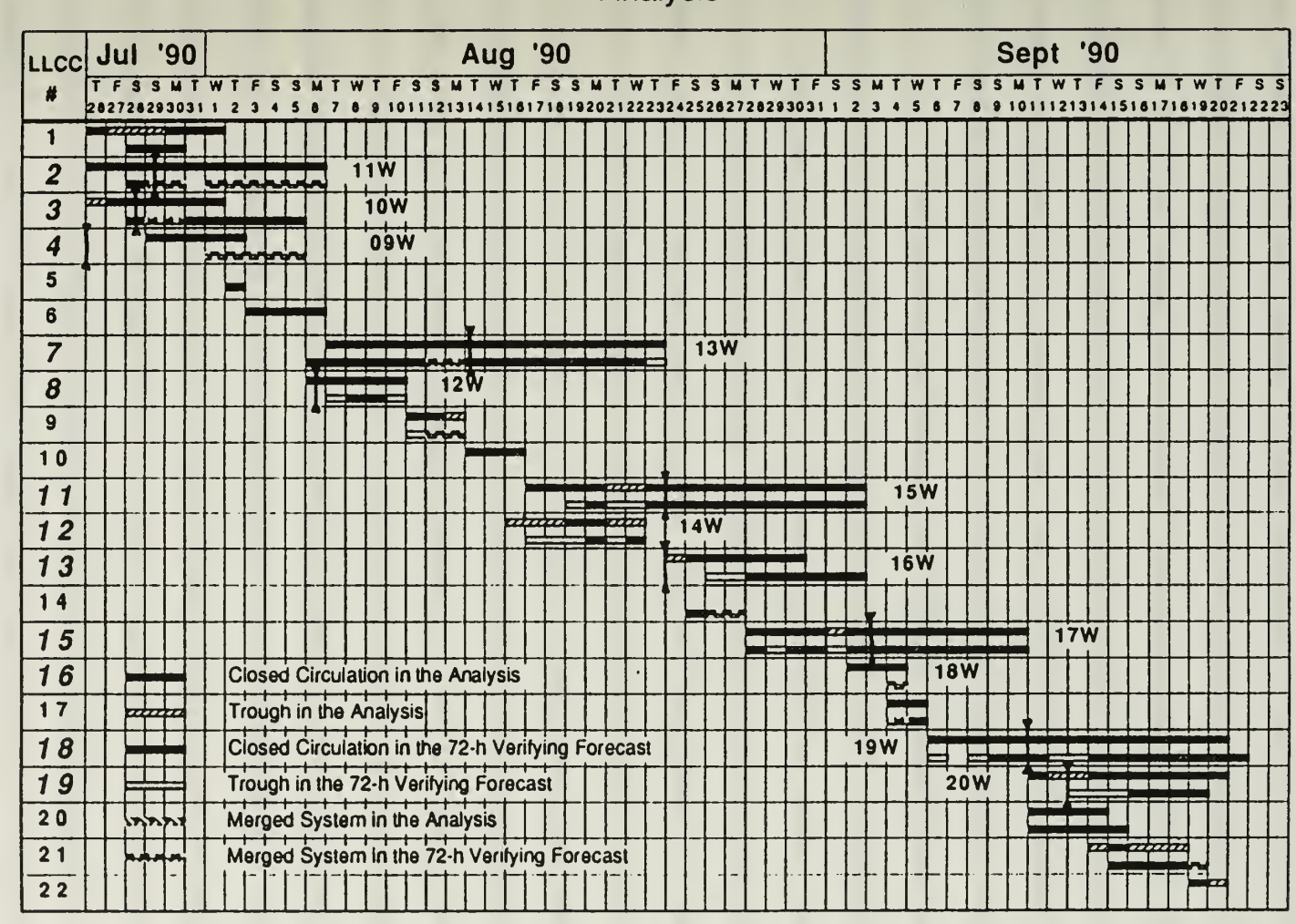


Fig. 24 Sample time line indicating numbered low-level cyclonic circulations (LLCC) in the FNOC global model (left column) analyses and forecasts (see code insert). Named tropical cyclones are indicated by the bold LLCC number and the number designator is indicated to the right of the time lines, with a genesis time indicated by a vertical line with triangular ends (Fiorino *et al.* 1993).

larger than the cases with synthetic observations. Whereas only 66% of the forecasts without synthetic observations maintained a traceable circulation to 72 h, the percentage increased to 87% for the forecasts beginning with synthetic observations. Notice also that the FNOC T79 model forecast errors with synthetic observations in Table 9 are about equivalent to the ECMWF T106 model forecast errors during 1990-91 (Table 8). The percent improvement of the FNOC global model errors relative to the operational CLIPER forecast errors are 9%, 31% and 33% at 24 h, 48 h and 72 h respectively. These numbers indicate skill relative to CLIPER even at the 24-h time interval.

(6) Summary. These limited evaluations of the various global models indicate that the tropical cyclone track forecasts have improved and are competitive with other objective aids. More complete and systematic evaluations of these global models for tropical cyclone forecasting are needed. The tropical cyclone forecaster needs to understand when they will fail to provide a forecast, and the synoptic conditions when the forecast is likely to be good or poor.

The advantage of the global baroclinic models relative to the limited region baroclinic models (Section 3) is the absence of artificial boundaries that eventually limit the useful forecast interval. The Muroi and Sato (1992) assessment suggests that useful track forecasts to 120 h may be produced in certain cases with advanced global models (Fig. 23). Goerss and Jeffries demonstrate that improvements in track forecasts with the FNOC T79 global model are almost linearly related to improvements in initial positions. Miller (1992) suggests that insertion of bogus vortices (such as the UKMO and JMA models in Fig. 23) may have contributed to larger error growth rates relative to the EMCWF model that has no insertion of synthetic observations. Nevertheless, it would be interesting to know if an improved initial position in the ECMWF T213 model would be translated into an additional forecast improvement. If so, such a global model would provide significantly improved guidance to tropical cyclone track forecasters at all intervals.

The lack of timeliness of the global model forecasts is a disadvantage. The

ECMWF model is only integrated once a day for 12 UTC conditions, and after a long time delay (~ 10 h) to allow maximum collection of data. Other global models are integrated twice a day at about 8 h after synoptic times. Although the global model resolution continues to improve, a higher resolution limited-region baroclinic model can always be integrated with the same computer resources. In addition to having more timely track forecasts, the higher-resolution models are more likely to provide intensity trends, structure change and precipitation distribution forecasts than the global models. At least for shorter time intervals, the limited-resolution baroclinic models are likely to have an important role in tropical cyclone forecasting for some time.

c. Research global models

(1) Florida State University. For a number of years, Professor T. N. Krishnamurti and his research group at Florida State University (FSU) have been developing and testing global numerical weather prediction models. A review by Krishnamurti *et al.* (1993) summarizes the various data assimilation and forecast model improvements related to the tropical cyclone life cycle and track forecasts. One of the key advances has been the physically-based initialization system that has been developed to make use of the diverse data sources, and especially the satellite-based rainfall rates. Davidson and Puri (1992b) have patterned their Australian limited-region baroclinic model initialization (Table 2b) after the FSU system to improve the initial divergent winds and diabatic heating to be consistent with the prescribed rain rates. The reader is referred to Krishnamurti *et al.* (1993) and the references therein for detailed descriptions of the physical processes in the FSU model. Here, only a brief description of the numerical characteristics and the initial conditions for tropical cyclones will be given to compare with the operational global models described above.

As shown in Table 5a, the FSU global model is typically integrated with T170 horizontal resolution, which is surpassed only by the T213 ECMWF model. As only 12 levels are used in the vertical, the FSU has less resolution than the operational models.

Krishnamurti *et al.* (1988) tested the effect of horizontal resolution for tropical cyclone prediction with T21, T31, T42, T63 and T106 spectral waves. Systematic improvements in the formation and motion of the storms were achieved for several case studies when the horizontal resolution was improved and an additional vertical level within the surface layer was utilized to improve the surface flux calculations.

As shown in Table 5b, no synthetic wind and height observations are included in the FSU model to define the tropical cyclone position. Rather, the extensive physical initialization package based on the observed rain rates in and around the tropical cyclone are used to force a rotational and divergent circulation in the initial conditions. Thus, a tropical cyclone is indeed present in the initial conditions, and the initial motion is governed by the environmental flow that has been spun-up during the physical initialization step. Bedi *et al.* (1993) have included Special Sensor Microwave Imager (SSM/I) data in the physical initialization of three typhoons.

Krishnamurti *et al.* (1993) summarizes several case studies of five-day predictions of the life cycle and motion of tropical cyclones. Krishnamurti *et al.* (1992) and Beven (1993) have used the model outputs from a successful prediction of Typhoon Colleen to diagnose the dynamics of the recurvature period. They suggest that the region immediately outside the heavy rain area of the model storm experiences strong divergent outflows that contribute significantly to the advection of divergence aloft. Enhancement of low-level convergence in response to the upper-level divergence contributes to an asymmetric distribution of deep convection, which contributes to the storm motion. Increased vertical resolution in the outflow layer is shown to result in stronger divergence amplitudes in the outflow layer, and thus contribute to improved forecasts of recurvature in the model. The complexity of the baroclinic models with feedbacks between convection and lower tropospheric convergence and generation of vorticity is consistent with the idealized baroclinic model studies in Appendix A. Whereas the research models such as the FSU model offer the potential for improved prediction of tropical cyclone formation and

motion, the difficulties of adapting the physical initialization and other aspects of the high-resolution model to operational forecasting are certainly a challenge.

(2) JMA high-resolution test case. A single case study of Typhoon Flo striking Japan during September 1990 was simulated with a T213 version of the JMA global model (Iwasaki 1991). The second aspect of this research was to test the impact of the convective parameterization scheme. Heckley *et al.* (1987) had earlier indicated the sensitivity of the ECMWF model track forecasts of Hurricane Elena to the replacement of the Kuo parameterization scheme with a convective adjustment scheme. Ueno (1991) also had used a modified Kuo parameterization technique in the JMA global model and found that a poleward bias in the track of a low-latitude typhoon was reduced.

Iwasaki (1991) found the operational GSM could not predict the development of Typhoon Flo, nor maintain the proper intensity of Typhoon Ed, which was present in the initial conditions (Fig. 25). The T213 version with the standard Kuo scheme maintained Typhoon Ed, but could not predict the development of Typhoon Flo. The high resolution model with the modified Kuo scheme was able to predict the occurrence, development and recurvature of Typhoon Flo. However, the movement and filling of Typhoon Ed over land was not well predicted by this version. This experiment indicates again the possibility of 5-day tropical cyclone predictions in high-resolution global models with improved physical process representations. The potential needs to be explored in the future.

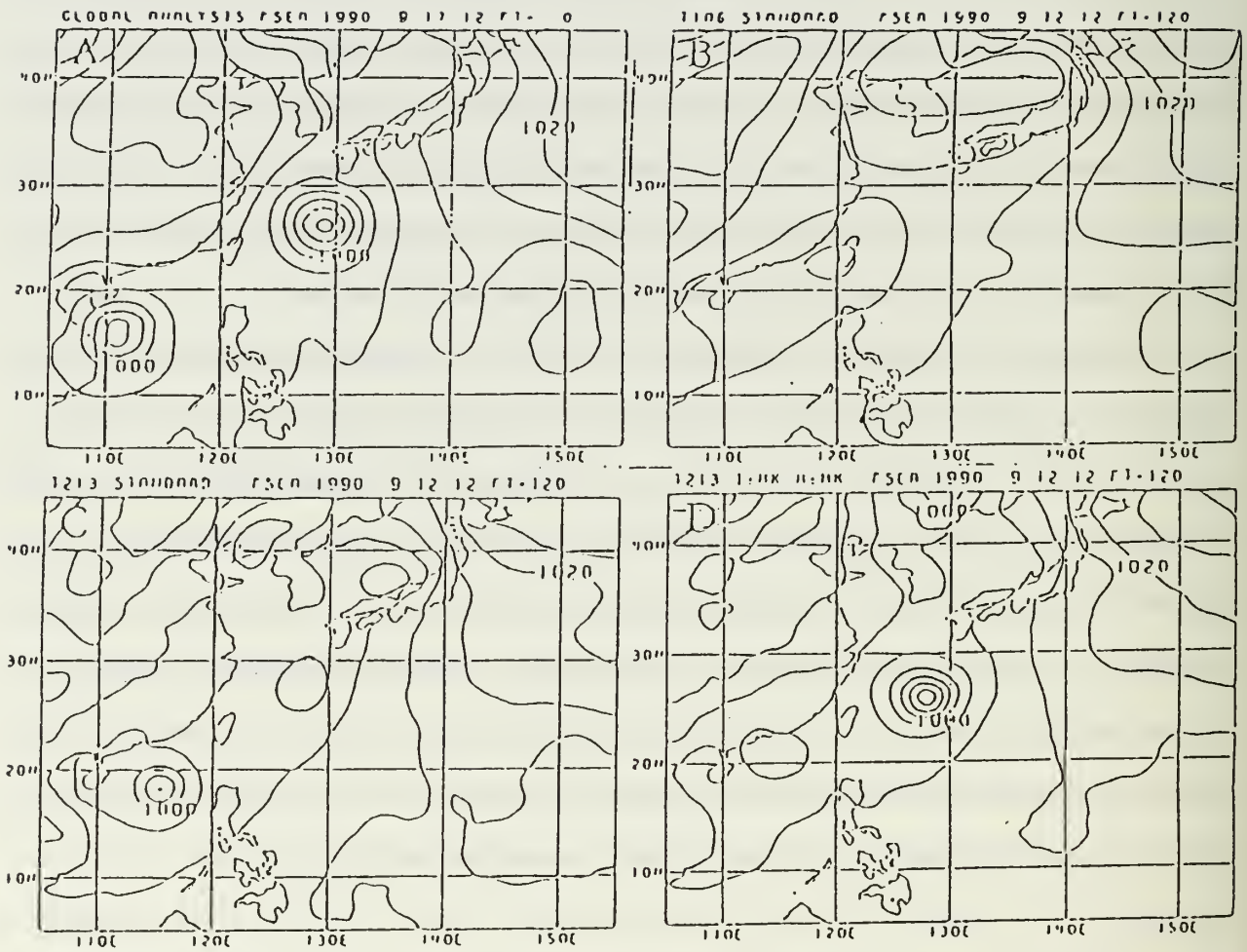


Fig. 25 (a) Verifying sea-level pressure analysis at 12 UTC 17 September 1990, and 5-day forecasts from 12 UTC 12 September for (b) the operational GSM of JMA, (c) research T213 version with standard Kuo parameterization scheme, and (d) T213 version with modified Kuo scheme (Iwasaki 1991).

## 5. References


Andersson, E., and A. Hollingsworth, 1988: Typhoon bogus observations in the ECMWF data assimilation system. ECMWF Research Department Tech. Memo. No. 148.

Bedi, H. S., T. N. Krishnamurti and K. Ingles, 1993: Impact of physical initialization using SSM/I data on prediction of typhoons. Preprints, 20th Tech. Conf. on Hurricanes and Tropical Meteorology, American Meteor. Soc., Boston, MA 02108.

Bengtsson, L., H. Bottger and M. Kanamitsu, 1982: Simulation of hurricane-like vortices in a general circulation model. Tellus, **34**, 440-457.

Bender, M. A., R. J. Ross, R. E. Tuleya and Y. Kurihara, 1993: Improvements in tropical cyclone track and intensity forecasts using the GFDL initialization system. Submitted.

Bennett, A. F., L. M. Leslie, C. R. Hagelberg and P. E. Powers, 1992: Tropical cyclone prediction using a barotropic model initialized by a generalized inverse method. Submitted to Mon. Wea. Rev.

Beven, J. L., III, 1993: Tropical cyclone-environmental interactions during recurvature. Preprints, 20th Tech. Conf. on Hurricanes and Tropical Meteorology, American Meteor. Soc., Boston, MA 02108.

Carr, L. E., III, 1989: Baroclinic vortex adjustment to asymmetric forcing with application to tropical cyclones. Ph.D. dissertation, Naval Postgraduate School, Monterey, CA 93943, 143 pp.

Carr, L. E., III, and R. L. Elsberry, 1992: Analytical tropical cyclone asymmetric circulation for barotropic model initial conditions. Mon. Wea. Rev., **120**, 644-652.

Chan, J. C.-L., 1992: A preliminary investigation of the performance of global and regional models during SPECTRUM. Tech. Doc. WMO/TD-No. 472, World Meteor. Organiz., Geneva, pp. V.12 - V.21.

Chan, J. C.-L., and H. Lam, 1989: Performance of the ECMWF model in predicting the movement of typhoon Wayne (1986). Wea. and Forecasting, **4**, 234-245.

Davidson, N. E., and K. Puri, 1992a: Limited area tropical prediction for AMEX. Aust. Meteor. Mag., **40**, in press.

_____, 1992b: Tropical prediction using dynamical nudging, satellite-defined convective heat sources, and a cyclone bogus. Mon. Wea. Rev., **120**, 2501-2511.

DeMaria, M., 1987: Tropical cyclone track prediction with a barotropic spectral model. Mon. Wea. Rev., **115**, 2346-2357.

DeMaria, M., S. D. Aberson, K. V. Ooyama, and S. J. Lord, 1992: A nested spectral model for hurricane track forecasting. Mon. Wea. Rev., **120**, 1628-1643.

DeMaria, M., and R. W. Jones, 1993: Optimization of a hurricane track forecast model with the adjoint model equations. Mon. Wea. Rev., in press.

Dietachmeyer, G. S., 1992: On the application of continuous dynamic grid adaptation techniques to meteorological modelling. Part II. Efficiency. Mon. Wea. Rev., **120**, 1707-1722.

Dietachmeyer, G. S., and K. K. Drogemeir, 1992: On the application of continuous dynamic grid adaptation techniques to meteorological modelling. Part I. Basic formulation and accuracy. Mon. Wea. Rev., **120**, 1675-1706.

Elsberry, R. L., 1979: Applications of tropical cyclone models. Bull. Amer. Meteor. Soc., **60**, 750-762.

Elsberry, R. L., 1987: Tropical cyclone motion. Chap. 4, A Global View of Tropical Cyclones. Office of Naval Research, Arlington, VA 22217, 91-171.

Elsberry, R. L., 1990: International experiments to study tropical cyclones in the western North Pacific. Bull. Amer. Meteor. Soc., **71**, 1305-1316.

Elsberry, R. L., and R. F. Abbey, Jr., 1991: Recent advances in the understanding of tropical cyclone motion. Tech. Rep. NPS-MR-91-003, Naval Postgraduate School, Monterey, CA 93943, 92 pp.

_____, 1992: Typhoon motion and environmental steering. Tech. Doc. WMO/TD No. 472, World Meteorological Organization, Geneva, Switzerland, pp. III.1 - III.19.

Elsberry, R. L., B. C. Diehl, J. C.-L. Chan, P. A. Harr, G. J. Holland, M. Lander, T. Neta, and D. Thom, 1990: ONR Tropical cyclone Motion Initiative: Field experiment summary. Tech. Rep. NPS-MR-91-001, Naval Postgraduate School, Monterey, CA 93943, 106 pp.

Elsberry, R. L., and R. H. Bohner, Jr., 1992: Three-component decompositions of tropical cyclone wind fields: Relation to tropical cyclone motion. International Symposium on Tropical Cyclone Disasters, Beijing, 12-16 October 1992.

Fiorino, M., and R. L. Elsberry, 1989: Some aspects of vortex structure in tropical cyclone motion. J. Atmos. Sci., **46**, 979-990.

Fiorino, M., J. S. Goerss, J. J. Jensen and E. J. Harrison, Jr., 1993: An evaluation of the real-time tropical cyclone forecast skill of the Navy Operational Global Atmospheric Prediction System in the western North Pacific. Wea. and Forecasting, **8**, 3-24.

Franklin, J. L., 1990: Dropwindsonde observations of the environmental flow of hurricane Josephine (1984): Relationships to vortex motion. Mon. Wea. Rev., **118**, 2732-2744.

Fujita, T., 1952: Pressure distribution within a typhoon. Geophys. Mag., **23**, 437-451.

Goerss, J. S., L. R. Brody and R. A. Jeffries, 1991: Assimilation of tropical cyclone observations into the Navy Operational Global Prediction System. Proc. 9th Conf. on Num. Wea. Pred., Denver, CO, 14-18 October, Amer. Meteor. Soc., Boston, MA 02108, 638-641.

Goerss, J. S., and R. L. Jeffries, 1993: Assimilation of synthetic tropical cyclone observations into the Navy Operational Global Atmospheric Prediction System. Wea. and Forecasting, (in review).

Hall, C. D., 1987: Verification of global model forecasts of tropical cyclones during 1986. Meteor. Mag., **116**, 216-219.

Harr, P. A., T. Neta and R. L. Elsberry, 1991: ONR Tropical Cyclone Motion Research Initiative: Data users guide to observations. Tech. Rep. NPS-MR-91-002, Naval Postgraduate School, Monterey, CA 93943, 123 pp.

Heckley, W. A., M. J. Miller and A. K. Betts, 1987: An example of hurricane tracking and forecasting with a global analysis-forecasting system. Bull. Amer. Meteor. Soc., **68**, 226-229.

Holland, G. J., 1980: An analytic model of the wind and pressure profiles in hurricanes. Mon. Wea. Rev., **108**, 1212-1218.

Holland, G. J., L. M. Leslie, E. A. Ritchie, G. S. Dietachmayer, P. E. Powers and M. Klink, 1991: An interactive analysis and forecast system for tropical cyclone motion. Wea. and Forecasting, **6**, 415-424.

Holland, G. J., and G. S. Dietachmayer, 1992: On the interaction of tropical-cyclone scale vortices. Part III: Continuous barotropic vortices. Quart. J. Roy. Meteor. Soc., submitted.

Holland, G. J., and L. M. Leslie, 1993: On the bogussing of tropical cyclones in numerical models: A comparison of vortex profiles. Wea. and Forecasting, submitted.

Iwasaki, T., 1991: Status report on numerical prediction of typhoons. Preprints, Second Workshop on Natural Disaster Reduction, Karuizama, Japan.

Iwasaki, T., H. Nakano and M. Sugi, 1987: The performance of a typhoon track prediction model with cumulus parameterization. J. Meteor. Soc. Japan, **65**, 555-570.

Jones, R. W., and M. DeMaria, 1991: A variational method for including persistence in a hurricane track forecast model. Preprints, 19th Conf. on Hurr. and Trop. Meteor., Amer. Meteor. Soc., Boston, MA 02108, 331-334.

_____, 1993: Further results of variational data assimilation with a barotropic hurricane track forecast model. Preprints, 20th Conf. on Hurr. and Trop. Meteor., Amer. Meteor. Soc., Boston, MA 02108.

Krishnamurti, T. N., D. Oosterhof and N. Dignon, 1989: Hurricane prediction with a high resolution global model. Mon. Wea. Rev., **117**, 631-669.

_____, H. S. Bedi, K. S. Yap, D. Oosterhof and G. Rohaly, 1992: Recurvature dynamics of a typhoon. Meteor. Atmos. Phys., **50**, 105-126.

_____, H. S. Bedi, K. S. Yap and D. Oosterhof, 1993: Hurricane forecasts in the FSU models. Adv. Atmos. Sci., **10**, 121-131.

Kuo, H.-L., 1974: Further studies of the parameterization of the influence of cumulus convection on large-scale flow. J. Atmos. Sci., **31**, 1232-1240.

Kurihara, Y., R. E. Tuleya, M. A. Bender and R. J. Ross, 1992: Advanced modeling of tropical cyclones. Proc., International Symposium on Trop. Cyclone Disasters, Beijing, 12-16 October.

Kurihara, Y., M. A. Bender and R. J. Ross, 1993a: An initialization scheme of hurricane models by vortex specification. (submitted).

Kurihara, Y., M. A. Bender, R. E. Tuleya and R. J. Ross, 1993b: Hurricane forecasting with the GFDL automated prediction system. Preprints, 20th Conf. on Hurr. and Trop. Meteor., 10-14 May, Amer. Meteor. Soc., Boston, MA 02108.

Leslie, L. M., and G. J. Holland, 1992: Data assimilation techniques for tropical cyclone track prediction. Proc., International Symposium on Trop. Cyclone Disasters, Beijing, 12-16 October.

Liu, Z., and Q.-C. Zeng, 1992: The application of adaptive mesh to the numerical forecasting of tropical cyclone track. Proc., International Symposium on Trop. Cyclone Disasters, Beijing, 12-16 October.

Lord, S. J., 1991: A bogussing system for vortex circulations in the National Meteorological Center global model. Preprints, 19th Tech. Conf. on Hurricanes and Trop. Meteor., American Meteor. Soc., Boston, MA 02108, 328-330.

Lord, S. J., and J. L. Franklin, 1987: The environment of Hurricane Debby (1992). Part I. Winds. Mon. Wea. Rev., **115**, 2760-2780.

Mathur, M. B., 1991: The National Meteorological Center's Quasi-Lagrangian Model for hurricane prediction. Mon. Wea. Rev., **115**, 1419-1447.

Mathur, M. B., and A. M. Shapiro, 1992: A procedure to reduce northward drift of tropical storms in a numerical model. Tech. Memo. NWS NMC 71, National Weather Service, Washington, DC, 20 pp plus figures.

Miller, M. J., 1992: The analysis and prediction of tropical cyclones by the ECMWF global forecasting system: Progress, problems and prospects. ICSU/WMO International Symposium on Trop. Cyclone Disasters, Beijing, 12-16 October.

Muroi, C.-A., and N. Sato, 1992: Intercomparison of tropical cyclone track forecasts by ECMWF, UKMO and JMA operational global models. Tech. Rep. No. 30, Numerical Prediction Div., Japan Meteor. Agency, (in press).

Ohnishi, H., 1992a: Effect of the vortex structure on nonlinear beta drift. Tech. Doc. WMO/TD No. 472, World Meteor. Organ., Geneva, pp. IV.43-IV.51

_____, 1992b: How to improve typhoon motion forecast. Proc., International Symposium on Trop. Cyclone Disasters, Beijing, 12-16 October.

Peng, M. S., and R. T. Williams, 1990: Dynamics of vortex asymmetries and their influence on vortex motion on a beta-plane. J. Atmos. Sci., **47**, 1987-2003.

_____, B.-F. Jeng and C.-P. Chang, 1993a: Forecast of typhoon motion in the vicinity of Taiwan during 1989-1990 using a dynamical model. Wea. and Forecasting, in press.

_____, D.-S. Chen, S. W. Chang, C.-P. Chang and B.-F. Jeng, 1993b: Forecast of typhoon tracks near Taiwan by a numerical model incorporating past typhoon motion and different spin-up vortices. Preprints, 20th Conf. on Hurr. and Trop. Meteor., Amer. Meteor. Soc., Boston, MA 02108.

Puri, K., N. E. Davidson, L. M. Leslie, and L. W. Logan, 1992: The BMRC tropical limited area model. Aust. Meteor. Mag., **40**, 81-104.

Ross, R. J., and Y. Kurihara, 1992: A simplified scheme to simulate asymmetries due to the beta effect in barotropic vortices. J. Atmos. Sci., **49**, 1620-1628.

Shapiro, L. J., 1992: Hurricane vortex motion and evolution in a three-layer model. J. Atmos. Sci., **49**, 140-153.

Shapiro, L. J., and K. V. Ooyama, 1990: barotropic vortex evolution on a beta plane. J. Atmos. Sci., **47**, 170-187.

Shun, C. M., 1992: Performance of the ECMWF model in tropical cyclone track forecasting over the western North Pacific during 1990-1991. Tech. Memo. No. 184, European Centre for Medium-range Weather Forecasts, Shinfield Park, UK, 32 pp.

Sitnikov, I. G., 1991: Numerical modeling of tropical cyclones in the USSR. Hydrometeor. Res. Centre, Moscow, USSR.

Smith, R. K., 1991: An analytic theory of tropical cyclone motion in a barotropic shear flow. Quart. J. Roy. Meteor. Soc., **117**, 685-714.

_____, 1992: On the theory of tropical cyclone motion. Proc., International Symposium on Trop. Cyclone Disasters, Beijing, 12-16 October.

Smith, R. K., and W. Ulrich, 1990: An analytical theory of tropical cyclone motion using a barotropic model. J. Atmos. Sci., **47**, 1973-1986.

Tatsumi, Y., 1986: A spectral limited-area model with time-dependent lateral boundary conditions and its application to a multi-level primitive equation model. J. Meteor. Soc. Japan, **64**, 637-663.

Ueno, M., 1991: Typhoon track forecast by JMA NWP models and current practive for improvement in the track forecast. Tech. Doc. WMO/TD No. 426, World Meteor. Organ., Geneva, 87-97.

Ueno, M., and K. Ohnogi, 1992: A change of the operational typhoon bogussing method. Tech. Doc. WMO/TD No. 472, World Meteor. Organ., Geneva, pp. II.21 - II.27.

Velden, C. S., and L. M. Leslie, 1991: The basic relationship between tropical cyclone intensity and the depth of the environmental steering layer in the Australian region. Wea. and Forecasting, **6**, 244-253.

WMO, 1990: Proceedings of the Second International Workshop on Tropical Cyclones. Tech. Doc. WMO/TD No. 361, World Meteor. Organ., Geneva, 122 pp.

Yamasaki, M., 1986: A three-dimensional tropical cyclone model with parameterized cumulus convection. Papers Meteor. Geophys., **37**, 205-234.

_____, 1987: Parameterization of cumulus convection in a tropical cyclone model. Special issue, J. Meteor. Soc. Japan, 665-678.

_____, 1992: A study of tropical cyclone motion with a nested-grid model including rain water prediction. Papers Meteor. Geophys., **43**, 61-77.

Zhu, Y.-T., 1992: Recent advances in numerical simulation of tropical cyclone activities in China. Proc., International Symposium on Trop. Cyclone Disasters, Beijing, 12-16 October.

# APPENDIX A

## A Review of Recent Idealized Baroclinic Models of Tropical Cyclone Motion

### a. Introduction

It is convenient to first discuss the baroclinic effects associated with the tropical cyclone structure in a no-shear environment and then those associated with an environment that has a vertical wind shear. The structure effects have been modelled on a beta-plane for comparison with the barotropic models (see Elsberry and Abbey 1991). Vertical shear effects have been studied first on an *f*-plane to illustrate the basic principles, and then on a beta-plane to better simulate real vortices. Another option in the numerical model simulations is to include or to remove the diabatic processes (especially latent heat release) and the frictional processes that are essential aspects of tropical cyclones. The goal of these idealized baroclinic model studies is to understand each aspect of the physical processes that combine to cause the motion of real tropical cyclones.

Wu and Emanuel (1993) have raised an issue regarding the environment of the tropical cyclone. They have estimated the potential vorticity $[(f + \varsigma)/(-\partial p/\partial\theta)]$ on isentropic surfaces by interpolation from the U. S. National Meteorological Center (NMC) Northern Hemisphere final analyses on a 2.5° x 2.5° latitude-longitude grid. In the example in Fig. A-1, Hurricane Bob is moving northward along the east coast of the U. S. under the influence of a strong Bermuda high pressure cell. Thus, the anticyclonic (negative) relative vorticity is large and the absolute vorticity values are reduced in the subtropics. A common assumption is that the static stability that appears in the denominator of the potential vorticity is nearly constant in the horizontal across the tropical and subtropical oceans. Whether some additional static stability compensation (i.e., larger vertical gradients of $\theta$ in anticyclonic regions and at low latitudes compared to cyclonic regions and high latitudes) may also be occurring is somewhat uncertain due to the scarcity of rawinsondes (Bermuda is the only regular station north of the Caribbean). Wu and Emanuel conclude that a constant potential vorticity gradient associated with a beta-

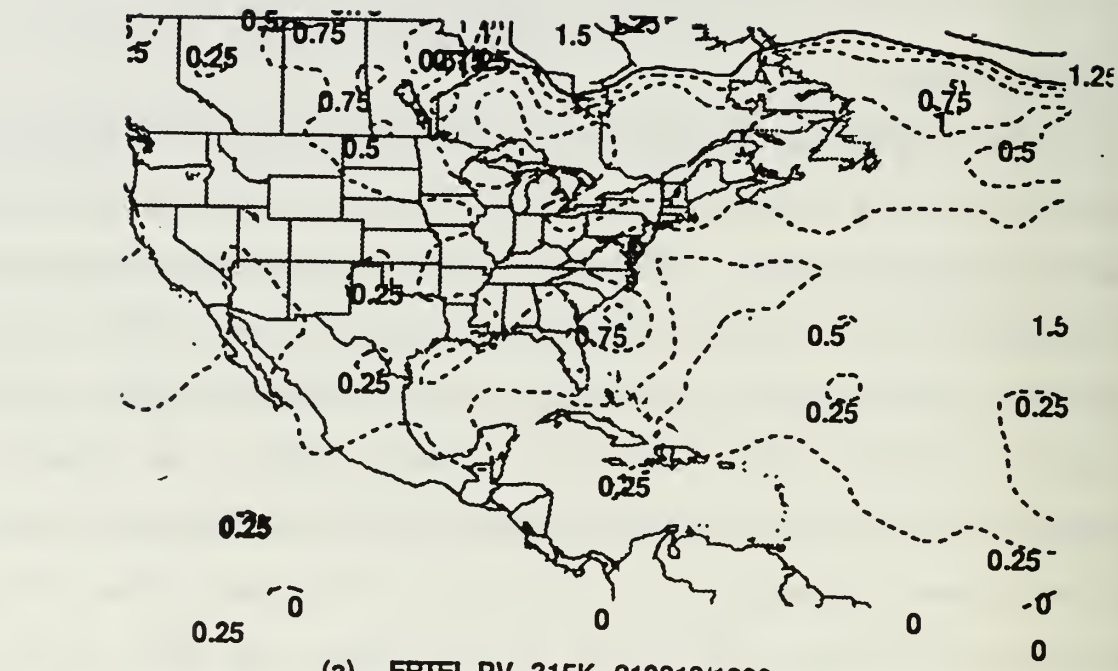


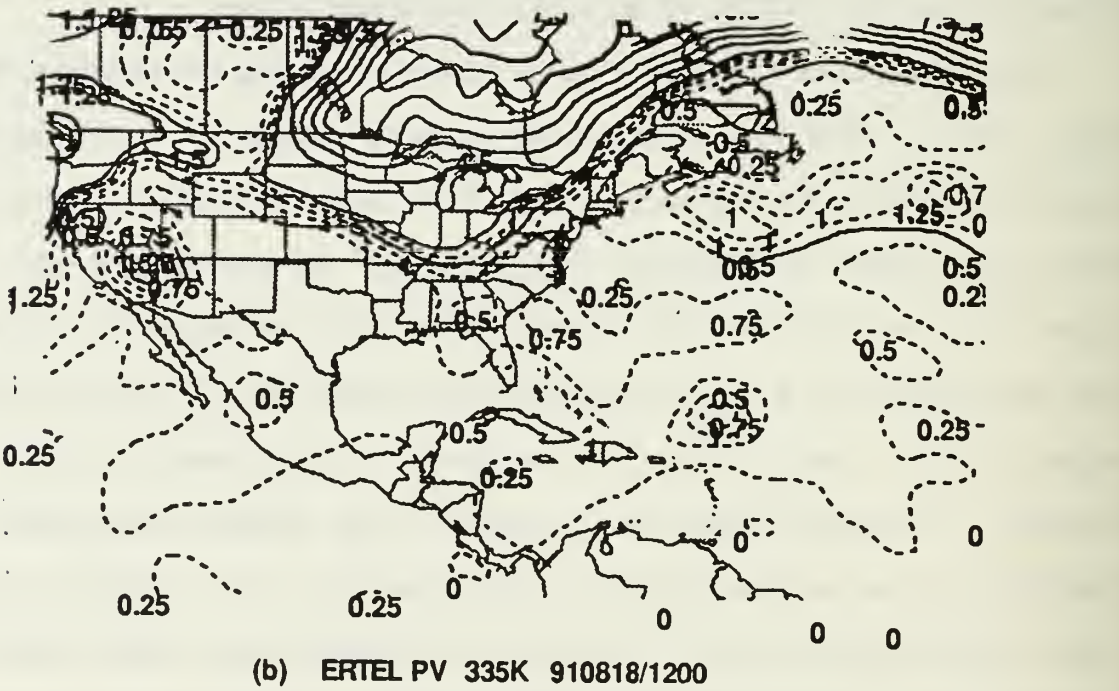


Fig. A-1 Ertel potential vorticity (PV) at 12 UTC 18 August 1991 on the (a) 315°K and (b) 335°K isentropic surface (Wu and Emanuel 1993). Potential vorticity values smaller than (larger than or equal to) 1.5 PVU are shown as dashed (solid) lines with unequal contour intervals of 0.25 PVU (1.5 PVU).

plane approximation would not apply in the environment of Hurricane Bob.

Significant potential vorticity gradients are found at the tropopause level because of the near-discontinuities in static stability between the tropopause and the lower stratosphere. Thus, Wu and Emanuel propose that the anticyclonic flow near the tropopause in a tropical cyclone may interact with these potential gradients, which would propagate the anticyclonic cells westward and equatorward. If these anticyclonic cells have an indirect effect on the tropical cyclone vortex motion via vertical tilt effects (to be described below), the outflow layer may have an important role in the motion process. Clearly, similar potential vorticity calculations should be attempted in other tropical cyclone regions to test the generality of Wu and Emanuel's contention. The TCM-90 enhanced data set of rawinsondes over normally data-sparse tropical oceans, and the 50 km resolution in the TCM-90 final analyses, are likely to provide a more representative potential vorticity distribution than the archived $2.5^{o}$ x $2.5^{o}$ NMC grid.

b. Tropical cyclone baroclinic structure

In the barotropic model simulations, the tropical cyclone vortex is represented as a deep-layer mean. Near the center, the vertical wind shear is small in the lower troposphere and the cyclonic circulation extends to great depths. However, an anticyclone is found aloft, especially at outer radii. Thus, a tropical cyclone can be represented as a pyramid-shaped cyclonic vortex penetrating upward into an anticyclone aloft.

Because the radial extent of the cyclonic vortex decreases with increasing elevation, the propagation vector associated with the beta effect should diminish aloft (based on barotropic model reasoning, see Elsberry and Abbey 1991). Wang and Li (1992) tested this effect with a 10-level baroclinic model of a quiescent environment in which the tropical cyclone vortex had maximum winds at 900 mb and decreased linearly to zero at 100 mb (Fig. A-2). Such a vertical wind shear is consistent with a warm core in the tropical cyclone. The radial variation (not shown) has a maximum at 200 km and decreased to zero at 750 km. The relative angular momentum (RAM), which is the product of the radius and

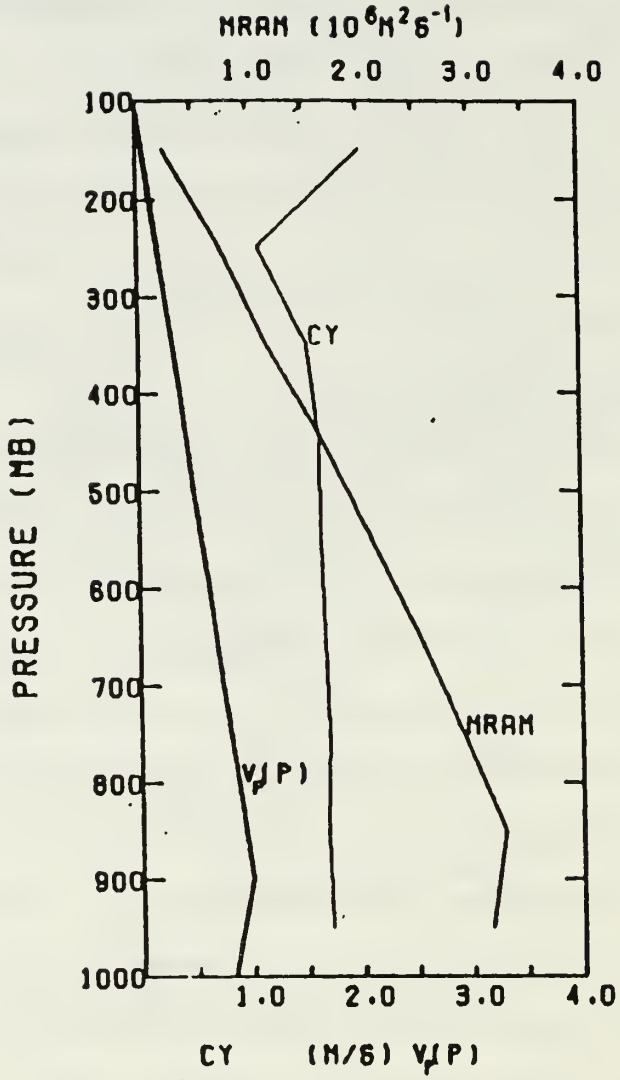


Fig. A-2 Initial tangential wind $V_p$ (normalized by maximum wind) and mean relative angular momentum (MRAM) variations with pressure in the Wang and Li (1992) 10-level numerical model. Mean meridional drift speed $C_y$ of the vortex at 24 h is also shown.

the tangential wind component integrated over the domain, was positive (no anticyclonic wind aloft were included) and had a vertical variation similar to the tangential wind structure (Fig. A-2).

Because the Wang and Li model was adiabatic and frictionless (no heating or convective momentum mixing to maintain the warm core and vertical tilt), it was expected that the differential beta-effect propagation with elevation would disperse the vortex. However, the vortex maintained a vertically coherent structure as indicated by the essentially constant meridional propagation at all levels (Fig. A-2). This propagation vector is close to that expected from a barotropic model initialized with the vertically-integrated vortex wind structure.

c. Conceptual model of secondary circulation coupling

Why did the upper (lower) levels of vortex in the Wang and Li model propagate faster (slower) than expected based on beta-plane reasoning for the size of the cyclonic vortex at those levels? A first-order explanation can be provided in terms of the quasi-geostrophic omega equation considering only the differential vorticity advection with elevation,

$$\alpha \nabla^2 \omega + f_0 \frac{\partial^2 \omega}{\partial p^2} \approx -f_0 \frac{\partial}{\partial p} (-V \cdot \nabla \zeta). \tag{1}$$

Again applying barotropic model reasoning within each of the 10 layers in the Wang and Li model, wavenumber one gyres will develop over 24-36 h. The flow between the anticyclonic and cyclonic gyres to the northeast and southwest respectively will advect the vortex to the northwest. The speed of propagation will be a maximum at 900 mb and will decrease linearly with elevation because of the assumed structure in Fig. A-2.

In terms of the vorticity budget,

$$\frac{\partial \zeta}{\partial t} = -V \cdot \nabla \zeta - \beta v - \omega \frac{\partial \zeta}{\partial p} - (f + \zeta) \nabla \cdot V \tag{2}$$

the tropical cyclone is a positive vorticity center that moves toward (away from) the positive

(negative) vorticity tendencies. In non-divergent, barotropic model simulation of a tropical cyclone vortex on a beta-plane, Fiorino and Elsberry (1989) showed that the advection of the asymmetric vorticity by the symmetric vortex nearly balanced the beta term. Since the last two terms in (2) are zero in their model, this left only the advection of the symmetric vorticity by the asymmetric circulation (wavenumber one gyres) as the mechanism for vorticity change. Fiorino and Elsberry demonstrated that the advecting velocity between the gyres was almost equal to the propagation vector C. Thus, the horizontal vorticity advection is given by this C vector passing through the positive vorticity maximum representing the symmetric vortex. In particular, positive (negative) vorticity advection regions are found in advance (behind) the propagating storm.

Since both C and the vorticity maximum decrease with elevation, the positive vorticity advection decreases (nonlinearly) with decreasing pressure. Based on equation (1) above, this differential vorticity advection will lead to an downward (upward) vertical motion ahead (behind) the propagating storm (Fig. A-3). Given the nonlinear decrease in the vorticity advections from 900 mb upward, the maxima in the vertical motion will be in the lower troposphere and will decrease toward zero at 100 mb. Consequently, a deep secondary circulation is established with horizontal convergence into the subsidence regions ahead and horizontal divergence from the ascent regions behind the storm. The existence of a vertical motion couplet with downward motion ahead and upward motion behind (Fig. A-4) was confirmed in a five-layer adiabatic model by Wang and Holland (1993) and by Jones (1993). In Wang and Holland, the vertical profile of tangential winds was nearly constant up to about 600 mb, so the maximum vertical motion was near this level. In addition, the vertical motion was reversed in the uppermost layer of the model after 48 h of integration.

In each of these adiabatic, baroclinic models, the last two terms in equation (2) are not zero as in the barotropic model of Fiorino and Elsberry. The horizontal convergence

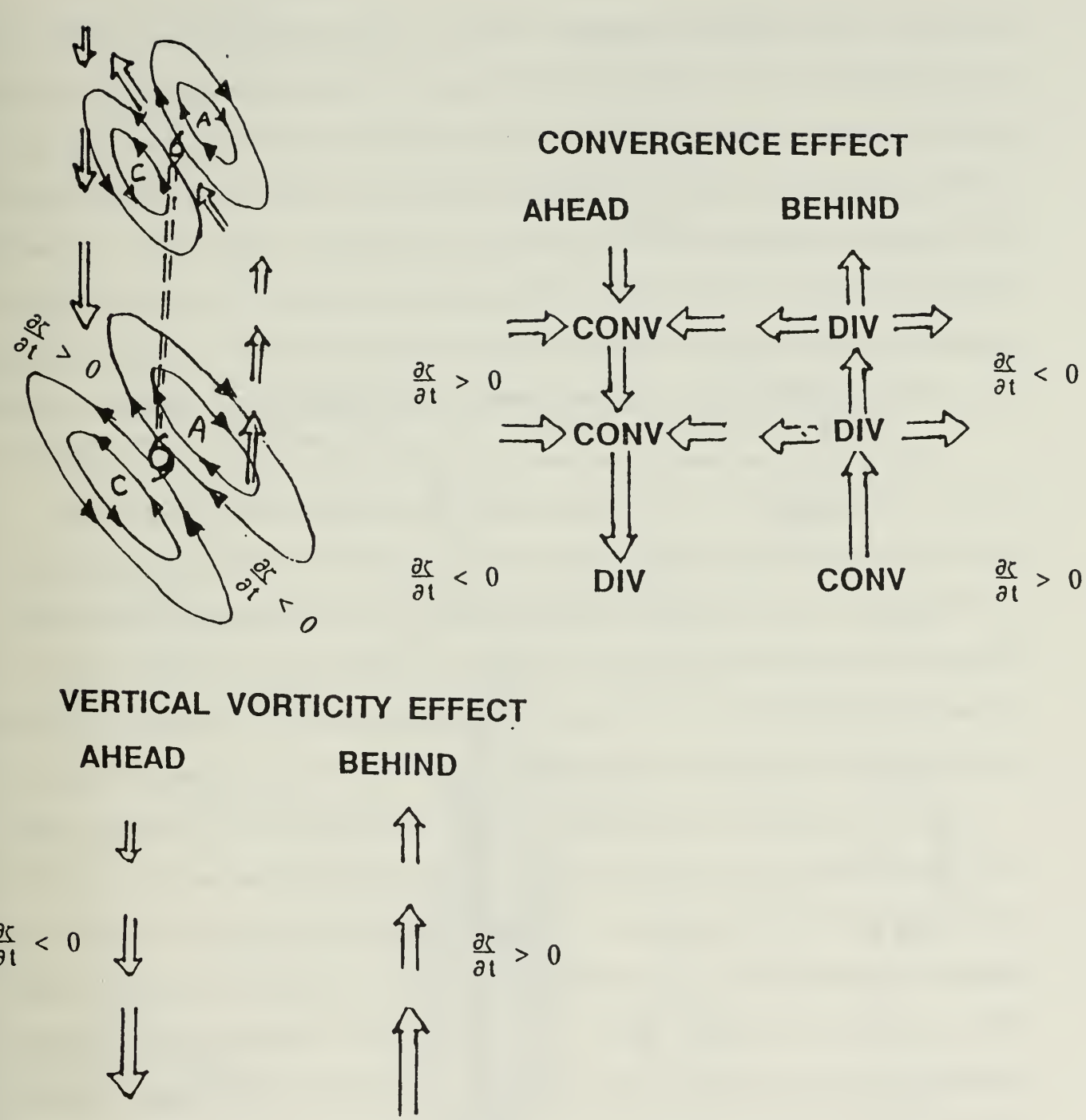


Fig. A-3 Schematic conceptual model of the secondary circulation in an adiabatic tropical cyclone vortex on a beta plane. The asymmetric circulation sets up propagation vectors that create positive (negative) vorticity advection regions ahead and behind the vortex. Differential advection creates vertical motions and horizontal convergence and divergence (see text).

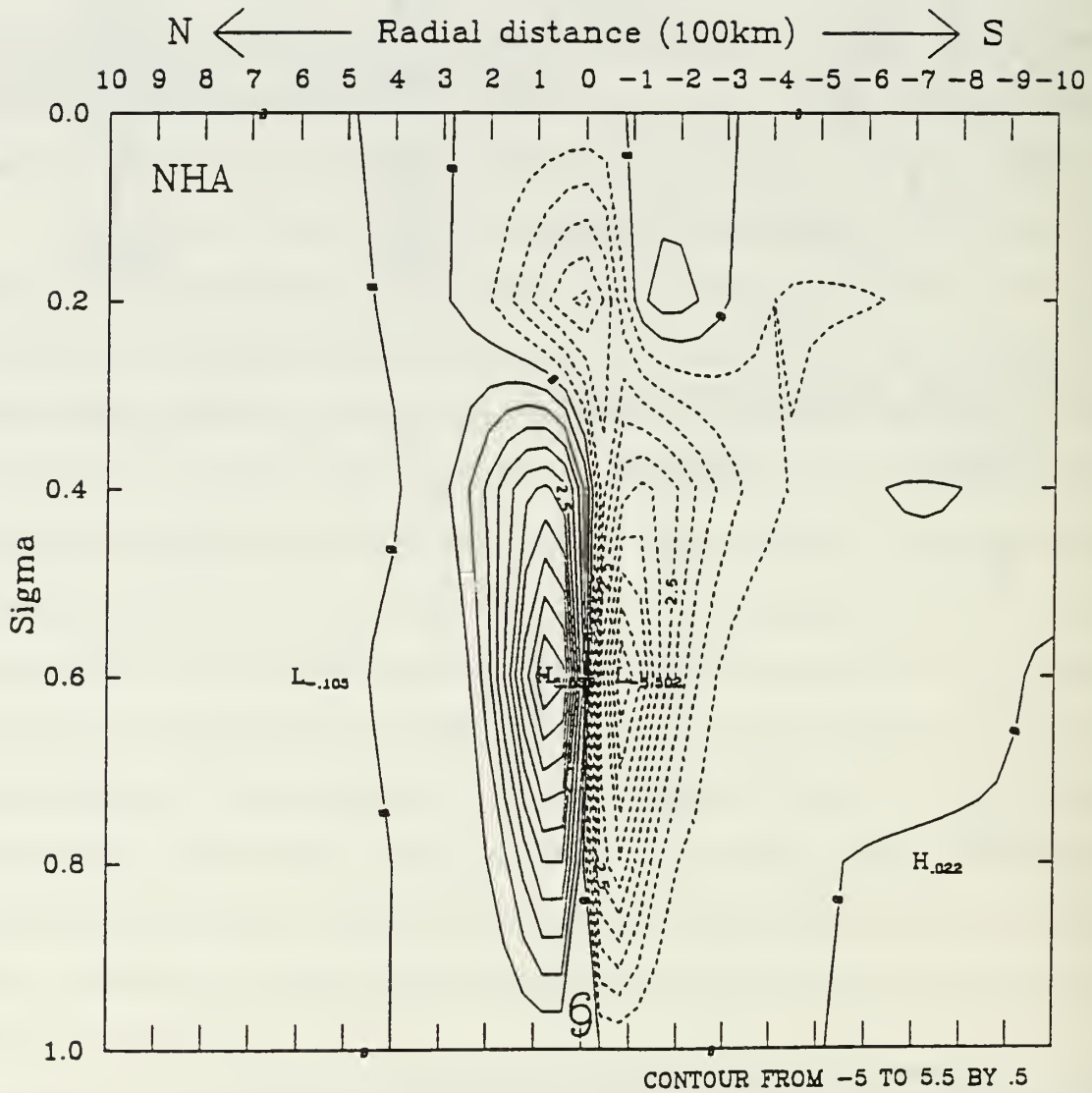


Fig. A-4 Meridional cross-section through the adiabatic tropical cyclone vortex in the Wang and Holland (1993) model illustrating the vertical motion couplet of descent ahead and ascent behind as in the conceptual model of Fig. A-3.

ahead of the storm will create positive vorticity tendencies aloft ahead of the cyclone, and negative vorticity tendencies will be created behind the cyclone due to the divergence (Fig. A-3). Because the cyclone vortex aloft will tend to move toward the positive vorticity tendency region, it will actually be displaced faster than the beta-plane propagation vectors expected at upper levels. In addition, the vertical vorticity advections associated with vertical motions in the secondary circulation (Fig. A-3) contribute to negative (positive) vorticity tendencies at low levels ahead (behind) the vortex. Therefore, the net translation of the vortex at low levels is slower than the beta-plane propagation expected for the vortex structure.

The various terms in the vorticity budget equation (2) are displayed (Fig. A-5) by Wang and Holland (1993) for their five-layer adiabatic model. The horizontal advection of vorticity does indeed contribute to a positive (negative) vorticity tendency at 900 mb ($\sigma$ = 0.9) ahead (behind) the storm center. Although a more complicated pattern of horizontal advection is found at $\sigma$ = 0.3, the magnitudes are almost a factor of 10 smaller and thus are not a major contributor to the motion. As suggested by the meridional cross-section of vertical motion in Fig. A-4, horizontal divergence (convergence) is found at low levels ($\sigma$ = 0.9) below the downward (upward) vertical motion maximum to the north (south) of the center. The corresponding vorticity tendencies at $\sigma$ = 0.9 (Fig. A-5) are negative (positive) ahead of (behind) the storm as in the conceptual model of Fig. A-3. Conversely, horizontal convergence (divergence) is found at $\sigma$ = 0.3 north (south) of the center. The corresponding vorticity tendencies at $\sigma$ = 0.3 (Fig. A-5) are positive (negative) ahead of (behind) the storm, which also agrees with the conceptual model of Fig. A-3. Similarly, the vertical advection contribution to the vorticity tendency (Fig. A-5) at $\sigma$ = 0.9 and $\sigma$ = 0.3 are generally consistent with the conceptual model of Fig. A-3, except they are rotated about $90^{o}$ relative to the storm motion vector. Notice that the vertical vorticity advection contributions are more than an order of magnitude smaller than the leading horizontal advection contributions in this adiabatic model of the tropical cyclone.

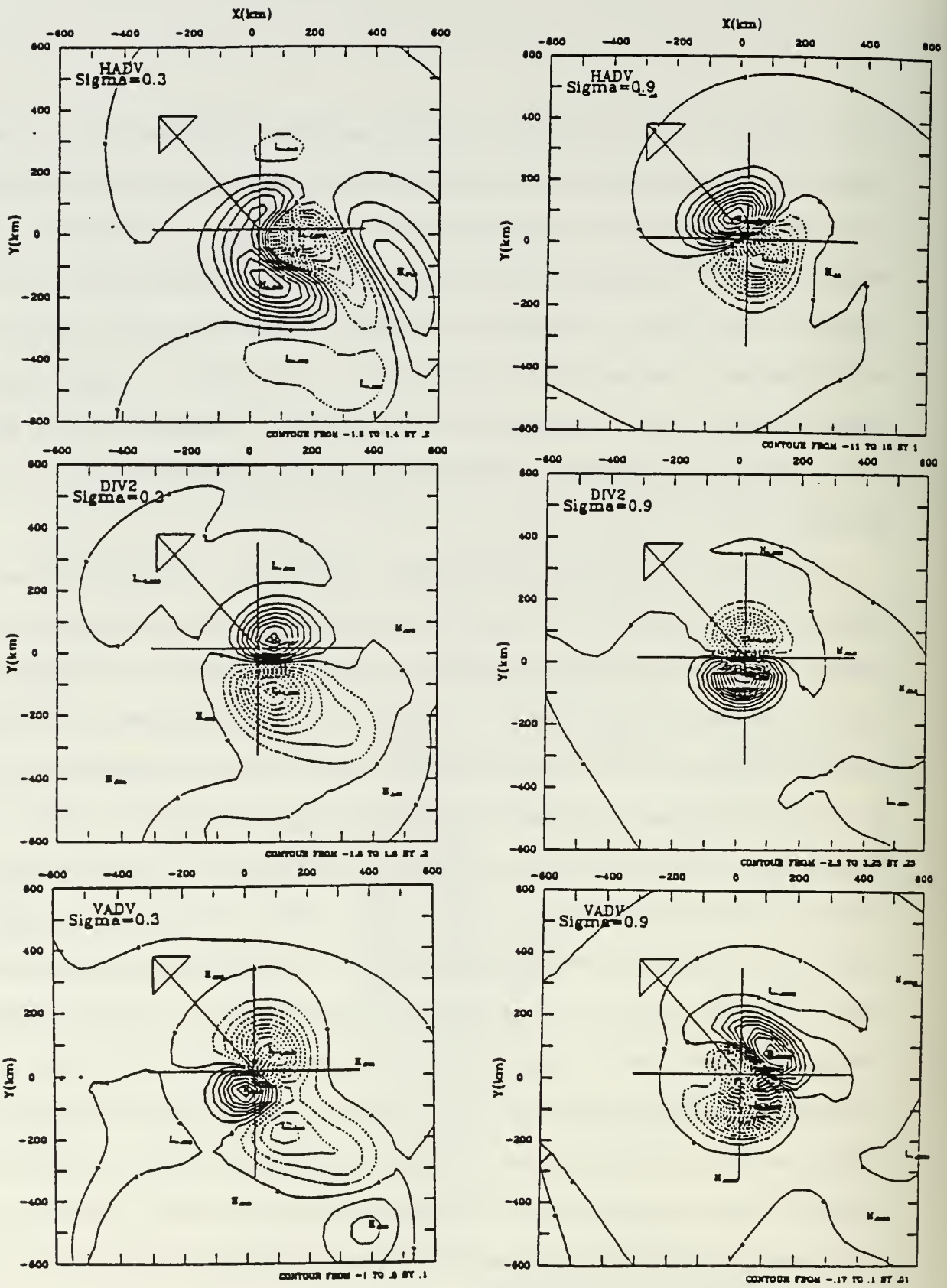


Fig. A-5 Vorticity tendency contributions in the adiabatic tropical cyclone model of Wang and Holland (1993) due to horizontal advection at $\sigma$ = 0.3 and $\sigma$ = 0.9 (top), divergence generation at $\sigma$ = 0.3 and $\sigma$ = 0.9 (middle) and vertical vorticity advection at $\sigma$ = 0.3 and $\sigma$ = 0.9 (bottom). Units are in $10^{-9}$ $s^{-2}$, but different contour intervals are used in each panel. The long arrow indicates the direction of the vortex on the beta-plane.

The combined barotropic-baroclinic reasoning in Fig. A-3 leads to a secondary circulation that is consistent with a propagation vector that is slower (faster) than expected values at lower (upper) levels. As Wang and Li (1992) demonstrate, a completely cyclonic vortex as in Fig. A-2 can remain vertically coherent. Notice that the above reasoning is that the primary vortex motion is associated with beta-plane propagation due to the asymmetric circulation. However, the vertical variations in the propagation vector set up the vertical motion pattern (secondary circulation). The associated vertical vorticity advection and horizontal convergence/divergence terms lead to modifications of the vorticity tendencies in the budget equation (2). A similar reasoning will be applied below in more complicated baroclinic model simulations.

When Wang and Li added an anticyclonic flow aloft to better represent the tropical cyclone structure, the anticyclone moved west-southwest while the cyclone below moved northwest. This separation of the centers occurred due to the lack of a vertical coupling mechanism as in the secondary circulation associated with the completely cyclonic vortex in Fig. A-2. An adiabatic model can not sustain the anticyclone aloft over the tropical cyclone against the beta-effect dispersion.

d. Diabatic contributions to vertical coupling

Each of the adiabatic experiments above was essentially a vortex "spin-down" experiment. That is, a tropical cyclone-like structure was imposed, but the diabatic processes (and convective momentum) to sustain the vortex structure were not included. Although such a vortex must eventually dissipate, the horizontal dispersion due to the beta-effect did not (did) occur if the vortex was all cyclonic (had an anticyclone aloft). Inclusion of diabatic effects is expected to be more effective in maintaining the vertical coherence of the vortex as the different layers will be coupled by a more intense vertical circulation than the vertical circulation induced by quasi-geostrophic reasoning described in Fig. A-3.

The key question is: what is the proper formulation of the diabatic (and frictional) processes to properly represent a real tropical cyclone? The diabatic processes occur on a

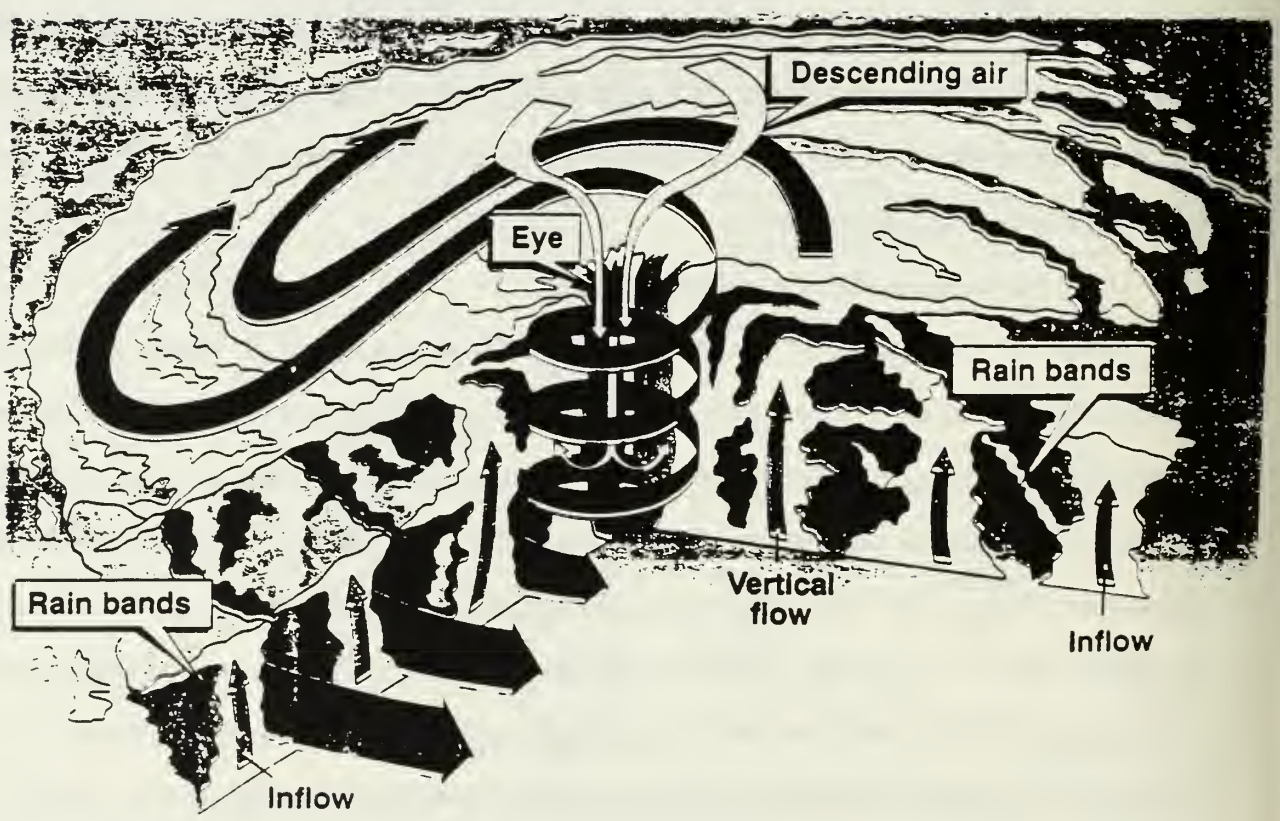


Fig. A-6 Schematic of the cloud structures on various scales in the mature tropical cyclone.

range of scales (Fig. A-6) from small convective towers, spiral rainbands and the primary circulation (inflow at low levels, ascent in the eyewall, and outflow aloft). Clearly a fine horizontal resolution is required to address the heating and flow responses on all of these scales. Even given the proper grid resolution, the physical processes in such clouds may not be well represented by latent heat parameterizations presently available. The relationships between the frictional and diabatic processes are critical in the tropical cyclone. At least in the mature stage, the frictional-CISK type of feedback between frictionally-induced convergence in the boundary layer and latent heat release in clouds is well established. In addition, the updrafts and downdrafts in or adjacent to the deep convection also have a frictional aspect via convective-scale transports of momentum. The point is simply that any representation of diabatic and frictional processes in present numerical models is an idealization of nature.

Shapiro (1992) included convective heat release in response to boundary layer friction and the convective momentum transports. Although only three layers were used in the vertical (Table A-1), a multiply-nested grid allowed a wide range of horizontal scales to be simulated. A tropical cyclone vortex was spun up on an *f*-plane for 48 h, and then the beta effect was introduced. As in the barotropic models with quiescent flow, the propagation vector is to the north-northwest at about 2.4 m $s^{-1}$. The asymmetric circulation in the middle layer (Fig. A-7a) is remarkably similar to the barotropic models with a cyclonic (anticyclonic) gyre to the west (east). These gyres are shown to form from the advection of low potential vorticity (rather than absolute vorticity in barotropic models) from the equatorward side and high potential vorticity from the poleward side (Fig. A-7b). Notice also the homogenization of the asymmetric potential vorticity field within about 300 km of the center, as occurred in the barotropic models (Elsberry and Abbey 1991). In this case, the barotropic stabilization process associated with the radial shear of the angular velocity also is tending to homogenize the asymmetric effects of the convective heating and momentum distributions. Although the flow between the cyclonic-anticyclonic gyre pair is

Table A-1 Characteristics of selected idealized baroclinic models to study tropical cyclone motion.

| Model | Number of layers | Horiz. Res. | Heat source | Friction | Convect. Moment. |
|---|---|---|---|---|---|
| Flatau et al. (1992) | 5 | Cylindr. Spectral s=3 | Constant | Small Newtonian | No |
| Shapiro (1992) | 3 | Nested 20, 40, 80, 160 320, 640 | Predicted | Boundary Layer | Yes |
| Wang and Holland (1993) | 5 | 40 km | Predicted | Boundary Layer | No |
| Wu and Emanuel (1993) | 2 | ? | Specified PV source | None | No |

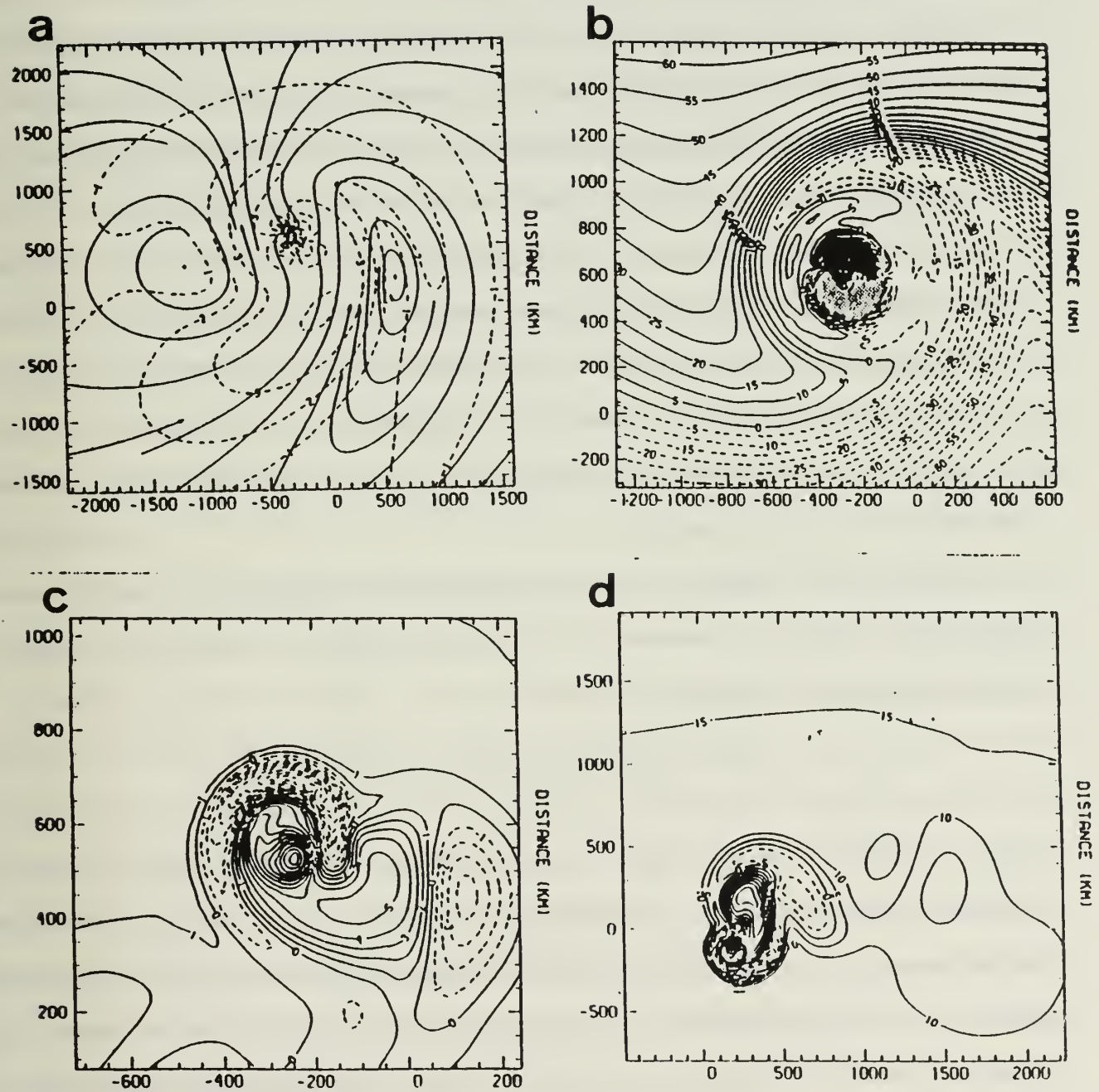


Fig. A-7 Asymmetric (a) wind (contour 1 m $s^{-1}$) and (b) potential vorticity (contour 5 x $10^{-10}$ $m^{-1}$ $s^{-1}$), shaded for less than -85 x $10^{-10}$ $m^{-1}$ $s^{-1}$ at 120 h in middle layer of the Shapiro (1992) baroclinic model for a vortex on a beta plane. (c) Potential vorticity (contour 1 x $10^{-10}$ $m^{-1}$ $s^{-1}$) in upper layer near center of vortex with no vertical shear, and (d) with westerly shear in upper layer (contour 5 x $10^{-10}$ $m^{-1}$ $s^{-1}$).

not as uniform as in the barotropic models, it clearly advects the vortex to the north-northwest. Even though Shapiro notes that enhanced convection on the forward side relative to the trailing side could also be contributing, the association of the propagation with the asymmetric circulation is quite convincing.

The vertical heating distribution creates negative potential vorticity anomalies in the upper layer of the Shapiro model, and the convective momentum flux deposits positive potential vorticity from below. Consequently, the potential vorticity distribution above the center is quite complex (Fig. A-7c). A wake of positive and negative anomalies with large magnitudes trails behind the center. On the larger scale, the outer anticyclonic circulation advects high (low) potential vorticity values to the east (west) side of the center, which will tend to create wavenumber one gyres in the upper layer that are in the opposite sense as the gyres in the middle layer. Although the upper-layer gyres tend to advect the lower portions of the vortex toward the south, this effect is small compared to the northward advection by the middle-layer gyres.

Flatau *et al.* (1992) do not attempt to dynamically predict the interaction between diabatic and frictional processes in the tropical cyclone. Rather, they specify a representative (but arbitrary) heat source

$$Q = a\,\hat{Q}\,\sin(\pi\sigma)\,\exp(-\alpha\sigma)\,\exp\left(-\frac{r^2}{r_0^2}\right),$$

where $\alpha = 0.554$, $\hat{Q} = 7.87^{\circ}$C/day, $r_0 = 150$ km, and $a$ is a normalization factor. A symmetric vortex is spunup in a two-dimensional version of their five-layer model (Table A-1) to provide the initial conditions. As in Shapiro (1992), the spun-up vortex is then added in the three-dimensional model on a beta-plane with no environmental flow. However, the diabatic processes are represented only by the constant heat source Q that is always positioned over the vortex center defined from the surface pressure field. No frictional boundary layer or convective momentum transport is included, and only a small Newtonian friction is added in the lowest layer to partially compensate for the energy

source. Thus, Flatau *et al.* avoid the complexities of the diabatic-frictional processes of real tropical cyclones by imposing a constant heat source, which has the advantage that the diabatic input is precisely known. Because the heat source is continually added over the low pressure center and minimal frictional damping is included, the vortex continues to develop in the three-dimensional model. This vortex advects the earth's vorticity, which creates a potential vorticity distribution in the lower troposphere similar to Fig. A-7b. As in the Shapiro (1992) model, the wavenumber one gyres associated with the asymmetric circulation produce a propagation to the northwest (Fig. A-8). Notice that the diabatic track is to the right of the adiabatic track (heat source Q set to zero). Flatau *et al.* demonstrate that the anticyclone (potential vorticity minimum) in the upper-most layer is displaced westward and equatorward in a quiescent flow as expected on a beta plane. How this outflow layer feature contributed to the difference in tracks in Fig. A-8 is not clear because of the differences in vortex wind profiles for the diabatic and adiabatic model integrations.

Flatau *et al.* note that the diabatic processes should couple the anticyclonic circulation aloft to the cyclonic vortex below, and thus reduce the relative angular momentum (RAM) of the vortex. From the barotropic reasoning of Fiorino and Elsberry (1989), a decrease in the outer wind strength in the vortex should reduce the westward and poleward propagation on the beta plane. In spite of this enhanced vertical coupling, Flatau *et al.* conclude that the motion of the vortex in their five-layer baroclinic model is determined by the strength of the low-level, cyclonic circulation, rather than with a vertically-averaged RAM that included the anticyclonic flow aloft. Thus, the presence of an anticyclonic outflow layer aloft evidently had only a minimal effect on the track in this case of no environmental flow.

Wang and Holland (1993) also compared diabatic and adiabatic versions of a five-layer dynamical model (Table A-1). The only diabatic process they included was a CISK-type convective heating proportional to the relative vorticity in the lowest model layer.

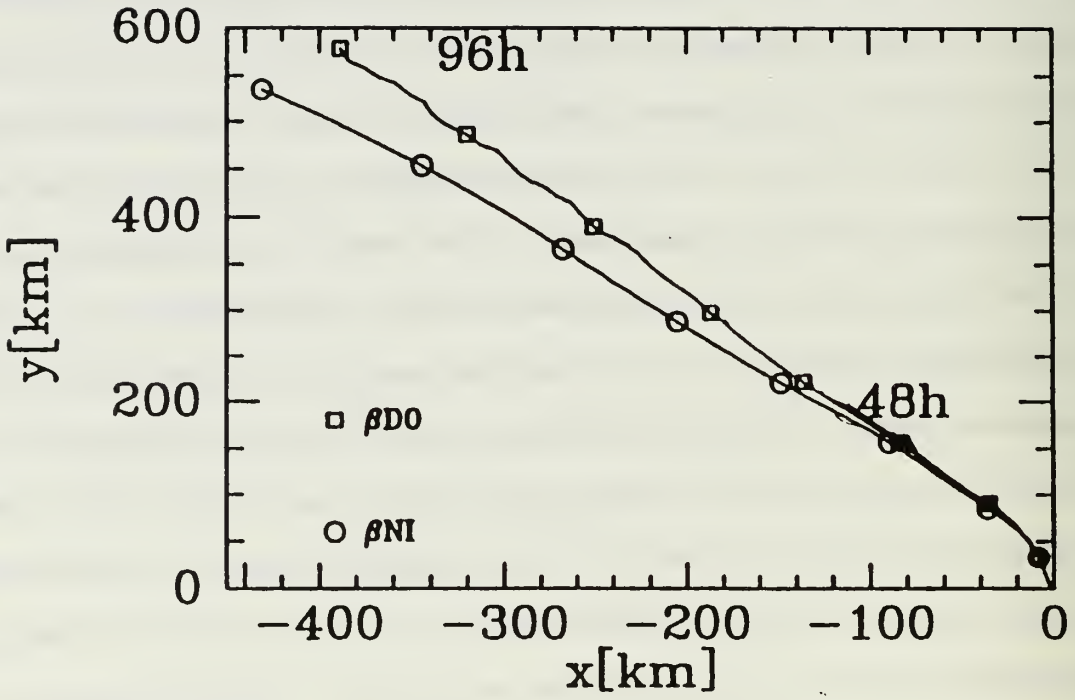


Fig. A-8 Vortex positions each 12 h in the Flatau *et al.* (1992) baroclinic model on a beta plane with (squares) and without (circles) diabatic heat source.

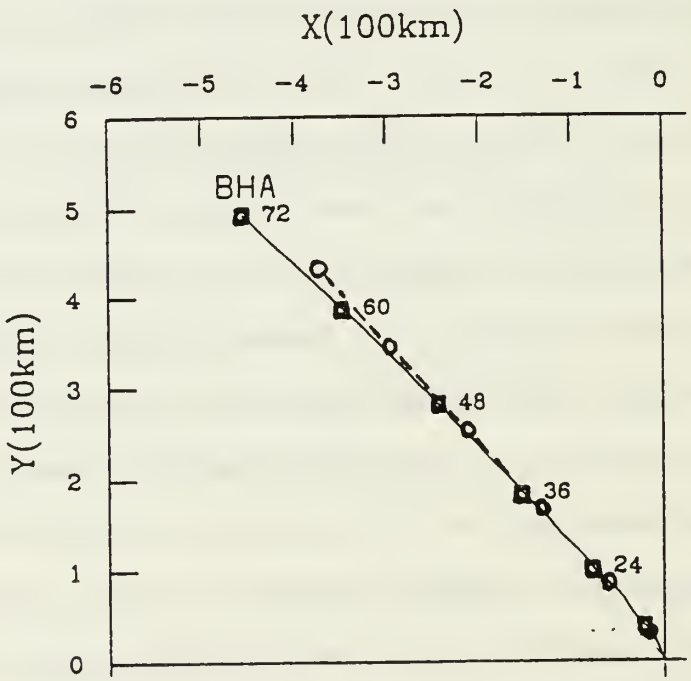


Fig. A-9 Vortex positions each 12 h in the Wang and Holland (1993) baroclinic model on a beta plane with (squares) and without (circles) diabatic heat source.

Wang and Holland include a frictional boundary layer with a wind speed dependent drag coefficient, and horizontal and vertical diffusion of momentum and heat on the grid scale. Thus, the Wang and Holland model is more similar to the Shapiro model than the Flatau *et al.* model. Two symmetric vortices were spun up on an *f*-plane to provide the initial conditions for the beta-plane experiment. A change in the vertical distribution of the cumulus convection heating created a vortex with a stronger and deeper upper-level anticyclone for illustrating the potential motion differences due to cyclone structure. As expected from barotropic models, the stronger cyclonic vortex propagated westward and poleward faster than the less cyclonic vortex. In contrast to the Flatau *et al.* comparison in Fig. A-8, the vortex track in the diabatic model of Wang and Holland was essentially in the same direction and was faster (about 0.5 m $s^{-1}$) that the adiabatic version (Fig. A-9).

The enhanced vertical coupling in a diabatic model is illustrated in Fig. A-10. In the three lowest layers, the local change of relative vorticity has a strong dipole of positive (negative) vorticity tendencies ahead (behind) the vortex center. The $\sigma$ = 0.3 layer appears to be a transition layer with a positive tendency area almost coincident with the vortex center and negative tendency areas ahead and behind the center. Notice that no consistent relationship is found between the positive and negative vorticity tendencies in the outflow layer ($\sigma$ = 0.1) and the vortex motion vector. This similar result as in the Shapiro and the Flatau *et al.* models again implies that the outflow layer has no significant effect on motion in the absence of environmental shear. This is true even though significant anticyclonic centers exist that are not co-located with the low-level vortex centers, and thus a vertical tilt exists (to be discussed below in response to vertical wind shear in the environment).

Wang and Holland (1993) examined the various terms in the vorticity budget (2) for the diabatic model as in Fig. A-5 for the adiabatic model. Although horizontal advection of vorticity contributes, the major change is the increase in relative importance of the vorticity generation due to the convergence at low levels in advance of the vortex. That is, the

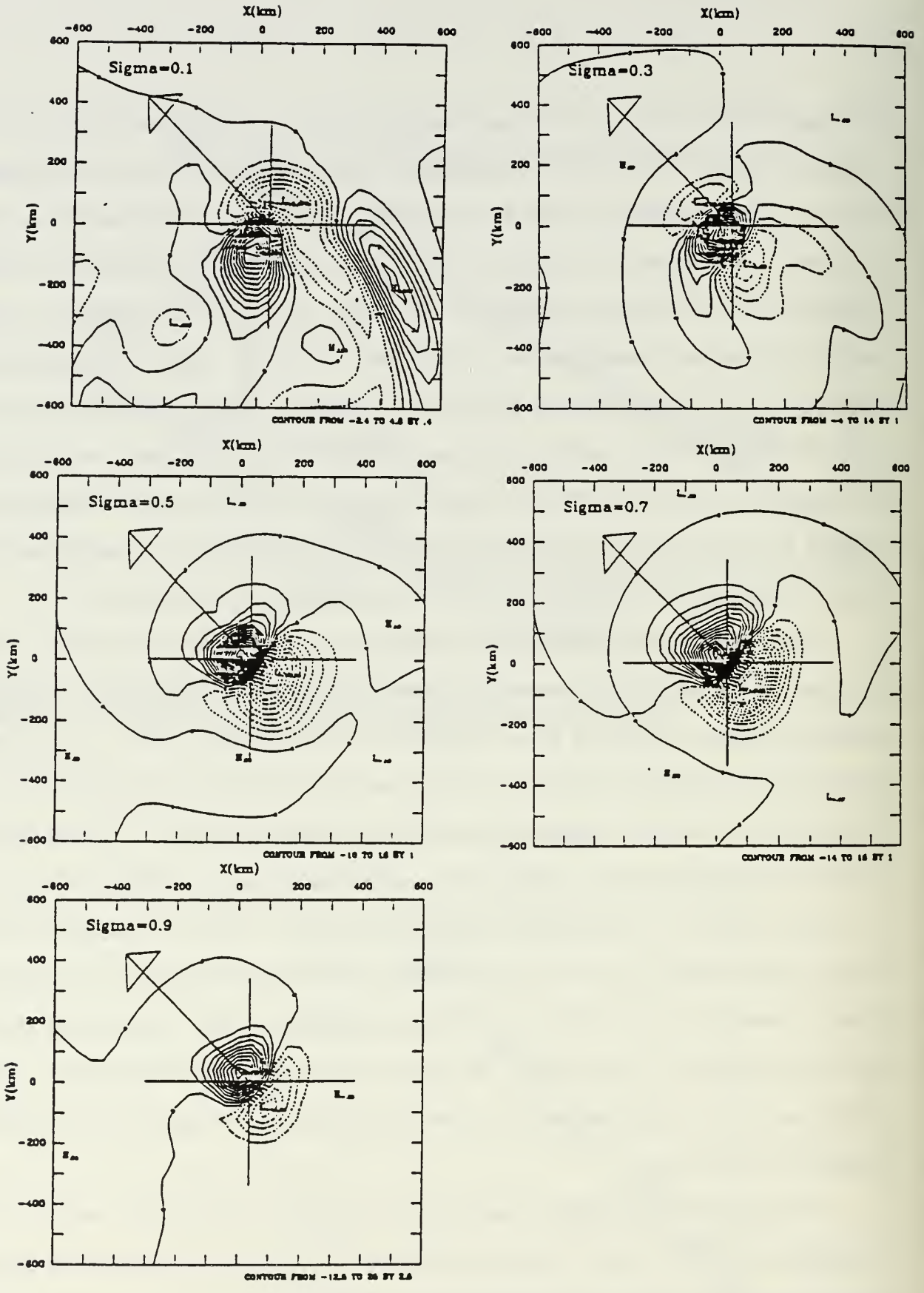


Fig. A-10 Relative vorticity time tendency ($10^{-9}$ $s^{-2}$) after 48 h integration of the Wang and Holland (1993) baroclinic model on a beta plane with a diabatic heat source. Cross hairs indicate the surface position and the large arrow indicates the direction of motion.

frictional convergence, and its positive feedback loop via the CISK-type parameterization in the Wang and Holland model, leads to a positive vorticity tendency in advance of the vortex position. The vertical advection of vorticity is an important term in the middle and upper troposphere in advancing the upper portion of the vortex to maintain a vertical consistency with the lower troposphere vortex. As in the adiabatic model (Fig. A-5), this vertical advection is a result of vertical motion induced by other physical processes, and thus is a secondary process rather than a first-order effect.

The contribution of low-level convergence in advance of the vortex center to positive vorticity tendencies is the likely explanation for why the diabatic vortex track in Fig. A-9 is faster than the adiabatic vortex. Recall that Flatau *et al.* (1993) superposed their analytical heating function directly over the surface pressure center, which would tend to maintain the low center in its present location. That is, the Flatau *et al.* application of the heat source would tend to retard the vortex motion relative to the horizontal vorticity advection that is tending to propagate the vortex forward (Fig. A-5). Thus, it is not surprising that the diabatic vortex track in the Flatau *et al.* model (Fig. A-8) is slower than the adiabatic version, whereas the opposite is true for the Wang and Holland model (Fig. A-9), in which the dynamically-predicted low-level convergence is in advance of the present position.

e. Vertical shear effects

In the above baroclinic model simulations, no environmental flow was included. Thus, the only contribution to the potential vorticity gradient was the poleward gradient of the Coriolis parameter. As Wu and Emanuel (1993) point out, the meridional gradient of potential vorticity q in a quasigeostrophic flow that has only a zonal component U is

$$\frac{\partial q}{\partial y} = \beta - \frac{\partial^2 U}{\partial y^2} - \frac{f_0^2}{N}\left[\frac{\partial^2 U}{\partial Z^2} + \frac{1}{H}\frac{\partial U}{\partial Z}\right], \qquad (3)$$

where $f_0$ is the Coriolis parameter in the middle of the domain, N is the Brunt-Vaisala

frequency (assumed constant in horizontal) and H is a scale height. Notice that the meridional gradient of potential vorticity will be different from $\beta$ if the environmental flow U has curvature in either the horizontal or the vertical, or if linear vertical shear exists. All of the idealized baroclinic models considered here do not include horizontal wind shears. Because the inclusion of vertical shear will change the potential vorticity gradient, which is the dominant factor in beta-effect propagation (Fig. A-7), the interpretation of the vertical shear experiments is complicated.

Wu and Emanuel were able to cancel out the meridional gradient of potential vorticity in their two-layer model by properly specifying the slopes of the upper and lower boundaries. They set the mean wind in the lower layer to zero and introduce vertical shear by specifying a non-zero zonal flow in the upper layer. The tropical cyclone is idealized as a point potential vortex (wind decreasing outward with 1/r dependence, but having no relative vorticity except at the center). The upward decrease in diabatic heating is represented as a source of (negative) potential vorticity. Thus, the negative potential vorticity anomaly associated with the anticyclone aloft expands in area due to a radial outward potential flow that emanates from a point mass source co-located with the lower vortex. If no vertical shear is present, the upper vortex patch simply expands in time, remains circularly symmetric and causes no lower vortex motion. If a moderate westerly wind is introduced in the upper layer (Fig. A-11), the vortex expands and is advected to the east. Due to barotropic instability, the vortex patch is rolled up. However, the outer winds around the upper-level anticyclone induce an advective flow in the lower layer that now crosses over the point vortex representing the tropical cyclone.

As shown in the schematic (Fig. A-12), the tilt of the anticyclone to the east due to a westerly shear will induce a northward deflection of the low-level vortex. Conversely, the flow around the low-level vortex will induce a northward deflection of the upper-level vortex. Thus, the cyclone-anticyclone couplet can translate northward together. With an easterly shear (Fig. A-12), the anticyclone aloft is tilted to the west, and this upper-level PV

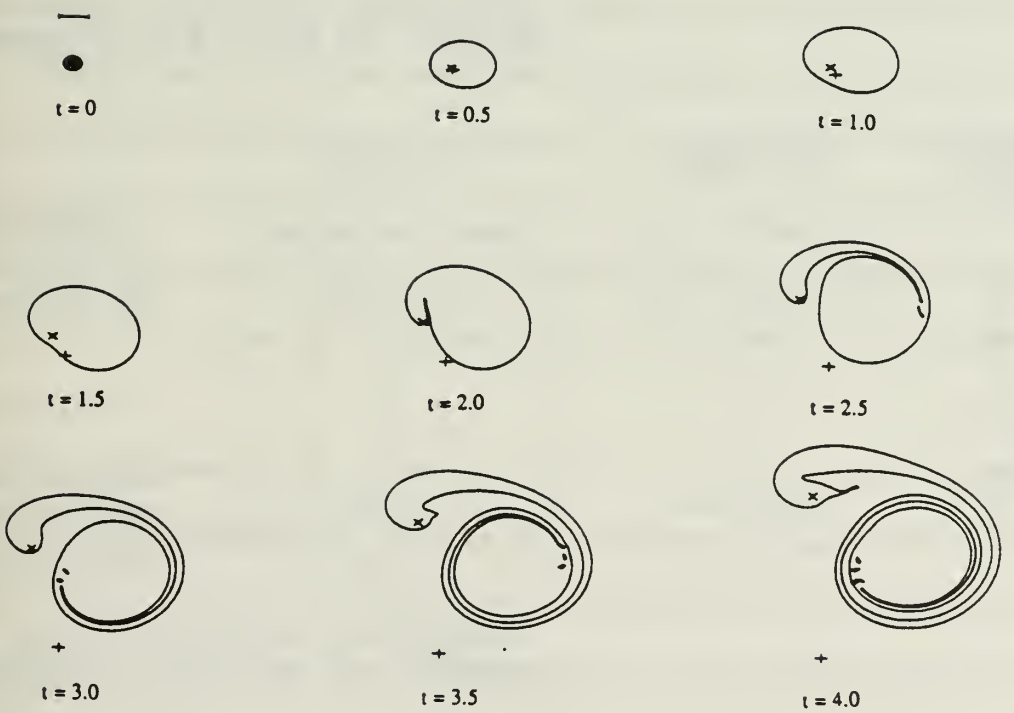


Fig. A-11 Evolution of the upper-layer vortex patch in the Wu and Emanuel (1993) baroclinic model with an upper-layer depth one quarter of the lower-layer depth and a moderate vertical wind shear ($\chi$ = 1.25). The lower-layer point vortex at the initial and present times are indicated by the + and x symbols respectively. The nondimensional time interval of 0.5 corresponds to about two days and a length scale of 500 km is indicated in the upper left corner.

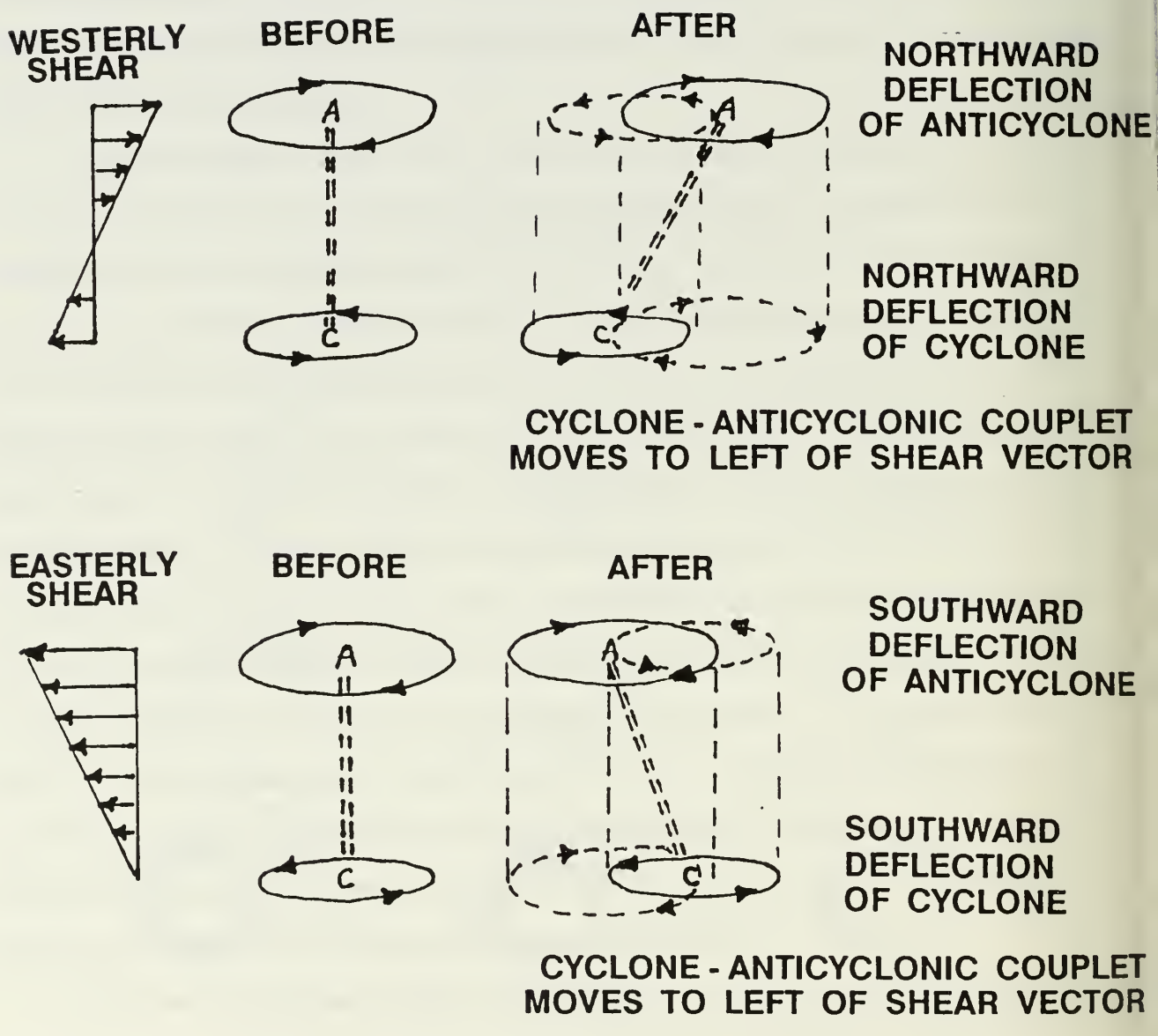


Fig. A-12 Schematic of the potential interaction between an upper-level anticyclone (A) and low-level cyclone that were initially vertically oriented (middle section), but were then exposed to a westerly shear (top) or an easterly shear (bottom). Following Wu and Emanuel (1993), the potential vorticity distributions in each layer induce circulations in the adjacent layer (dashed) lines that deflect the upper-level and lower-level circulations as indicated in the right column.

anomaly induces a southward flow across the upper-layer anticyclone. In this case, the cyclone-anticyclone couplet can translate southward together. Thus, Northern (Southern) Hemisphere tropical cyclones are expected to translate to the left (right) of the vertical wind shear vector as the upper-level anticyclone becomes tilted relative to the center.

The induced zonal, meridional and total translation speeds for the case in Fig. A-11 are shown by the long-dashed lines in Fig. A-13. Since the anticyclonic center of the patch at t = 0.5 (dimensional time about two days) is northeast of the low-level vortex, a westward (negative zonal) and northward (positive meridional) component is induced across the low-level vortex. The westward component grows until about t = 1.7, and then rapidly decreases to zero around t = 2.8, when the upper-level anticyclone is due east of the low-level vortex (Fig. A-11). As the anticyclone drifts farther to the southeast, the low-level zonal translation is toward the east (positive). The magnitudes of these translations are quite large (1-3 m $s^{-1}$) for this "optimal shear" case. Either smaller or larger shear values eventually lead to smaller translation speeds (Fig. A-13c), as well as a different evolution of meridional and zonal components. The trajectories of the lower-level vortex are shown in Fig. A-13d for the three wind shears. In each case, the initial deflections are toward the north-northwest. With smaller than optimal shear, the trajectory curves toward the northeast. The optimal shear trajectory also is curving toward the northeast by the end of the integration.

The magnitudes of the deflections in Fig. A-13d are critically dependent on the relative ratio of the upper-layer depth to the lower-layer depth (Wu and Emanuel 1993). In the case shown, this ratio was 0.25, which would correspond to a 200 mb outflow layer over a 800 mb cyclonic flow layer. This is similar to the configuration in the five-layer baroclinic models of Flatau *et al.* (1992) and Wang and Holland (1993) described above. However, the outflow layer may be considerably shallower in real storms. For example, the NASA DC-8 observations at 195 mb in Supertyphoon Flo (Dunnavan *et al.* 1991) indicated nearly cyclonic flow to about 200 km radius. Thus, the outflow must have been at some

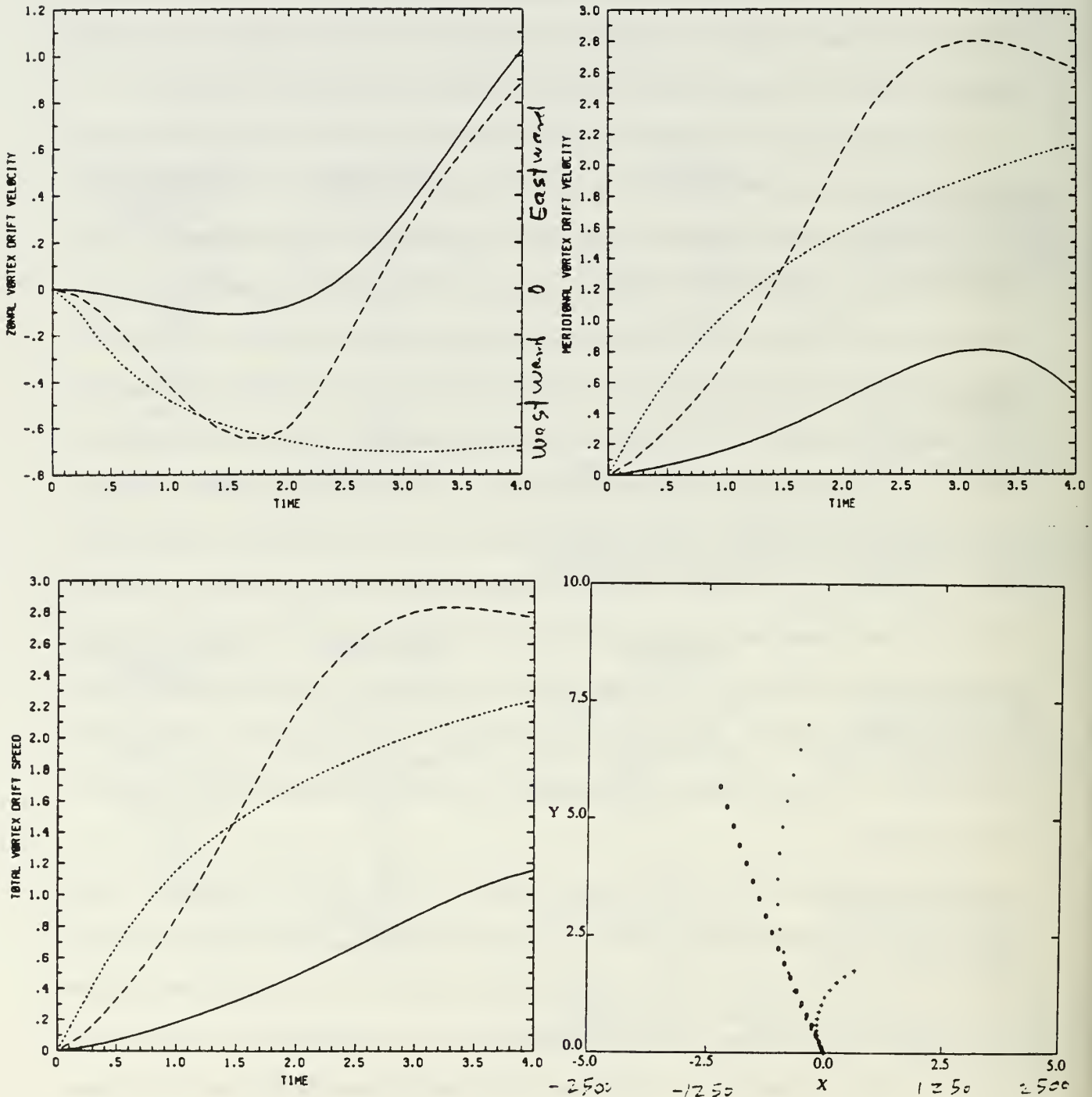


Fig. A-13 Evolution of the induced lower-layer vortex (a) zonal and (b) meridional velocity, (c) total speed, and (d) trajectories in units of 500 km with time in the Wu and Emanuel (1993) model for the same conditions as in Fig. A-11 (long-dashed line) and for weaker vertical wind shear (solid) and stronger vertical wind shear (short-dashed) conditions. The symbols each t = 0.5 along the trajectories in (d) for the three shear conditions are dots, crosses and circles respectively.

higher elevation. If the outflow was confined below the tropopause (around 100 mb), the outflow may have only been 50-75 mb deep, and the cyclonic flow 950-925 mb thick. In that case, the depth ratio is 0.053 - 0.081. If similar reductions in the track deflections can be assumed, the zonal and meridional components in Fig. A-13 would be only 1/5 to 1/3 of the values shown.

In the two-layer Wu and Emanuel model, a PV anomaly in one layer necessarily implies an induced circulation in the adjacent layer (Fig. A-12). In a multi-layer model, the circulation response may not extend throughout the depth as in the Wu and Emanuel model. The depth of penetration will be inversely proportional to the static stability.

Shapiro (1992) illustrates how the inclusion of vertical wind shear also introduces a meridional gradient of potential vorticity on an *f*-plane. Shapiro sets the zonal basic current equal to zero in the lowest two layers and adds a westerly wind only in the upper layer. Based on (3), the increase in shear from zero between layers 1 and 2 to a positive shear between layers 2 and 3 means the second derivative in Z is positive, and thus the $\partial q/\partial y$ is negative because the beta term is zero on the *f*-plane. Thus, two counter-balancing effects are introduced: (*i*) horizontal advection of potential vorticity by the symmetric vortex circulation of this negative $\partial q/\partial y$ should lead to a southward and eastward propagation (in the Northern Hemisphere); and (*ii*) vertical tilt of the anticyclonic vortex aloft to the east by the westerly shear should lead to a northward propagation as in Fig. A-12.

Shapiro (1992) found that the horizontal advection of potential vorticity gradient dominated, as the motion of the vortex was southward and eastward at an average speed of about 0.9 m $s^{-1}$. He showed that the cyclonic circulation now advected the low (high) potential vorticity values in the middle layer southward (northward) on the west (east) side of the cyclone, which is the opposite of the beta plane result in Fig. A-7b. With the negative $\partial q/\partial y$, the anticyclonic (cyclonic) gyre formed on the west (east) side, so the flow between the gyres was to the southeast, which resulted in the southeastward motion. The

westerly shear did advect the upper-layer air to the east and formed a wavenumber one asymmetry (Fig. A-7d). This low potential vorticity anomaly is analogous to the vortex patch in the Wu and Emanuel model (Fig. A-11), which is expected to move the low-level vortex toward the north (Fig. A-13d). However, the heat source and convective momentum transport in the Shapiro model maintained a nearly vertical vortex that moved southeastward with the vortex in the middle layer. Shapiro concludes that the northward gradient of potential vorticity in the upper layer deflects the anticyclone to the north, but the Wu and Emanuel mechanism has little effect on the vortex motion. Rather, the southward gradient of potential vorticity in the middle layer is both necessary and sufficient to explain the southeastward drift.

Shapiro (1992) also demonstrated the importance of the depth of the upper outflow layer. When Shapiro reduced the thickness of this layer, the southeastward speed in the negative $\partial q/\partial y$ on an *f*-plane experiment was reduced from 0.9 m $s^{-1}$ to 0.3 m $s^{-1}$. This decrease in propagation was nearly equal to the reduction in the potential vorticity gradient associated with the larger middle layer depth. A stronger anticyclonic vorticity occurred in the shallower outflow layer, which should have produced a northward motion tendency. However, the horizontal advection of the potential vorticity gradient by the cyclonic circulation in the middle layer was an even more dominant effect.

Flatau *et al.* (1992) and Wang and Holland (1993) impose linear vertical wind shears in their five-layer models. According to equation (3) above, this introduces a small meridional gradient of potential vorticity. For example, the westerly wind shear in Flatau *et al.* introduces a meridional PV gradient of $0.51 \times 10^{-6}$ $km^{-1}$ even though *f* was set equal to a constant. Because this value is more than an order of magnitude less than the PV gradient (about $0.7 \times 10^{-5}$ $km^{-1}$) on a beta plane, the major effect is expected to be due to the vertical shear rather than the horizontal advection of PV by the symmetric circulation.

The vortex trajectories on a *f*-plane with westerly and easterly shear in the Flatau *et al.* (1992) model are shown in Fig. A-14. The control case of a uniform easterly flow has a

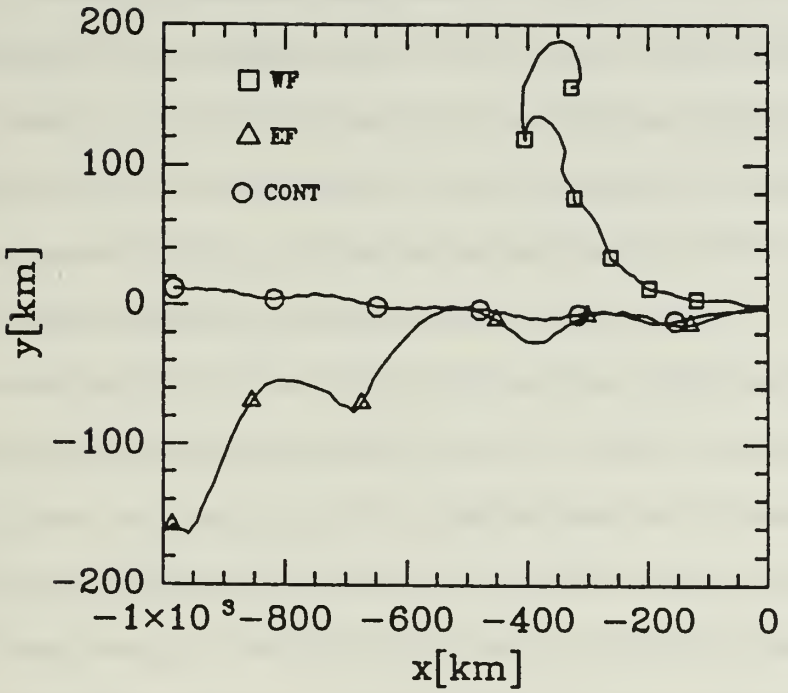


Fig. A-14 Vortex positions each 12 h in the Flatau *et al.* (1993) baroclinic model on an *f*-plane for the uniform easterly wind control (circles), westerly shear (squares) and easterly shear (triangles).

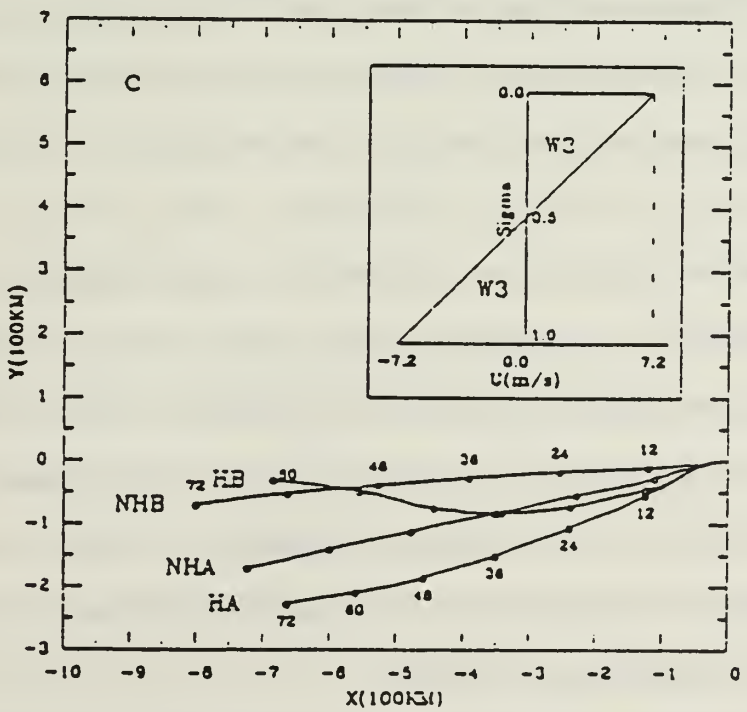


Fig. A-15 Vortex positions each 12 h in the Wang and Holland (1993) model on an *f*-plane with (H) and without (NH) diabatic heat source for the strong westerly shear case indicated in the inset. Vortex B has a deeper anticyclonic layer aloft than Vortex A.

very small meridional drift due to the small Newtonian friction in the lowest layer (Table A-1). The differences in westward displacements between the westerly shear and the easterly shear cases in Fig. A-14 are due to the differences in depth-averaged basic currents, with a stronger easterly flow in the easterly shear case. Notice that meridional deflections to the left of the imposed shear vector begin to develop after 24-36 h, which is in the proper sense for the vertical tilt mechanism (Fig. A-12). The magnitudes are of the order of 0.5 m $s^{-1}$. As described above, the westerly (easterly) shear induces a small poleward (equatorward) PV gradient, which also would contribute to a slow poleward (equatorward) drift after 24-36 h when the beta-type gyres would have developed. Although the Flatau *et al.* demonstration is thus ambiguous, it does indicate that the magnitudes are considerably smaller than implied by Wu and Emanuel (Fig. A-13).

Wang and Holland (1993) obtained a quite different response to the imposition of a large westerly shear (Fig. A-15). The two vortices they tested moved westward with the lower layer flow between 900-500 mb. The surprising result is that the meridional deflection was to the right of the westerly shear vector, rather than to the left as in the Wu and Emanuel and Flatau *et al.* models. Wang and Holland (1993) attribute the rightward deflection of the low-level Vortex A, which was almost entirely cyclonic throughout the layer, to a cyclone-cyclone tilt mechanism. A further rightward deflection relative to the vertical shear vector was attributed to stretching, vertical advection and twisting terms associated with the diabatic heat source. The smaller rightward deflection of the low-level Vortex B, which had a deeper anticyclonic layer aloft, was attributed to a larger contribution from the anticyclone-cyclone tilt mechanism. In the Vortex B case with a diabatic heat source, the alternating dominance of the rightward deflection associated with the tilt mechanism led to an oscillatory trajectory. It is again emphasized that the meridional deflections in these cases are often small (~ 100 km over 72 h).

f. Vertical shear effects on a beta plane

Given the Shapiro (1992) demonstration that the horizontal advection mechanism

with only a small negative $\partial q/\partial y$ induced by westerly shear dominated the vertical tilt mechanism, it is not surprising that experiments of Shapiro, Flatau *et al.* (1992) and Wang and Holland (1993) with vertical shear on a beta plane are controlled by the beta effect. In contrast to the Flatau *et al.* *f*-plane deflections (Fig. A-14), the meridional displacements on the beta plane are toward the north (Fig. A-16) as expected. Large differences in zonal displacements are also noted, but these are associated with different lower-tropospheric wind profiles in the westerly shear and easterly shear cases.

Flatau *et al.* suggest that the 100 km difference in meridional displacements (versus about 300 km after 72 h in Fig. A-14) indicates the net motion is not just a superposition of the shear effect and the beta effect. They argue that the upper-level anticyclone also responds to the beta effect by moving to the south, and is not as far east as expected from the westerly shear case on an *f*-plane. With the upper-level anticyclone (negative potential vorticity anomaly) to the southeast (rather than to the east), the effect of the PV anomaly across the lower-level vortex is from the southwest (Fig. A-17) rather than from the south. This could account for the smaller meridional displacement for the westerly shear case in Fig. A-16. However, only small directional differences in the horizontal potential vorticity advection mechanism associated with the different vortex structures in the easterly and westerly shear cases may also cause similar magnitudes of meridional displacements over 72 h.

Recall also that the Flatau *et al.* five-layer model has an outflow layer thickness of about 200 mb, which may imply a larger role for the upper-layer potential vorticity anomaly (Fig. A-17) than may exist in nature. Wang and Holland (1993) also found some smaller differences in meridional displacements (not shown) when the vertical shear was added on a beta plane rather than on an *f*-plane. Wang and Holland suggest that the difference is a function of the vortex structure (depth of the anticyclonic layer), which influences both the vertical tilt mechanism and the extent to which the anticyclonic potential vorticity anomaly aloft is affected by the beta effect (as in Fig. A-17). Thus, the meridional propagation in a

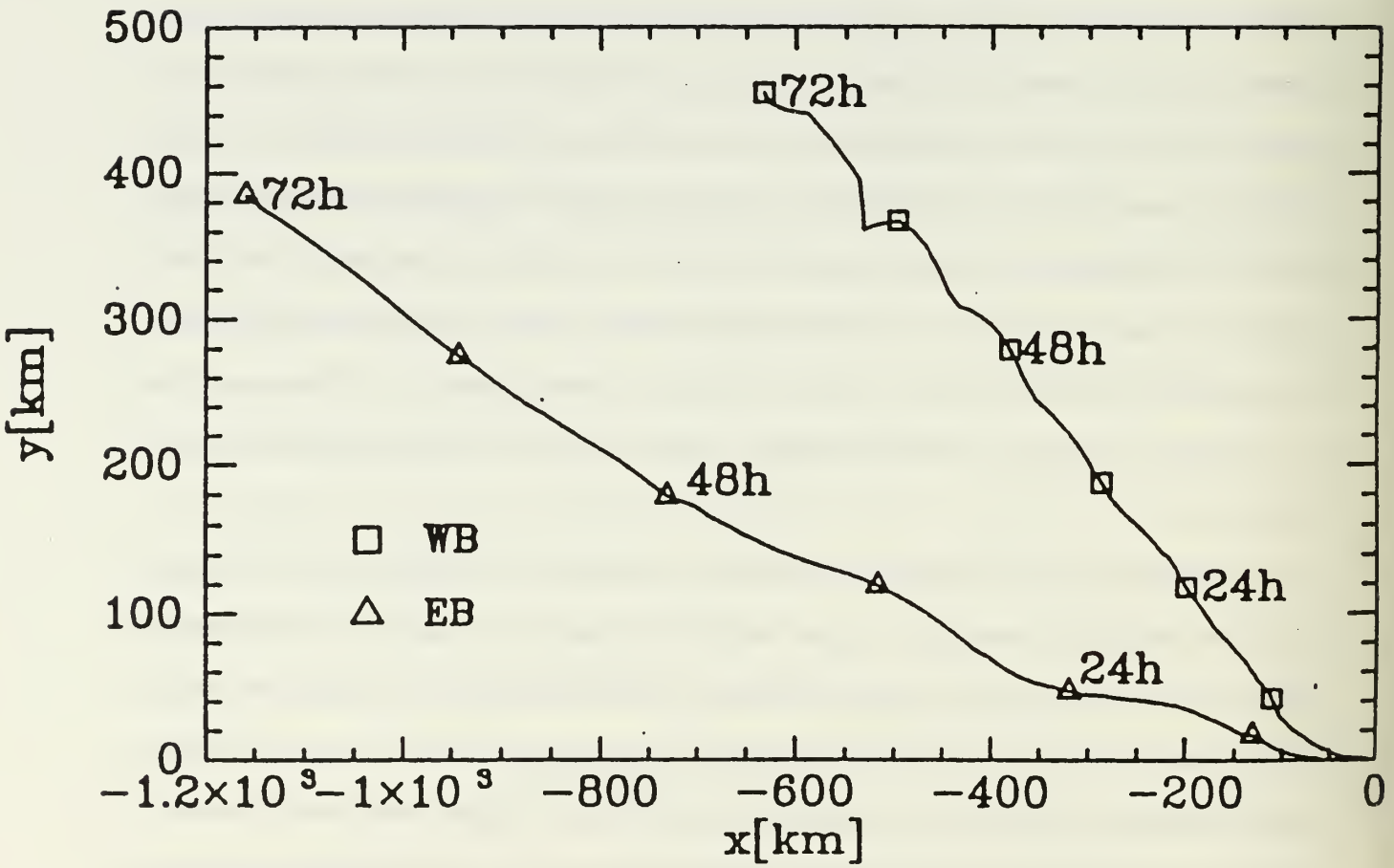


Fig. A-16 Vortex positions each 12 h for westerly shear (boxes) and easterly shear (triangles) on a beta plane in the Flatau *et al.* (1992) model.

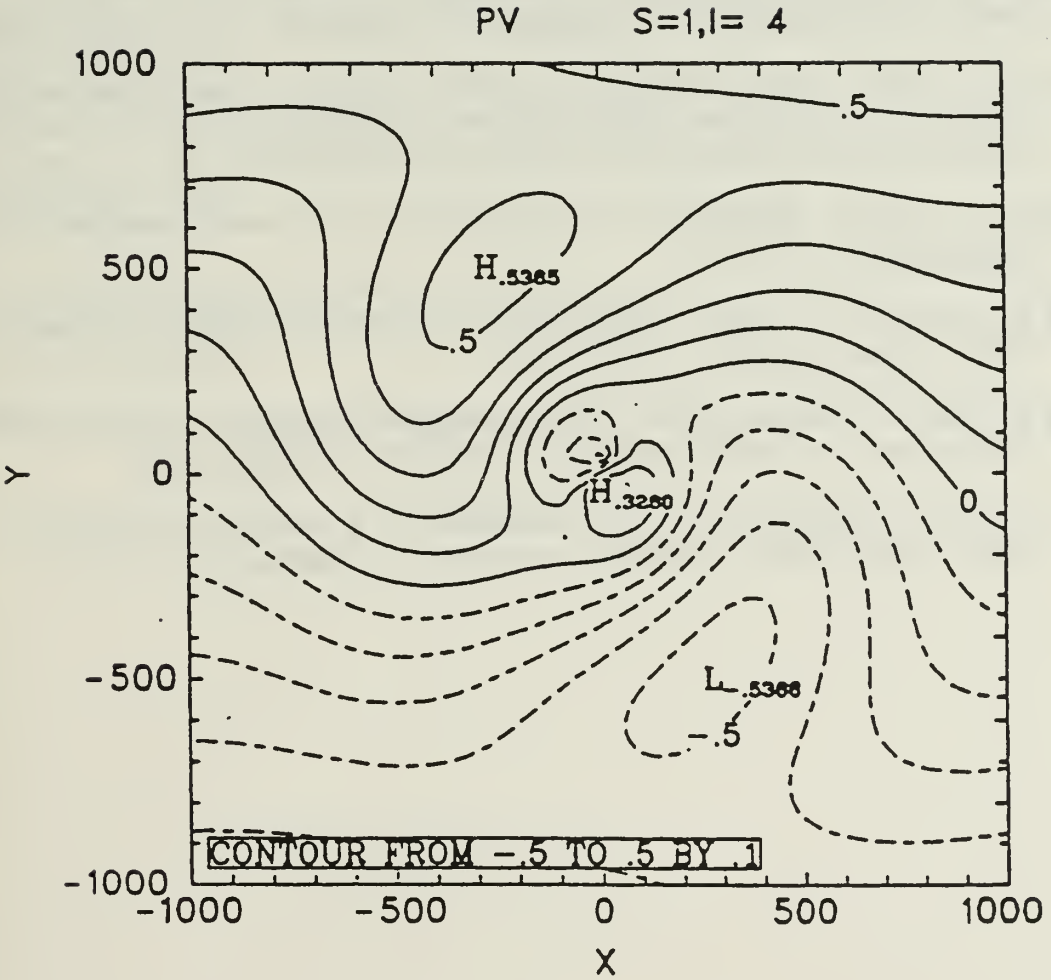


Fig. A-17 Wavenumber one contribution to the potential vorticity in the upper layer of the five-layer Flatau *et al.* (1992) model with westerly shear on a beta plane. Notice that the general orientation of the upper-level flow between the positive PV (cyclonic) and negative PV (anticyclonic) anomalies is from the southwest across the low-level vortex position at (0, 0).

g. References

Dunnavan, G. M., R. L. Elsberry, E. A. Ritchie, G. J. Holland and D. Lauritsen, 1991: Structure of Supertyphoon Flo during TCM-90. Preprints, 19th Conference on Hurricanes and Tropical Meteorology, American Meteorological Society, Boston, MA 02108, 21-26.

Elsberry, R. L., and R. F. Abbey, Jr., 1991: Recent advances in understanding tropical cyclone motion. Tech. Rep. NPS-MR-91-003, Naval Postgraduate School, Monterey, CA 93943, 92 pp.

Fiorino, M., and R. L. Elsberry, 1989: Some aspects of vortex structure in tropical cyclone motion. J. Atmos. Sci., **46**, 979-990.

Flatau, M., W. H. Schubert and D. E. Stevens, 1992: The role of baroclinic processes in tropical cyclone motion: The influence of vertical tilt. Submitted to J. Atmos. Sci.

Jones, S. C., 1993: The motion of dry baroclinic vortices: The role of vertical shear and vortex tilting. Preprints, 20th Conference on Hurricanes and Tropical Meteorology, American Meteorological Society, Boston, MA 02108.

Shapiro, L. J., 1992: Hurricane vortex motion and evolution in a three-layer model. J. Atmos. Sci., **49**, 140-153.

Wang, B., and X.-F. Li, 1992: The beta drift of three-dimensional vortices: A numerical study. Mon. Wea. Rev., **120**, 579-593.

Wang, Y., and G. J. Holland, 1993: On the baroclinic dynamics of tropical cyclone motion: The influence of vertical structure. Submitted to J. Atmos. Sci.

Wu, C.-C., and K. Emanuel, 1993: Interaction of a baroclinic vortex with background shear: Application to hurricane movement. J. Atmos. Sci., **50**, 62-76.

Distribution List

| | |
|---|---|
| Office of Naval Research (Code 1122MM)<br>800 N. Quincy Street<br>Arlington, VA 22217-5000 | 1 |
| Dr. Robert L. Haney (Code MR/Hy)<br>Chairman, Department of Meteorology<br>Naval Postgraduate School<br>Monterey, CA 93943-5000 | 1 |
| Dr. Russell L. Elsberry (Code MR/Es)<br>Department of Meteorology<br>Naval Postgraduate School<br>Monterey, CA 93943-5000 | 193 |
| Library (Code 0142)<br>Naval Postgraduate School<br>Monterey, CA 93943-5000 | 2 |
| Dean of Research (Code 08)<br>Naval Postgraduate School<br>Monterey, CA 93943-5000 | 1 |
| Defense Technical Information Center<br>Cameron Station<br>Alexandria, VA 22304-6145 | 2 |